

**STABILITY ANALYSIS OF A GLULAM DOME**

**WITH**

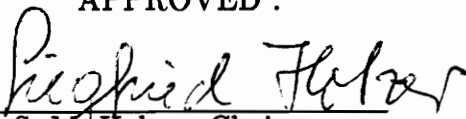
**NONLINEAR MATERIAL LAW**

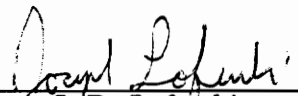
by

Niket M. Telang

Thesis submitted to the Faculty of the  
Virginia Polytechnic Institute and State University  
in partial fulfillment of the requirements for the degree of  
Master of Science  
in  
Civil Engineering

APPROVED :

  
S. M. Holzer, Chairman

  
J. R. Loferski

  
D. A. Garst

January 1992

Blacksburg, Virginia

C.2

L D

5655

V855

1992

T442

C.2

# Stability Analysis of a Glulam Dome with Nonlinear Material Law

by

Niket M. Telang

Committee Chairman: Dr. S. M. Holzer

Civil Engineering

## (ABSTRACT)

The object of this study is to incorporate a nonlinear material law for wood in the finite element program ABAQUS to develop effective finite element models of glulam domes, and to investigate the buckling behavior of glulam domes using this finite element program. The material law is implemented with a FORTRAN subroutine. Results from thorough testing of the subroutine are presented. The dome is then modeled with I-DEAS and, analysed with ABAQUS. The modeling procedure is briefly discussed, and the results from the stability analysis of the dome are presented. Finally, conclusions and further research scope based on this study are presented.

## Acknowledgements

I am truly grateful to Dr. S. M. Holzer for his excellent teaching, and his continued support and encouragement throughout this study. I wish to express my gratitude to Professor D. A. Garst and Dr. J. R. Loferski for their help and suggestions during the course of my study, and for serving on my committee.

I am very thankful to my fellow students, Raul Andruet, Jacem Tissaoui, Chris Earls, Nathan Madutujuh and Budi Widjaja for their lively discussions, probing questions, and innovative ideas.

I am extremely grateful to my family and friends, without whose support this task would have been impossible. I am especially grateful to Dr. Shirley and Mr. Robert Farrier, and to Dr. Laura J. Harper. Last but not the least, I am grateful to my parents and sister, whose love, affection and everlasting support have made my dreams a reality.

# TABLE OF CONTENTS

- 1. INTRODUCTION.....1
- 2. THE MATERIAL MODEL .....6
  - 2.1 Material Behavior of Wood .....7
  - 2.2 The Material Model .....8
    - 2.2.1 Compression Zone .....9
    - 2.2.2 Tension Zone .....12
  - 2.3 ABAQUS Material Library .....16
  - 2.4 User Material Option .....17
  - 2.5 The User Subroutine .....20
- 3. VERIFICATION OF THE MATERIAL MODEL .....23
  - 3.1 Testing of User Subroutine Option .....24
  - 3.2 Sensitivity Analysis and Accuracy Studies .....26
  - 3.3 Tests on the Cantilever Beam .....28
    - 3.3.1 Effect of Mesh Refinement .....29
    - 3.3.2 The Effect of Other Factors .....34
  - 3.4 Cantilever Column Loaded Through Its Base .....40

3.5	Torsion Tests on Cantilever Beam .....	45
3.5.1	Tests on Curved Cantilever Beam .....	49
3.5.2	Torsion Tests on Cantilever Beam .....	49
4.	MODELLING THE DOME .....	52
4.1	The Geometric Model .....	54
4.2	The Finite Element Model .....	54
4.3	Boundary Conditions.....	61
4.4	Material Properties .....	63
4.5	Dome Loading.....	65
4.6	Creation of ABAQUS Input File .....	67
4.6.1	Pre-processing Using I-DEAS .....	67
4.6.2	Nodal Loads .....	70
4.6.3	Beam Orientations and File Modifications .....	71
5.	DOMES ANALYSIS .....	74
5.1	Nonlinear Analysis Procedure .....	74
5.2	Proportional Limits and the Ultimate Stresses .....	76
5.3	Dome Cap Analysis.....	78
5.4	Effect of Shear Modulus on Dome Cap Model .....	79
5.5	Effect of Material Nonlinearity on the Dome Cap Behavior .....	87
5.6	Mesh Refinement Studies on the Dome Cap Model .....	93
5.7	Analysis of the Dome .....	97
5.8	Effect of Shear Modulus on the Dome Behavior .....	98

5.9 Effect of Material Nonlinearity on the Behavior of the Dome Models....	
.....	102
5.10 Mesh Refinement Studies of the Dome Model .....	107
6. CONCLUSIONS AND RECOMMENDATIONS .....	113
6.1 Conclusions.....	113
6.2 Recommendations .....	115
REFERENCES .....	117
APPENDIX A .....	121
APPENDIX B .....	125
VITA .....	144

## LIST OF ILLUSTRATIONS

Figure 2.1: Compression stress-strain curve .....	10
Figure 2.2: Tension stress-strain curve .....	13
Figure 2.3: Strain-strain curve for wood .....	15
Figure 3.1: (a) Cantilever beam model; (b) Elastic-plastic stress-strain law .....	25
Figure 3.2: Load deflection curves for user material and plastic option .....	27
Figure 3.3: Load deflection curves for the mesh refinement studies .....	30
Figure 3.4: Load deflection curves for beams in the selective mesh refinement studies .....	33
Figure 3.5: Original and modified stress-strain graphs for steel; (a) curve I; (b) curve II; (c) curve III .....	36
Figure 3.6: Load deflection curves for beams with different stress strain curves.	37
Figure 3.7: Load deflection curves for beams with different number of integration points .....	39
Figure 3.8: Hollow cantilever column .....	41
Figure 3.9: Stress-strain graph for the column .....	43
Figure 3.10: Load deflection curve for the column .....	44

Figure 3.11: Curved beam .....	46
Figure 3.12: Load deflection curve for the curved beam .....	48
Figure 4.1: Plan of the Triax dome .....	53
Figure 4.2: One sector of the dome .....	55
Figure 4.3: Dome model with refined mesh .....	57
Figure 4.4: Dome cap model .....	59
Figure 4.5: Dome cap with refined mesh .....	60
Figure 4.6: Dome model shown with the constraints .....	62
Figure 4.7: The types of stress strain curves used in the dome model .....	64
Figure 4.8: Beam orientations with respect to the spherical center .....	72
Figure 5.1: Dome cap with full snow load, response for different shear moduli...	83
Figure 5.2: Dome cap with half snow load, response for different shear moduli..	85
Figure 5.3: Dome cap nodes, original mesh .....	86
Figure 5.4: Dome cap with full snow load, response for different material laws..	89
Figure 5.5: Dome cap with half snow load, response for different material laws..	91
Figure 5.6: Dome cap mesh refinement studies, bilinear material law and half snow load .....	94
Figure 5.7: Dome cap mesh refinement studies, nonlinear material and half snow load .....	96
Figure 5.8: Dome with half snow load, effect of change in shear .....	99
Figure 5.9: Dome nodes, original mesh .....	100
Figure 5.10: Dome with full snow load, bilinear and nonlinear dome behavior....	103

Figure 5.11: Dome with half snow load, bilinear and nonlinear material behavior .....105

Figure 5.12: Dome with half snow load, mesh refinement studies, bilinear response .....108

Figure 5.13: Dome with half snow load, mesh refinement studies, nonlinear response .....109

Figure 5.14: Stress and strains at the limit point for the dome with refined mesh .....111

**LIST OF TABLES**

Table 5.1: Proportional limit and ultimate stresses for linear material law.....77

Table 5.2: Proportional limits and ultimate stresses for nonlinear material law .78

Table 5.3: Range of values for shear modulus .....80

## CHAPTER 1

# INTRODUCTION

The purpose of the present study is to incorporate a nonlinear material law for wood in the finite element program ABAQUS to develop effective finite element models of glulam domes, and to investigate the nonlinear buckling behavior of glulam domes using this finite element program.

A nonlinear material law of wood is incorporated by adding a user coded subroutine to ABAQUS. The subroutine is based on the mathematical model developed by Conners (1989) for the nonlinear constitutive behavior of wood. The mathematical model is obtained by simplifying the nonlinear stress-strain curve for wood by dividing it into several segments. Each segment is represented by a polynomial equation. In the discussion that follows, the term nonlinear behavior means the behavior of a structure with a nonlinear stress strain law.

The user coding option, the nonlinear material modelling procedure, and the

factors affecting the nonlinear behavior of beams and columns in ABAQUS analysis have to be thoroughly tested prior to their use in the analyses of any complex structure. As there are few analytical studies on the nonlinear behavior of wooden structures, a more commonly studied nonlinear material law for steel is used to gain experience and confidence in using ABAQUS by comparing the analysis results with the published data. The four steps given below are used to evaluate the material modelling capabilities of ABAQUS:

1. Testing of user subroutine option.

This is tested to determine if the user-coding option models a given material law correctly. In order to accomplish this, the elastic-plastic material law of steel is modelled using (a) the plastic option from the library of material models in ABAQUS; and (b) by the user-coding option in ABAQUS. A cantilever beam is assigned the material law using the two options. The results from the two analyses are then compared to see if the user-coding option is identical to the plastic option in ABAQUS for a given material law.

2. Testing of a cantilever in bending.

Finite element analyses of steel cantilever beams with nonlinear material law are carried out. Analysis runs are made for different mesh sizes, number of integration points, and modifications of the stress-strain curve. The results are compared with the continuum solution (Smith and Sidebottom, 1965).

### 3. Testing a cantilever column under combined bending and axial force.

Finite element analysis results for a pipe cantilever steel column are compared with experimental results presented by McGowan (1991).

### 4. Testing the torsional behavior.

A wooden cantilever beam with direct torsion, and a curved aluminum cantilever beam under bending and torsion are analysed to check the modelling of torsional properties in the user subroutine, and to evaluate the shear modulus computed by ABAQUS in the two cases. The results are compared with hand computations and with results by Jau (1985), respectively. The shear modulus used by ABAQUS in the analysis is thus evaluated and compared with the values assumed by Wu (1991), Tissaoui (1991), and Davalos (1989).

On completing the testing of user subroutine, a triax dome built in Raleigh, North Carolina, is modelled to study the material nonlinear buckling behavior of domes. Prior studies of elastic buckling behavior of this dome model have been conducted by Davalos (1991), Wu (1991), and by Holzer, Wu, and Tissaoui (1991). It was found from the previous studies that the maximum stresses in the dome members at the limit point were beyond the ultimate stresses ( Wu, 1991; Tissaoui, 1991; Holzer, Wu, and Tissaoui, 1991), and hence the assumption of linear elastic behavior had to be revised to include the nonlinear material law of wood.

Two types of dome models are created, based on the triax dome at Raliegh, N.C.

The first is of the dome cap model and the other is a complete dome model. The dome cap model consists of only the top ring of the complete dome. This model is created because it is much more economical to analyse in terms of computer time. Due to its smaller size, extensive testing of this model is possible. Also, since it is part of the complete dome, its behavior will be similar to that of the complete dome. Thus, potential modelling and analysis problems can be identified before analysis of the complete dome.

The dome models are created graphically using I-DEAS, which is a finite element program with excellent graphical capabilities. I-DEAS has the option for writing an input file for ABAQUS from the graphical model. The input file as obtained from I-DEAS is modified to include beam orientations and the nonlinear material law.

In the dome model, 2 noded straight beam elements are used. The tension ring, the purlins, and the bracing are modelled with truss elements. The truss bracing is used to model the bracing effect of the decking (Wu, 1991; Tissaoui, 1991; Holzer, Wu, and Tissaoui, 1991). The purlins are modelled as truss elements to minimize the degrees of freedom at the two ends and to represent the pinned connection of the beam-purlin joints (Wu, 1991).

Two load cases are considered. One is the symmetric load case of dead load and snow load over the complete dome (Full snow load). The other is dead load and

snow load over only half the dome (Half snow load). Studies by Wu (1991) show that for the half snow load case, the stresses in the dome members at failure are beyond the ultimate stresses. Hence this load case would be ideal to test the nonlinear buckling behavior of the dome, as the maximum stresses in this case would be in the nonlinear region of the stress strain curve. Also, the full and half snow load cases would allow the study of nonlinear dome behavior under cyclically symmetric and cyclically unsymmetric loading respectively. The uniformly distributed loads are discretized to the nodal loads by using shell elements (Wu, 1991; Tissaoui, 1991; Holzer, Wu, and Tissaoui, 1991).

In all, 13 dome cap models and 8 complete dome models are analysed. These models are obtained by changing the loading, the material law, and the mesh configuration. The results from the analyses of these models are used to:

1. compare the behavior of a dome with linear and nonlinear material laws.
2. determine the effect of the shear modulus on the predicted dome behavior.
3. determine the effect of two different loadings on the predicted dome behavior.
4. determine the effect of mesh refinement on the predicted dome behavior.

Equilibrium paths, critical loads, and maximum stresses at failure are presented in the study. Based on the present research, conclusions are presented and recommendations are made as to further study of glulam domes.

## CHAPTER 2

# MATERIAL MODEL

The studies conducted in the past on glulam triax domes (Holzer, Wu, and Tissaoui, 1991; Wu, 1991) indicate that the material properties of wood beyond the proportional limit must be incorporated in the model to determine the ultimate load capacity of the dome. In order to incorporate the material response of wood beyond the proportional limit, a segmented model suggested by Conners (1989) is chosen.

In this chapter, an attempt is made to explain:

- the material behavior of wood;
- the mathematical representation of this behavior;
- the incorporation of this nonlinear material law in the finite element program ABAQUS.

## 2.1 Material Behavior of Wood

Studies on the constitutive behavior of wood (Conners, 1989; Conners, 1985; Dietz, 1942) have indicated that wood has a nonlinear stress strain law, where the behavior in tension is considerably different from that in compression. This different behavior in tension and compression is explained on the basis of the cellular structure of wood (Davalos, 1989).

Wood is a biological material; it is made up of bundles of wood cells forming cylindrical tubes parallel to the axis of the tree. These parallel oriented bundles of wood cells or wood fibers are also called the grain of the wood. When compressed along the grain, these cylindrical tubes can buckle and be crushed. Consequently, wood has lesser strength in compression than in tension. The buckling and crushing of the wood fibres is depicted by the horizontal portion in the compression stress-strain curve of wood. In tension, wood can withstand higher stresses along the grain, and it does not show a marked horizontal yielding zone in the stress-strain curve.

The compressive strength parallel to the grain of wood is found to be about half of its tensile strength in a direction parallel to its grain, and the tensile strength

normal to the grain is about  $1/20^{th}$  of the tensile strength parallel to the grain (Davalos, 1989). Although wood is anisotropic in its behavior, it is modelled as transversely isotropic (Davalos, 1989). In this study, the material behavior in tension and compression parallel to grain is defined by a nonlinear uniaxial stress strain law, while the torsional behavior is described by a linear stress-strain law.

The model proposed by Connors (1989) is used to model the nonlinear bending and axial behavior of wood. The discussion which follow is primarily based on the paper by Connors (1989).

## **2.2 The Material Model**

The constitutive model proposed by Connors (1989) is represented by a curve composed of two segments for the tensile zone, and by three individual segments in the compression zone. Each segment is defined by a different mathematical equation. The mathematical equations which define the curve are based on nonlinear regression analyses of experimental stress strain data conducted by Connors (1989). The data is obtained for yellow poplar specimens with varying moisture contents and specific gravity. The mathematical equations and the

parameters used in these equations are described below in detail.

### 2.2.1. Compression Zone

The compression zone of the curve is modelled by three segments as shown in Fig.2.1. The first segment is linear from the origin to the strain point  $K_{1(compression)}$ . The second segment is nonlinear in the strain range from  $K_{1(compression)}$  to  $K_{2(compression)}$ . The third segment is linear and horizontal, implying a plastic behavior of the material beyond the strain value of  $K_{2(compression)}$ . The equations for the three segments of the curve are given below (Connors, 1989):

For the initial linear segment,

$$\sigma = \beta_1 \epsilon \quad (2.1)$$

$\beta_1$  is the longitudinal Young's modulus in compression.

For the second parabolic segment,

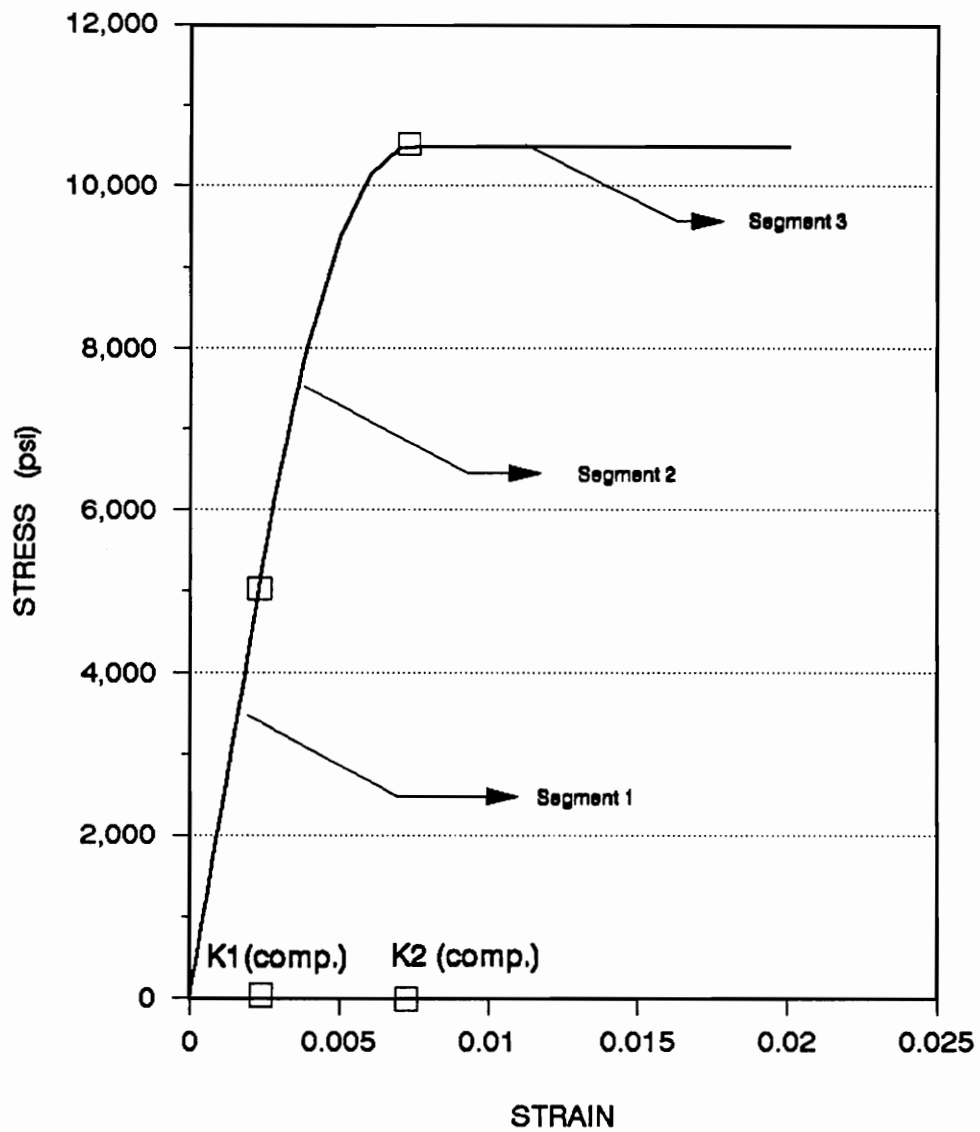


**Fig.2.1 COMPRESSION STRESS STRAIN CURVE**

$$\sigma = \alpha_1 + \beta_2 \epsilon + \beta_3 \epsilon^2 \quad (2.2)$$

For the third horizontal segment,

$$\sigma = \alpha_2 + \beta_4 \epsilon \quad (2.3)$$

By imposing continuity at  $K_{1(\text{compression})}$  and  $K_{2(\text{compression})}$ , and solving simultaneously Eqs. (2.1) through (2.3), the values for the constants are obtained:

$$\alpha_1 = \beta_3 K_1^2 \quad (2.4)$$

$$K_{1(\text{compression})} = (\beta_1 - \beta_2) / 2\beta_3 \quad (2.5)$$

$$\alpha_2 = \beta_3 (K_1^2 - K_2^2) \quad (2.6)$$

$$K_{2(\text{compression})} = (\beta_4 - \beta_2) / 2\beta_3 \quad (2.7)$$

The compression stress strain curve beyond the point  $K_{2(\text{compression})}$  is replaced by a straight horizontal line (zero slope). Therefore in Eq. (2.3),  $\sigma$  must have a constant value, which is obtained by making  $\beta_4$  equal to zero. The values of  $\beta_1$ ,  $\beta_2$ , and  $\beta_3$  are obtained from equations given below (Connors, 1989):

$$\beta_1 = 143900 + 441996(\text{MC}\%) - 28997(\text{MC}\%)^2 + 534(\text{MC}\%)^3 \quad (2.8)$$

$$\beta_2 = 5719340 - 258850(\text{MC}\%) + 4280(\text{MC}\%)^2 \quad (2.9)$$

$$\beta_3 = -1065588500 + 3449729(\text{MC}\%) + 1540914880(\text{SG}) \quad (2.10)$$

where

MC% = Percentage moisture content

SG = Specific gravity, based on oven-dry weight and green volume

### 2.2.2. Tension Zone

The tension zone of the stress strain curve is modelled by two segments as shown in Fig.2.2. The stress strain curve is linear from the origin to a strain value  $K_{1(tension)}$ , and is represented by the first segment. Beyond  $K_{1(tension)}$ , the curve is represented by the nonlinear second segment. The equations of the two segments of the curve are given below (Connors, 1989). Even though the nomenclature used here for the equations is the same as before, the values for the various constants are distinctly different than those used for the compression zone.

For the first segment,

$$\sigma = \beta_1^T \epsilon \quad (2.11)$$

For the second segment,

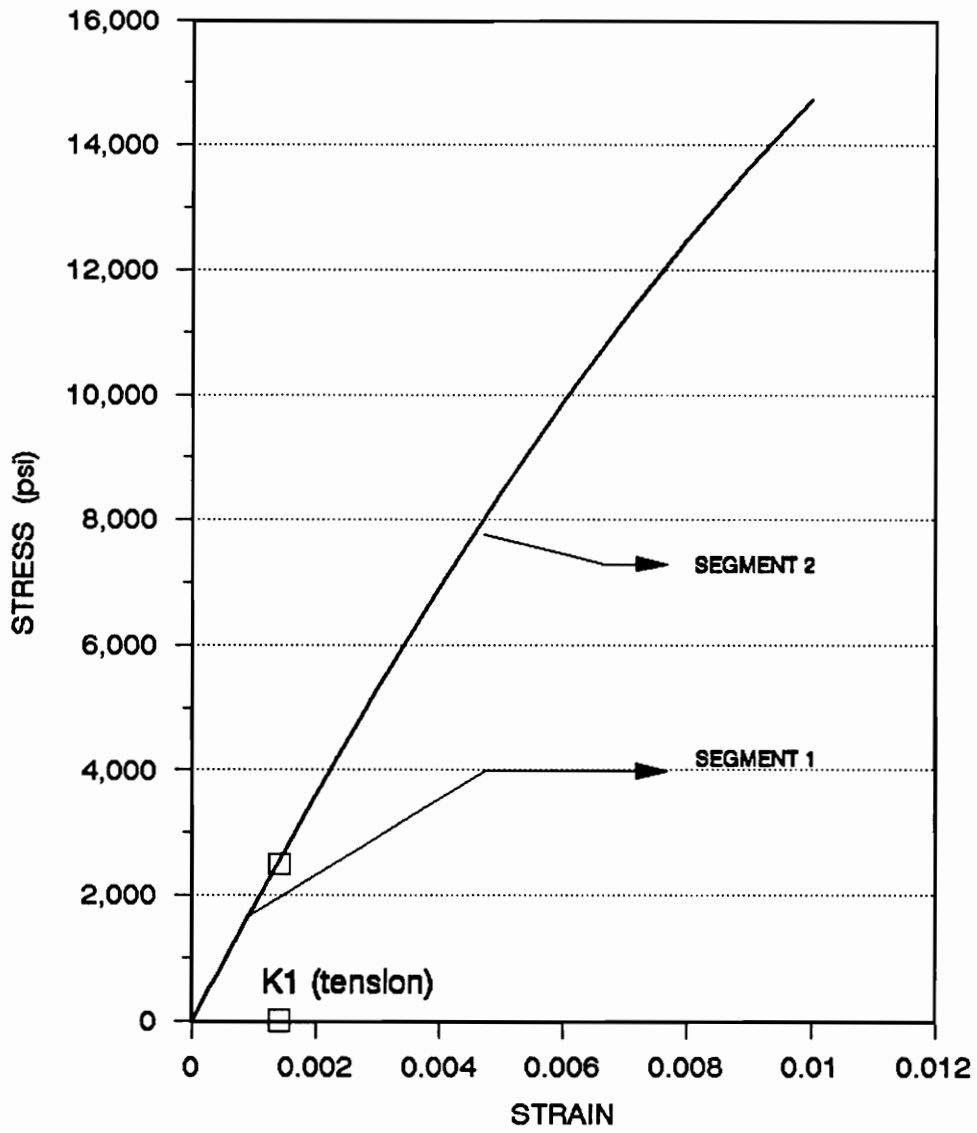


**Fig.2.2 TENSION STRESS STRAIN CURVE**

$$\sigma = \alpha_1^T + \beta_2^T \epsilon + \beta_3^T \epsilon^2 \quad (2.12)$$

$\beta_1^T$  is the longitudinal Young's modulus in tension.

$$\left( \frac{\partial \sigma}{\partial \epsilon} \right) \text{ same at } K_1$$

By imposing continuity at  $K_{1(tension)}$ , and solving simultaneously Eqs. (2.11) and (2.12), the values for the constants are obtained:

$$\alpha_1 = \beta_3^T K_1^2 \quad (2.13)$$

$$K_{1(tension)} = (\beta_1^T - \beta_2^T) / 2 \beta_3^T \quad (2.14)$$

The values for  $\beta_1^T$ ,  $\beta_2^T$ , and  $\beta_3^T$  for the tension zone are obtained from the equations given below (Connors, 1989):

$$\beta_1^T = 1822300 - 9.8(MC\%)^2 \quad (2.15)$$

$$\beta_2^T = 1934700 \quad (2.16)$$

$$\beta_3^T = 37045400 - 2204(MC\%)^3 - 150737800(SG) \quad (2.17)$$

where

MC% = Percentage moisture content

SG = Specific gravity, based on oven-dry weight and green volume

The equations presented above give a stress strain curve which matches reasonably

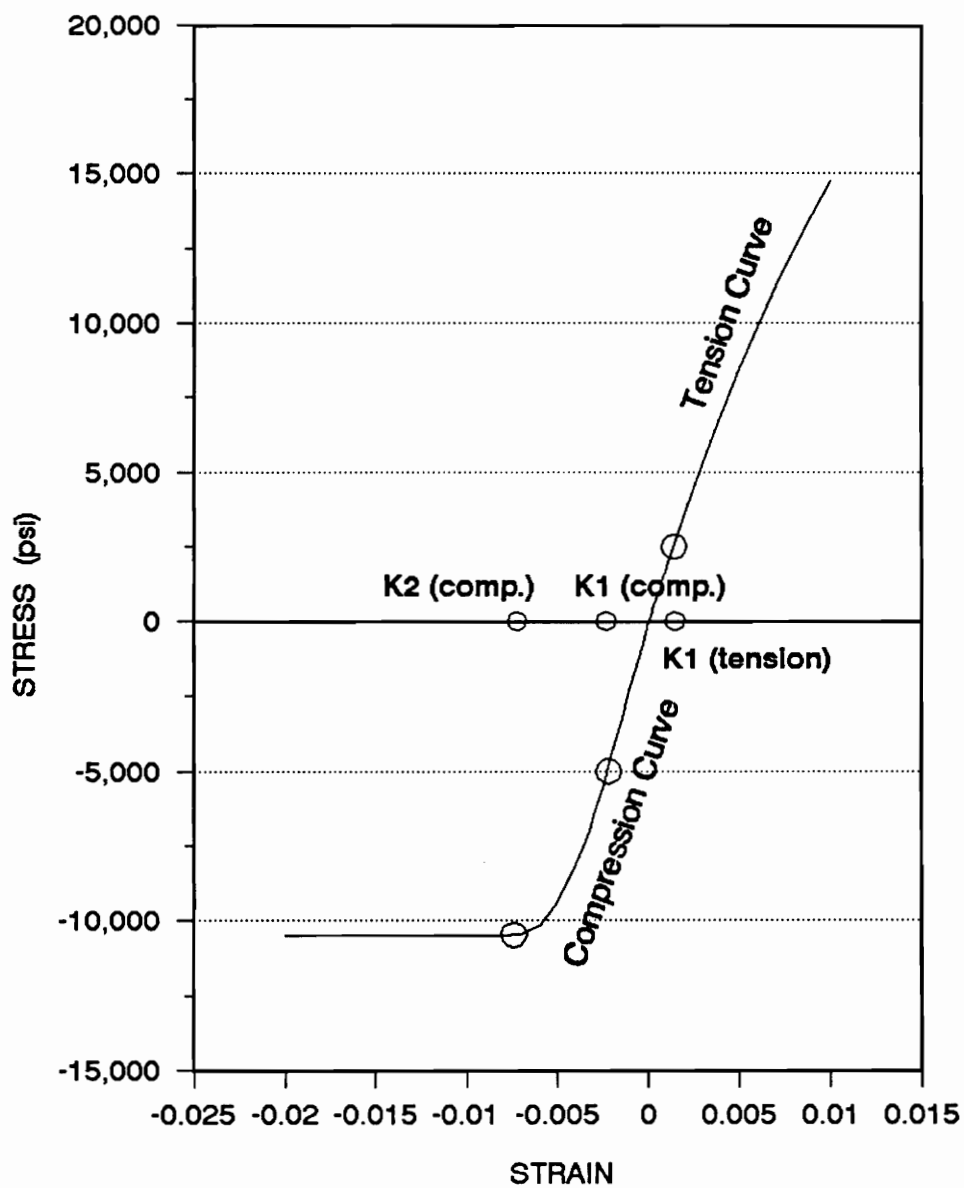


**Fig2.3 STRESS-STRAIN CURVE FOR WOOD**

well with the experimental data (Connors, 1989). In the above equations, both the tension and the compression equations use positive values for stresses and strains. In order to implement these equations in a finite element program, the compression equations are slightly modified so that they can work for a negative values of stresses and strains. The resulting stress strain curve is presented in Fig. 2.3.

### 2.3 ABAQUS Material Library

In ABAQUS, the material behavior of a structure can be defined by using one of the thirteen options available in the library of material models. Out of these thirteen model options, only three showed any potential for modelling the selected stress strain curve. The three options are:

1. Plastic
2. Hypoelastic
3. User Material

From the three options, the plastic and the hypoelastic options are the easiest to use. Although both of these options can be used to model a nonlinear material

law, they can not model a stress strain law which is different in tension and compression. While using these two options, only positive values for stresses and strains can be entered in the input file to define the curve. The program then uses the same values to define the curve in the tension and the compression regions.

The only remaining option is the user material option, which allows one to model any material behavior through a user coded FORTRAN subroutine. Thus, this option is used for defining the segmented stress strain law adopted for this study.

## 2.4 User Material Option

The user material option is a powerful tool to model material behavior not supported by the existing material models in the ABAQUS library. The material model is defined through a FORTRAN subroutine written in the input file. The option is activated by using the following set of commands in the input file:

```
*MATERIAL, NAME=WOOD
*USER MATERIAL, CONSTANTS=3
12, 0.52, 1.6E5
```

The value of the "constants" parameter can be changed to the number of constants required in the FORTRAN program. In the present program, three constants are needed to define the stress strain curve. These are: 1) the moisture content; 2) the specific gravity; and 3) the shear modulus. These constants are entered in the given order after the user material command.

The user coded FORTRAN subroutine is entered at the end of the input file. The last end step command in the input file is followed by the command \*USER SUBROUTINE, and the fortran code for the user subroutine is entered after this command. A complete input file for a triax dome along with the user subroutine is given in Appendix B.

When using beam and shell elements in combination with user material, the transverse shear stiffness for the section must also be provided. The value for the transverse shear stiffness is entered along with the other section properties of the beam section. The set of commands to describe the section properties and the transverse shear stiffness is given below:

\*\*Beam section dimensions are in inches.

\*BEAM SECTION, SECTION=RECT , ELSET=E1, MATERIAL=WOOD

6.75, 11.0

0.0993545, 0.9993732, -0.1324533

\*TRANSVERSE SHEAR STIFFNESS

10097800.54 , 10097800.54

The line with two stars is a comment line. The following line defines the element set with number E1 to have a rectangular beam section, and the material property identified by the name wood. In the next line is given the cross section of the beam followed by the direction cosines. The transverse shear stiffness command is given immediately following the direction cosines, and it is followed by the values for transverse shear stiffnesses in the two directions of the beam cross section. For a beam section, both of these values must be the same. The transverse shear stiffness for a beam element are computed from the equations given below (ABAQUS, 1991):

$$\text{Transverse shear stiffness} = f_p K_{\alpha 3} \quad (2.18)$$

where

$$K_{\alpha 3} = k G A \quad (2.19)$$

$$f_p = \frac{1}{(1 + 0.25 \times 10^{-4} \times \frac{l^2 A}{12 I})} \quad (2.20)$$

The value of k for a rectangular section is 0.85 and

$$\begin{aligned} G &= \text{Shear modulus} \\ &= \frac{E}{2(1 + \nu)} \end{aligned} \quad (2.21)$$

where

E = Young's Modulus

$\nu$  = Poisson's ratio

$A$  = area of cross section

$l$  = span of the beam

$I$  = minimum of the moment of inertia of the section

in the two principal cross sectional directions of the beam

The B33 beam used in the Triax dome does not model shear deformations, and thus does not require the value of transverse shear stiffness for any computational purpose. Even though this is the case, the ABAQUS run is terminated in the preprogram stage if this value is not provided. Hence a dummy value for the transverse shear stiffness must be provided if a B33 beam section is used along with user defined material property.

## 2.5 The User Subroutine

The fortran code for the material model is written in the subroutine UMAT. UMAT is called by ABAQUS at each material calculation point for which the material behavior is defined by the user material option. Each time the subroutine is called, it is provided with the state of the material in terms of stresses and

strains at the start of the increment. Using the values of stresses, strains and strain increments at the start of an increment, the subroutine has to perform the following two functions:

- update the stresses to those at the end of an increment
- provide the material Jacobian matrix for the constitutive model

The Jacobian matrix of the constitutive model is denoted as  $\frac{\partial \delta \sigma}{\partial \delta \epsilon}$  (ABAQUS 4.6 Users Manual, 1990), where  $\delta \sigma$  are the stress increments and  $\delta \epsilon$  are the strain increments. This matrix defines the change in the stress due to an infinitesimal change in the strain at the beginning of the time increment. The stresses at the end of an increment are determined by computing the stress increments from the strain increments, and adding those to the stresses at the beginning of the increment.

The B33 element is based on the Euler-Bernoulli beam theory, and as such is assumed to have axial (longitudinal) strains and torsional shear only (ABAQUS, 1991). These elements are also assumed not to warp out of their plane. Due to these assumptions, the Jacobian for B33 element is a 2-dimensional, diagonal matrix. The Jacobian matrix can be represented as:

$$J = \begin{bmatrix} J_{11} & 0 \\ 0 & J_{22} \end{bmatrix} \quad (2.22)$$

The first component of the Jacobian matrix,  $J_{11}$ , is the change in axial stress with infinitesimal change in axial strain, or in other words, the slope of the incremental stress strain curve. The second component,  $J_{22}$ , is the change in the torsional shear stress with infinitesimal change in torsional shear strain. In the present case, the torsional behavior of wood is linear. Hence the  $J_{22}$  is a constant, and is the shear modulus for wood. The value for the shear modulus is  $1.6 \times 10^5$  psi (Wu, 1991, Tissaoui, 1991).

The code for the subroutine UMAT which models the selected stress strain law of wood is presented in the Appendix B. The description of the variables and used in the FORTRAN code can be readily obtained from the ABAQUS user's manual (ABAQUS 4.6 User's Manual, pp. 8.18.1-1 to 8.18.1-9).

The user coded subroutine and the nonlinear material procedure has to be thoroughly tested prior to its use in the analyses of any complex structure. The results of this thorough and extensive testing are presented in the next chapter, along with recommendations on the finite element modelling of structures with material nonlinearity.

## CHAPTER 3

# VERIFICATION OF THE MATERIAL MODEL

The selection of a constitutive law for wood and its representation in ABAQUS as a material model was discussed in chapter 2. In this chapter, the results of materially nonlinear finite element analyses conducted on cantilever beams, and cantilever columns are presented.

In order to verify the analysis results, a comparative study has to be performed between the ABAQUS results and the numerical or continuum solutions found in the literature. As no numerical studies on the nonlinear material behavior of wooden structures are found in the literature, the ABAQUS material modelling capabilities are verified by modelling the nonlinear material law for steel.

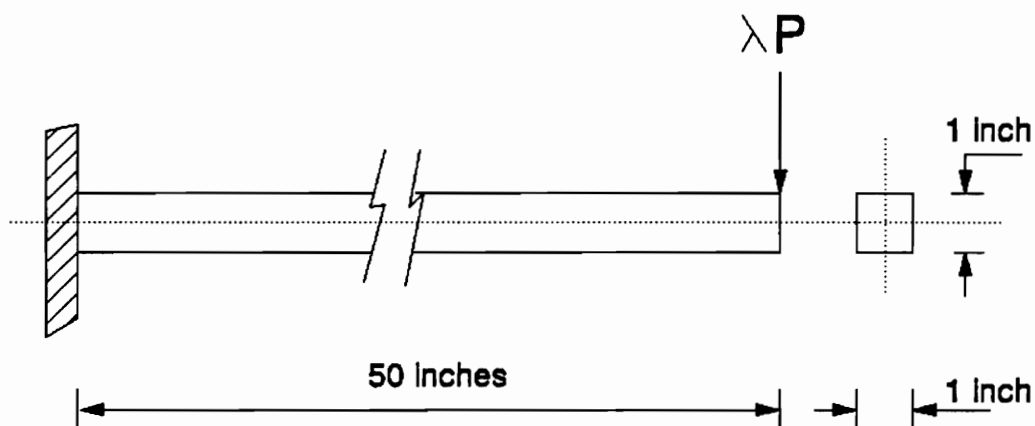
A two step approach is followed in the testing procedure. In the first step, the analysis results using the user subroutine option are compared with those using the plastic option. The plastic option is found in the ABAQUS library of material models.

In the second step, the factors affecting the analysis results for finite element analysis of simple structures with nonlinear material behavior are determined. Numerous ABAQUS runs are conducted on cantilever beams and columns which have nonlinear material behavior, with various mesh sizes, number of integration points, and the shape of the stress strain curves. Even though most of the analysis results discussed in this chapter are for steel beams and columns, they give a good background for understanding the factors influencing the accuracy of results for finite element analysis of wooden structures with nonlinear material behavior. The nonlinear Riks procedure in ABAQUS is used throughout the following analyses.

### **3.1 Testing of User Subroutine Option**

A cantilever beam as shown in Fig.3.1 is analysed using ABAQUS. Two models of the beam are analysed. Both have the elastic-perfectly plastic material property of steel. In the first model, the material law is assigned to the cantilever beam by using the user material option, while in the second model it is assigned using the plastic option from the ABAQUS library of materials.

The geometric and material properties of this beam are given below:



**(a) CANTILEVER BEAM MODEL**

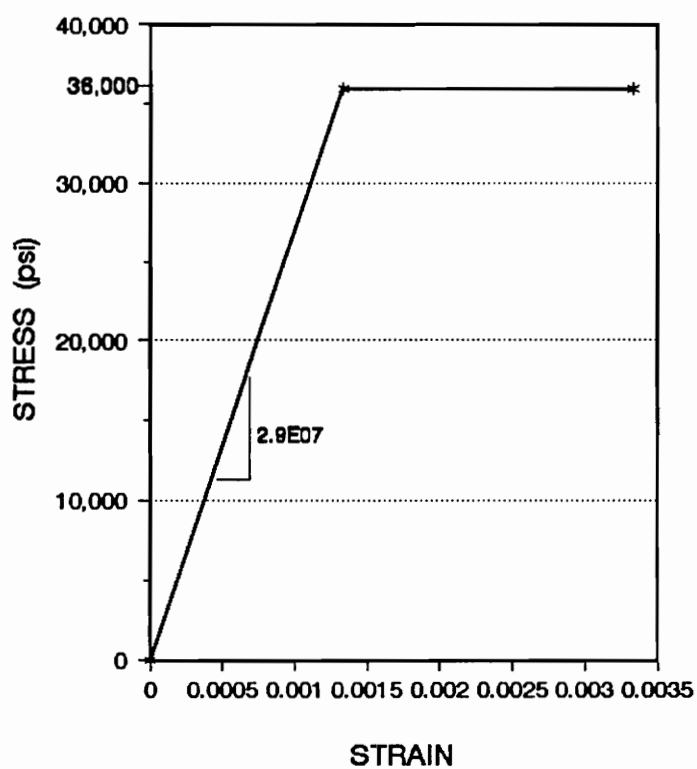


**FIG.3.1 (b) ELASTIC-PLASTIC STRESS-STRAIN LAW**

Span	: 50 inches
Cross-section	: 1x1 inches
Modulus of Elasticity	: $2.9 \times 10^7$ psi
Proportional Limit	: 36000 psi

The beams are modelled using two node space beam elements, denoted as B33 in the ABAQUS library of elements. As the effect of mesh refinement is not studied here, only one element is used for modelling the cantilever beam. Loading is in the form of point load applied at the tip of the cantilever.

The load factor versus the tip deflection curves of the beams are shown in Fig.3.2. It is observed that the curves for both the models are coincident. Thus, the user subroutine option gives exactly the same results as the plastic option.

Assuming that the plastic option from the ABAQUS library of materials correctly models the nonlinear material behavior, it can be safely stated that the user material option also models correctly the nonlinear material behavior for a given material for which a constitutive law is given. These analyses thus confirm that the user subroutine option works correctly, and gives a sound basis for coding the more complicated stress-strain law for wood using the user subroutine option.

### 3.2 Sensitivity Analyses and Accuracy Studies

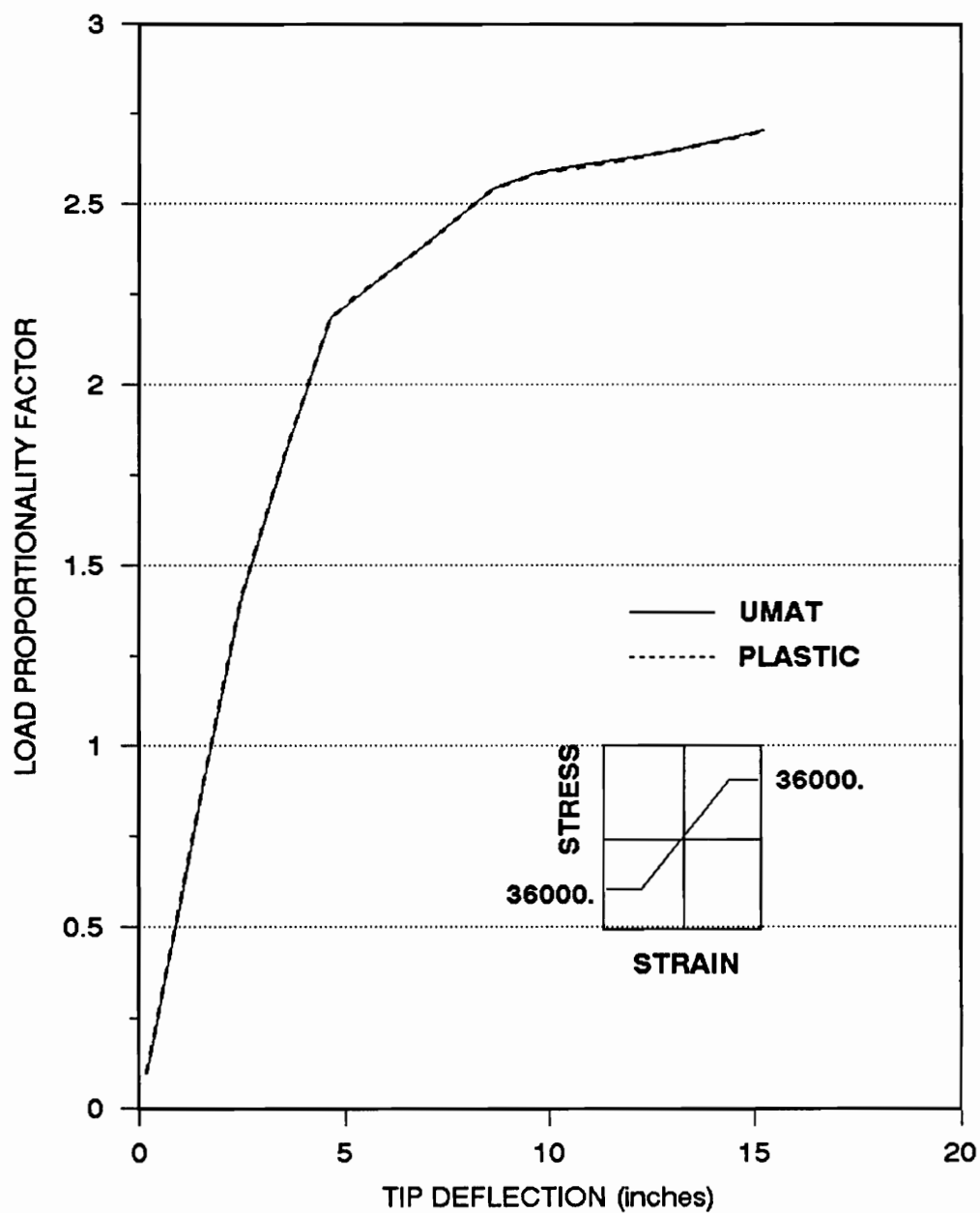


**Fig.3.2 LOAD DEFLECTION CURVES FOR  
USER MATERIAL AND PLASTIC OPTION**

A series of analysis runs are made with ABAQUS to study the sensitivity of the ABAQUS results to the following factors:

- The mesh size
- Selective mesh refinement, or the provision of hinge elements
- The shape of the stress-strain curve
- The magnitude of load increments in the Riks analysis
- The number of integration points in the cross-section

The study, taking into consideration the above points, is conducted in two parts. In the first part, a cantilever beam is analysed for the accuracy of its bending response under a point load applied at the tip. In the second part, a cantilever column is studied for the accuracy of its response under the action of a combined axial force and bending moment. For the cantilever column, the effect of imperfections is also included in the analysis.

### **3.3 Tests on The Cantilever Beam**

The same cantilever beam used in Section 3.2 is analysed in these studies. The material properties for most of the beam models are also the same as those given in Section 3.2. The material properties that are modified are explained in detail

while discussing those tests or beam models.

### **3.3.1. Effect of Uniform Mesh Refinement**

In the first set of analyses, three beam models with uniform mesh refinement are analysed. The response of the beams are compared with the continuum solution (Smith, and Sidebottom, 1965). The three beam models have meshes made up of 1, 5, and 10 elements, respectively. Load factor versus the tip deflection curves are shown in Fig.3.3.

The load deflection curve for the beam model with only one element shows a very stiff response, and it does not model accurately the nonlinear bending behavior of the cantilever. The model with 5 elements gives a much softer response which is closer to the continuum solution (Smith, and Sidebottom, 1965). The plastic failure load in this case is 191.8 pounds as compared to 180 pounds in the continuum analysis, an error of 6.5%. The beam model with a 10-element mesh gives the response closest to that of the continuum solution. The failure load in this case is 186.8 pounds, giving an error of only 4%.

From the above set of analyses, it can be concluded that successive refinement of

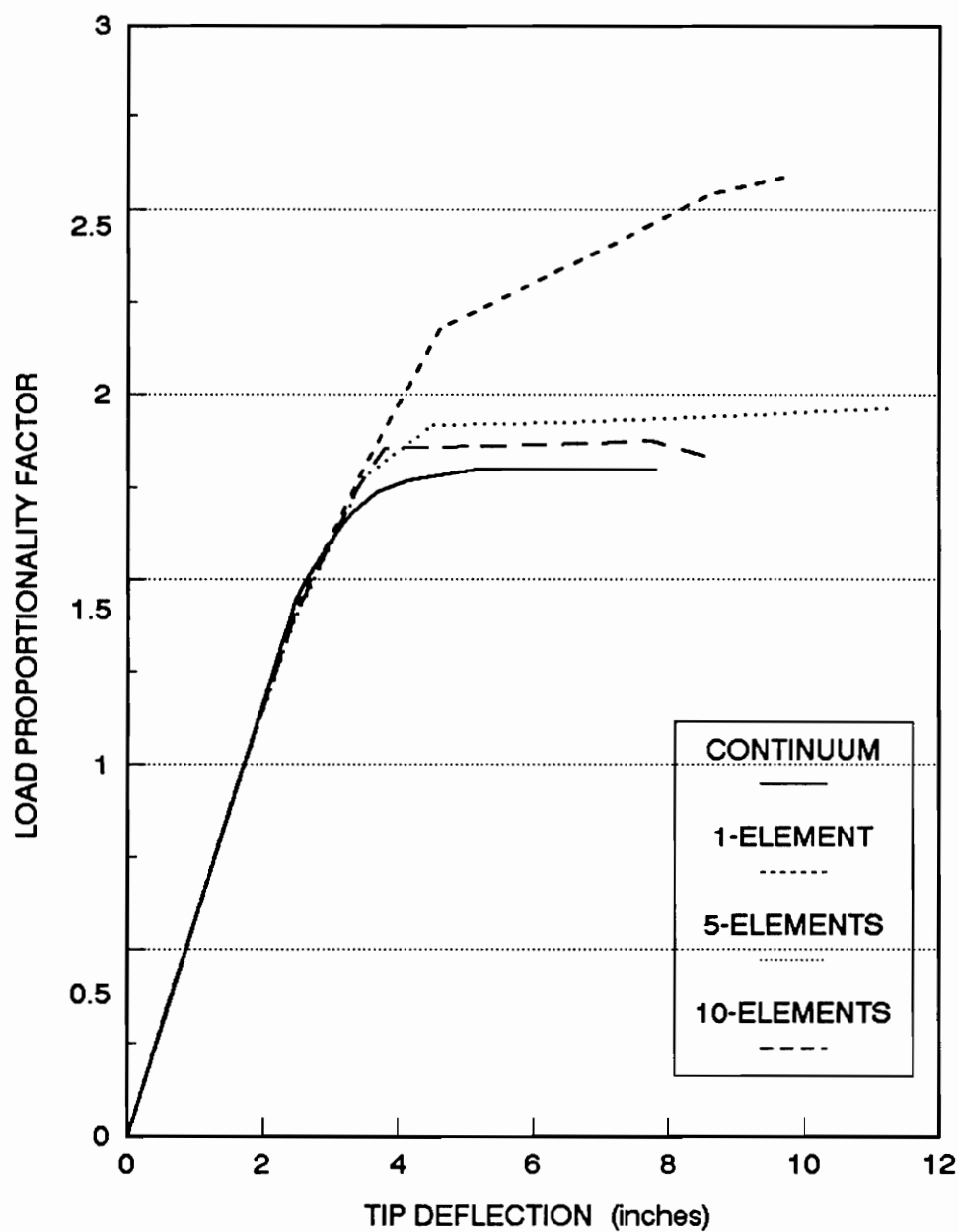


**Fig 3.3 LOAD DEFLECTION CURVES FOR THE  
FOR MESH REFINEMENT STUDIES**

the mesh would give more accurate results. Hence, the effect of mesh refinement on nonlinear material behavior of a structure is similar to that for elastic behavior.

For obtaining accurate results, an alternative approach of nonuniform mesh refinement is also tried. As the cost of analysis increases when the mesh is made finer, this alternative method would be more economical because it would require the mesh to be refined only at selected locations. Economy in terms of cost and time can become a big issue when analysing large structures. Hence the approach of selective mesh refinement looks more attractive than that of general mesh refinement, as it would save considerable time and money when analyzing large structures.

The method of selective mesh refinement is based on the plastic-hinge theory used in plastic analysis of steel structures. According to this theory, it is assumed that the structure behaves elastically until the proportional limit, and thereafter, the stresses at the critical section increase until the stresses at all the points on the section become equal to the yield stress. At this point, constant plastic moment is reached. This is idealised by the formation of a hinge, known as plastic hinge (Kaliszky, 1989), at the location of the maximum stress. Therefore, the method of selective mesh refinement consists of refining the mesh only at the location of maximum stresses, where a theoretical plastic hinge would be formed.

Two cantilever beam models are tested. Both beam models are made up of 2 elements. An element, one inch in length, is provided at the base of the cantilever

and the remaining part of the cantilever is modelled by the other. In the forgoing discussion, the one inch long element at the base of the cantilever is referred to as the hinge element.

In the first model, both elements are assigned the same elastic-plastic material property. In the second model, only the hinge element is assigned the elastic-plastic material property, whereas the other element is assigned a linear elastic material property. Out of these two runs, the second run is expected to be more efficient in terms of computing cost and time. This is because in the second model the program will have to conduct an iterative solution procedure for determining the material strength for only the hinge element, whereas in the first model, the iterative solution procedure will be required for both elements.

The load proportionality factor versus the tip deflection response for the two analysis runs are presented in the Fig.3.4, along with those for the continuum solution and the 10-element mesh. The two analyses runs with the hinge elements show very similar load deformation behavior. For the first model, the load deflection curve is linear till the yield load, becoming horizontal to indicate the plastic failure. For the second model, the load deflection curve becomes nonlinear before yielding, and is closer to the continuum response. The response of the cantilever beams with selective mesh refinement are softer than that for the 10-element mesh. Hence the selective refinement of the mesh seems to give better results than the general refinement of the mesh.

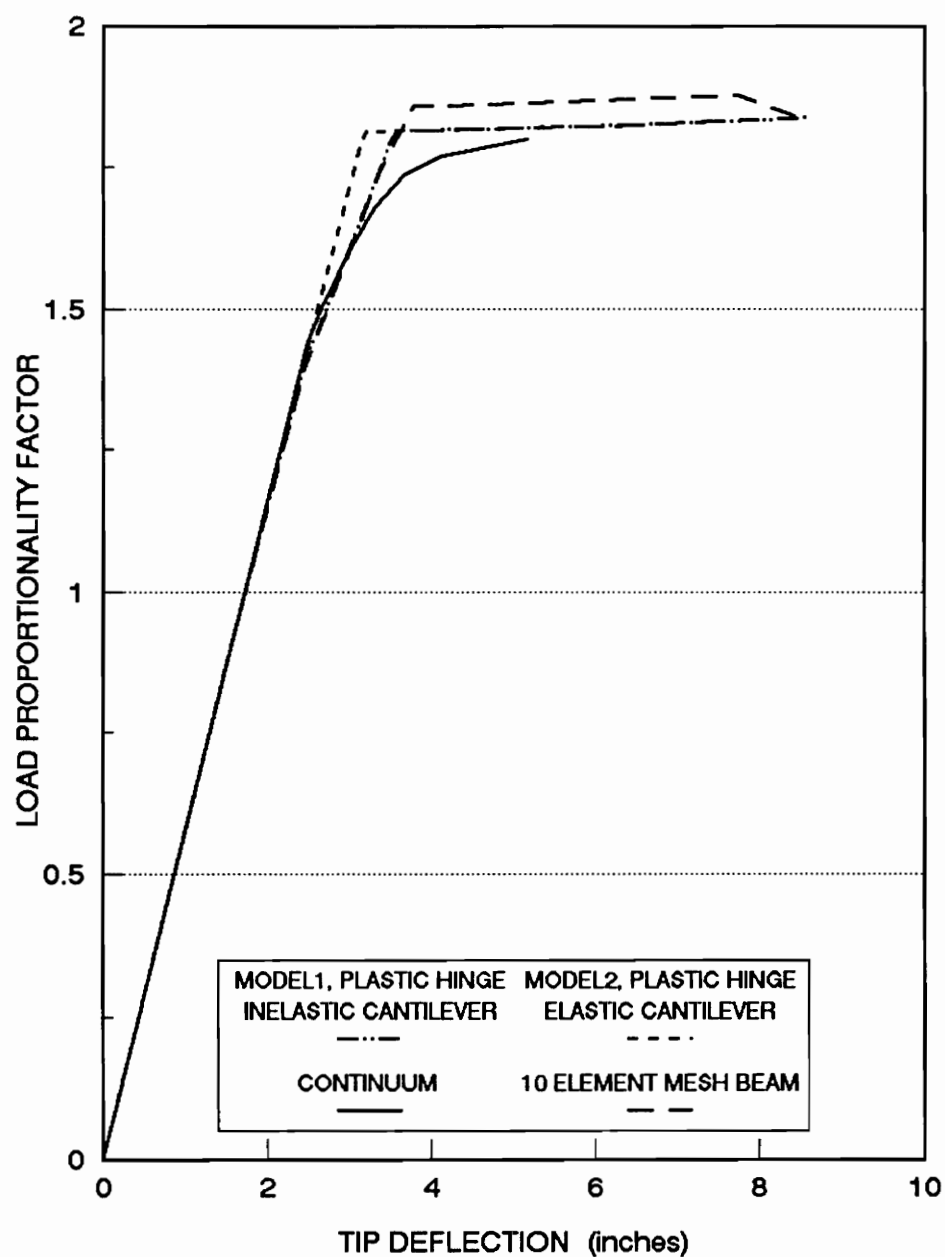


**Fig.3.4 LOAD DEFLECTION CURVES FOR BEAMS  
IN THE SELECTIVE MESH REFINEMENT STUDIES**

The plastic failure load obtained for the beams with hinge elements are 181 pounds, within 0.8% of the continuum solution (Smith, and Sidebottom, 1965). These failure load magnitudes are even better than the one obtained for the case of the 10-element mesh. Hence, providing hinge elements seems to be a very good method to obtain the most accurate as well as cost effective analysis results in a materially nonlinear analysis.

The method of providing a hinge element, though being very advantageous, has a drawback. In a large structure, it is very difficult to determine the location of critical sections by observation alone. To solve this problem, an initial approximate analysis must be carried out to determine the location of the critical sections. The skill of the structural engineer in deciding these critical sections is also very important. Although, to determine all the critical sections in a large structure, and to generate extra nodes and elements at these points is a formidable task, it has to be weighed against the accuracy of the solution and the savings in the cost of computing.

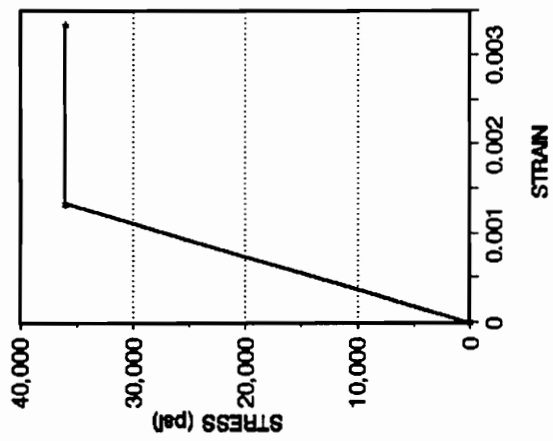
### **3.3.2. The Effect of Other Factors**

The sensitivity of ABAQUS solutions for its accuracy is further tested by varying

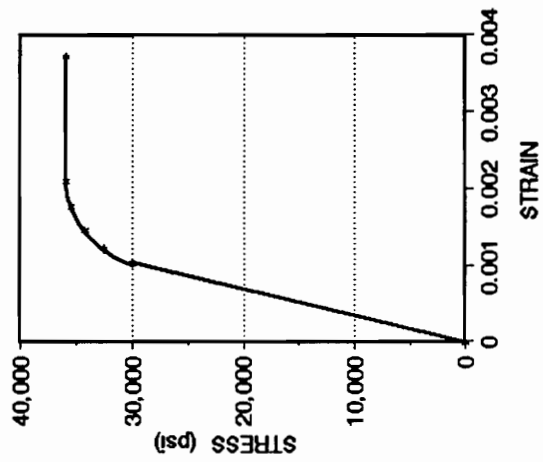
input parameters such as the smoothness of the stress strain curve, the number of integration points at a cross section, and the initial load increment in the Riks step. The results obtained by conducting a series of ABAQUS runs on the cantilever beam with a 5-element mesh are discussed below and are represented in graphical form for ease of comparison.

For this series of tests, the first parameter to be varied is the shape of the stress strain curve. Three different stress-strain curves are considered for modelling the material property of the cantilever, and are shown in Fig.3.5. All three curves have the same initial elasticity modulus and the same yield strength. The only difference between them is the shape of the transition curve between the initial linear portion and the plastic region of curve. The three graphs in Fig.3.5 indicate the increasing degree of smoothness of this transition curve.

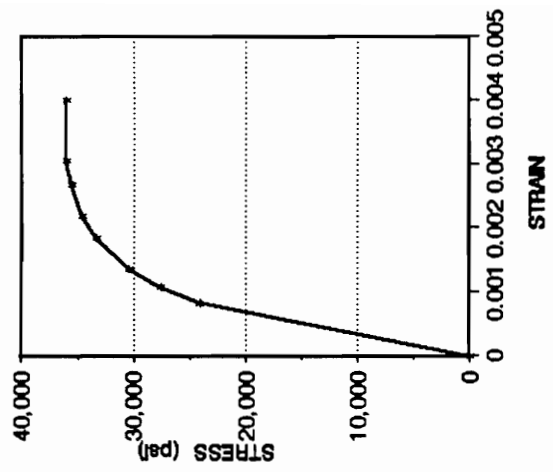
The results obtained from the analyses of the cantilever beams with the three stress strain laws do not show any considerable effect of the smoothness on their ultimate load. The final failure loads obtained in all three cases are nearly the same as observed from Fig.3.6. The shape of the stress strain curve, though, does affect the shape of the load deformation curve. When curve III from Fig.3.5 is used for the material, the load deformation response of the cantilever beam is smooth like that of the continuum case, whereas for the other two beams, the response is stiffer and is closer to the idealised elastic plastic response of a cantilever beam.



(a) CURVE I



(b) CURVE II



(c) CURVE III

FIG.3.5 ORIGINAL AND MODIFIED STRESS-STRAIN GRAPHS FOR STEEL

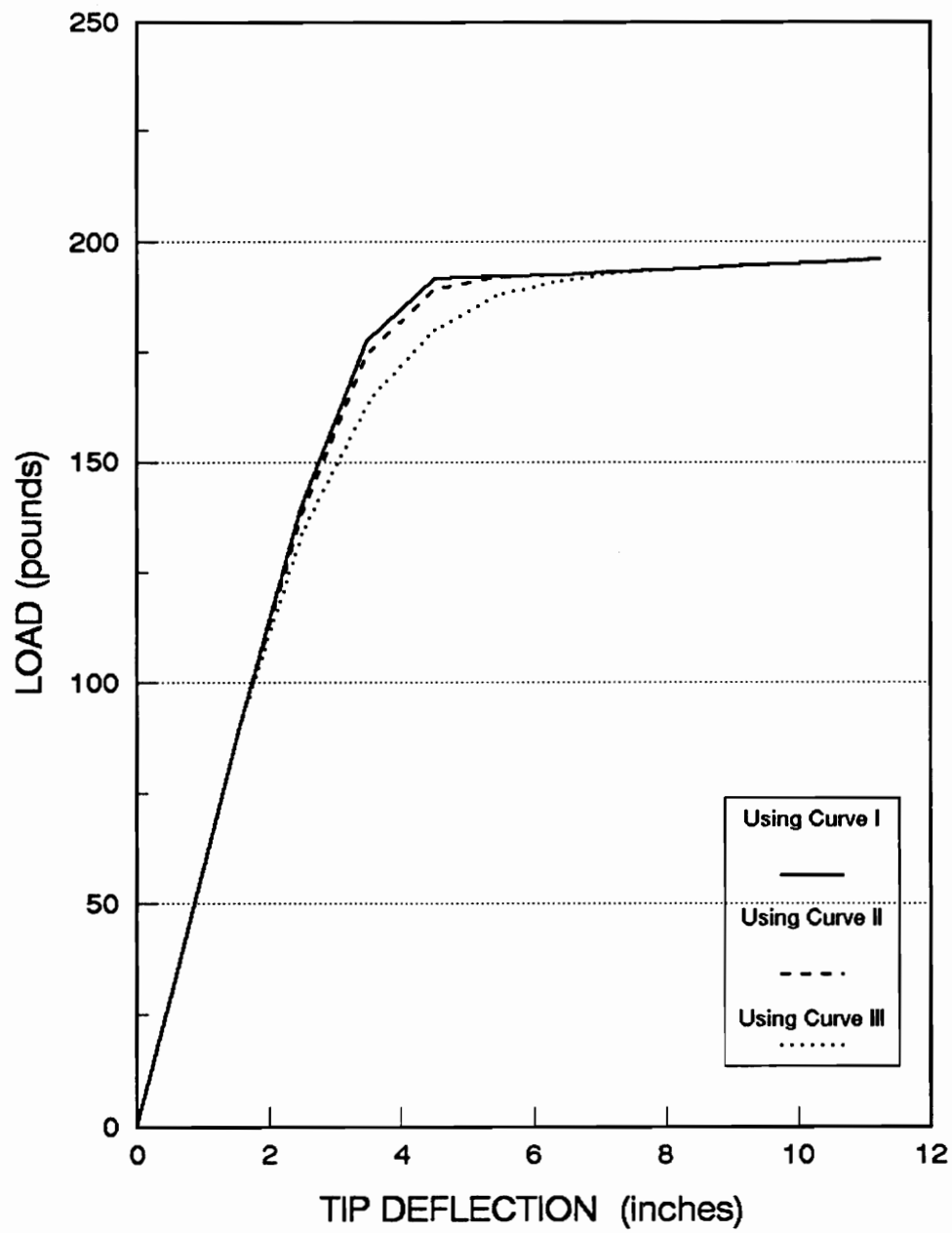


**FIG.3.6 LOAD DEFLECTION CURVES FOR BEAMS WITH  
DIFFERENT STRESS STRAIN CURVES**

The second parameter to be varied is the number of integration points across the depth of the beam cross section. The B33 beam has five integration points for the computation of mechanical and material behavior along its depth . The effect on the magnitude of the ultimate load and the accuracy of the load deformation response of the beam is studied by increasing the number integration points.

Two cantilever beam models are considered. The first model is same as before (5 elements, 5 integration points, and elastic-perfectly plastic material property), while the second model has seven integration points. The load deformation response for the two cases are plotted in Fig.3.7. The ultimate load for the cases when using 5 and 7 integration points are 191.2 and 185.5 pounds respectively. The nature of the load deformation curve for the second model is also much closer to the continuum case. Hence, this method of increasing the integration points could also be employed to improve the accuracy of the results. The only drawback seems to be the computing time. The analysis of the beam model with 10 element mesh and 5 integration points requires almost the same amount (30 seconds) of time as the model with 5 element mesh and 7 integration points. Hence the practicality of increasing the number of integration points while analysing large structures seems to be limited.

The third parameter to be changed was the initial load increment for the Riks analyses. This parameter was varied between 5 pounds to 30 pounds. It did not affect the accuracy of the ultimate load nor did it affect the nature of the load deformation curve.

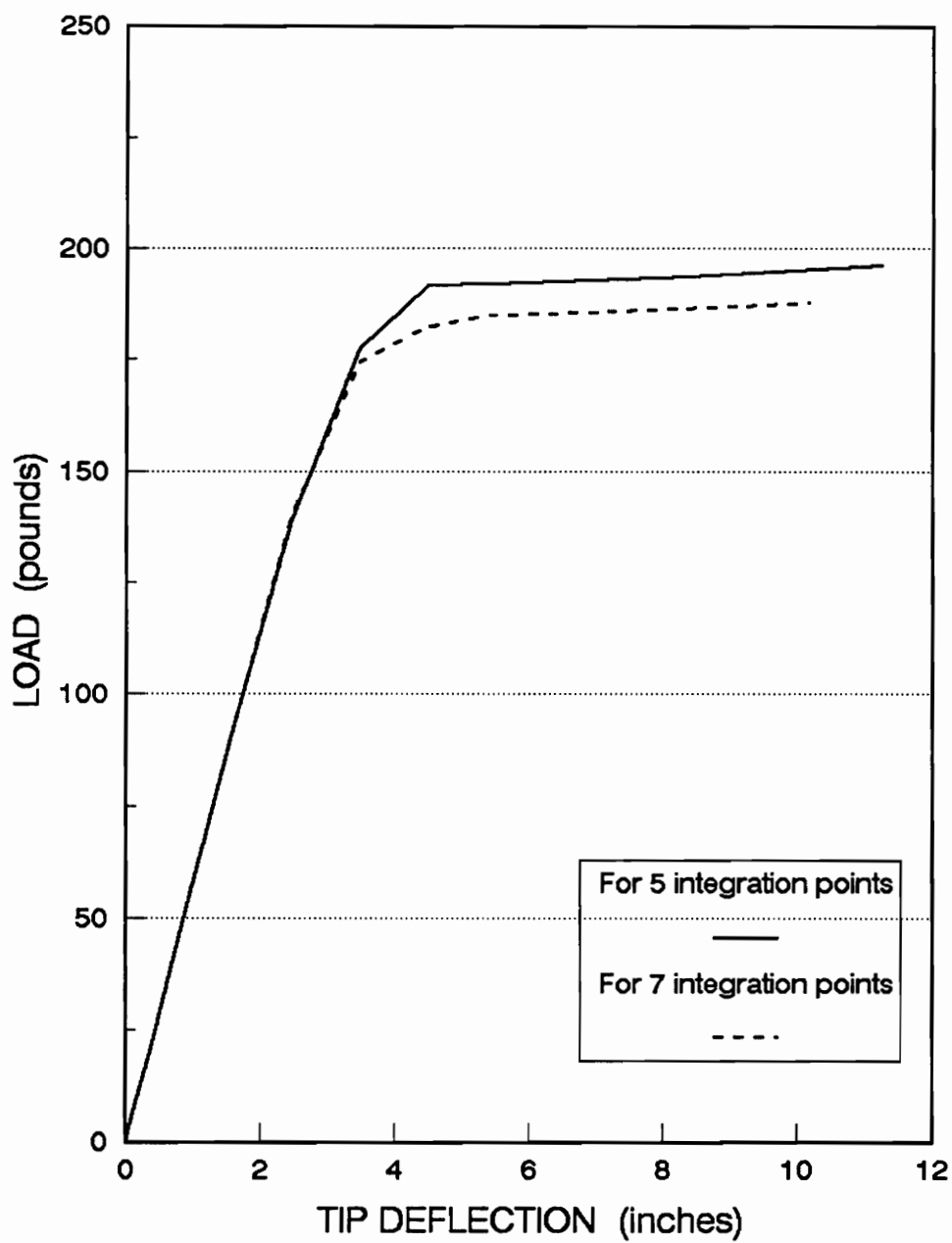


**FIG.3.7 LOAD DEFLECTION CURVES FOR BEAMS WITH  
DIFFERENT NUMBER OF INTEGARTION POINTS**

### 3.4 Cantilever Column Loaded Through Its Base

For testing the accuracy of ABAQUS analyses for the case of combined bending and axial loading along with a nonlinear material law, the solution is obtained for a steel cantilever column loaded through its base and as shown in Fig.3.8. This solution is compared with experimental tests conducted by McGowan on a similar cantilever column (McGowan, 1991 (pp.91-102)).

In the actual experiment, the column consists of a large diameter outer pipe, with a smaller diameter pipe passing through it. The outer pipe is fixed at the base along the circumference, whereas the inner pipe is free at the base and is attached to the outer pipe at the top. A vertical load is applied to the inner pipe at the base, thus causing the outer pipe to be loaded by a vertical force through its base. In the experimental tests, the eccentricity of the applied load is caused by the imperfections in the specimen and in the experimental setup. Due to this, bending of the column takes place, which eventually leads to the contact of the inner column with the outer column.

In the ABAQUS analyses, the outer pipe is modelled with ten two noded B23 plane beam finite elements, whereas the inner pipe is modelled by a two node C1D2 plane truss element. The imperfections in the actual experimental testing are modelled by applying the load at a certain eccentricity. The analysis of the

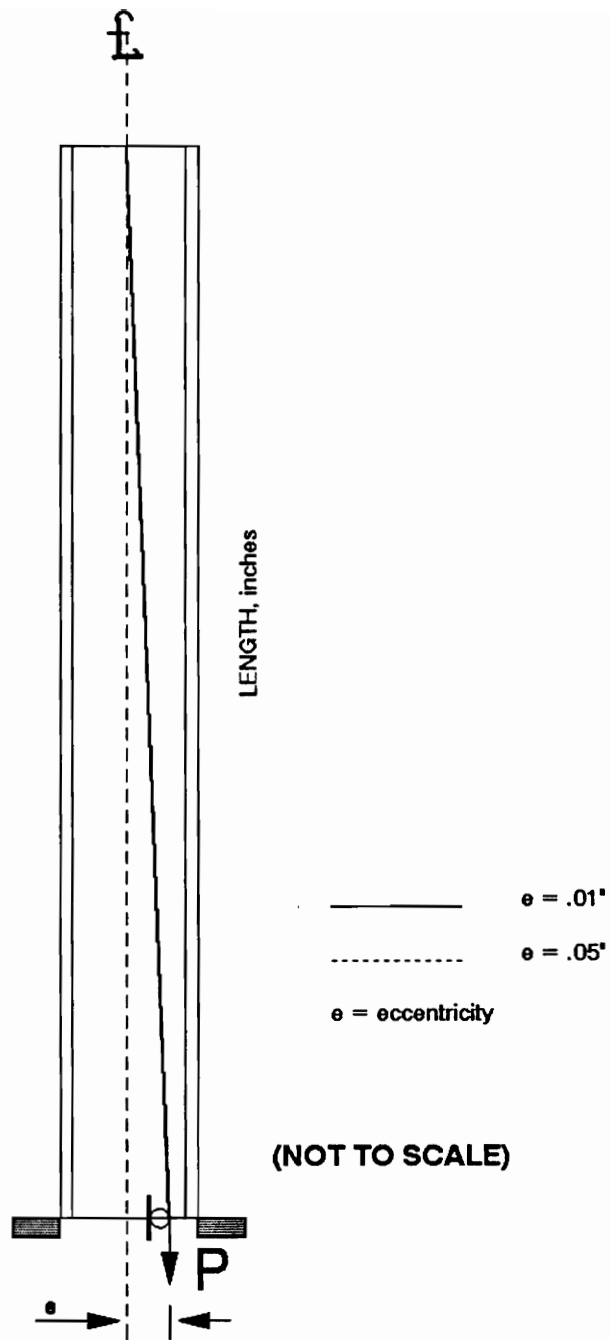


**Fig.3.8 HOLLOW CANTILEVER COLUMN**

contact problem is not attempted in this study, and hence the analysis is terminated before a contact problem is developed. The material behavior of the column is modelled on the basis of the data from the actual experimental tests.

The stress-strain law used for the column material is shown in the Fig.3.9, while the geometric specifications of the outer pipe are given below:

Outer diameter : 6.625 inches

Thickness : 0.188 inches

Length of Column : 182 inches

As it is not possible to directly equate the imperfections in the actual column with a numerical value of the eccentricity, two ABAQUS runs are made with different values of eccentricities to study their effect on the response of the column. In the first run, the eccentricity of the applied load is 0.01 inches, while in the second run the eccentricity is 0.05 inches.

The load deflection curves from the experimental tests and the ABAQUS analyses are presented in Fig.3.10. The analytical results for the model with eccentricity of 0.05 inches is close to the experimental results. The difference between the ABAQUS and experimental results is due to the difficulty in correlating the imperfections in the actual column with a numerical value of the eccentricity. The experimental load deflection curve is softer than the analytical results, indicating possibly greater imperfections than those modelled with the eccentricity of 0.05

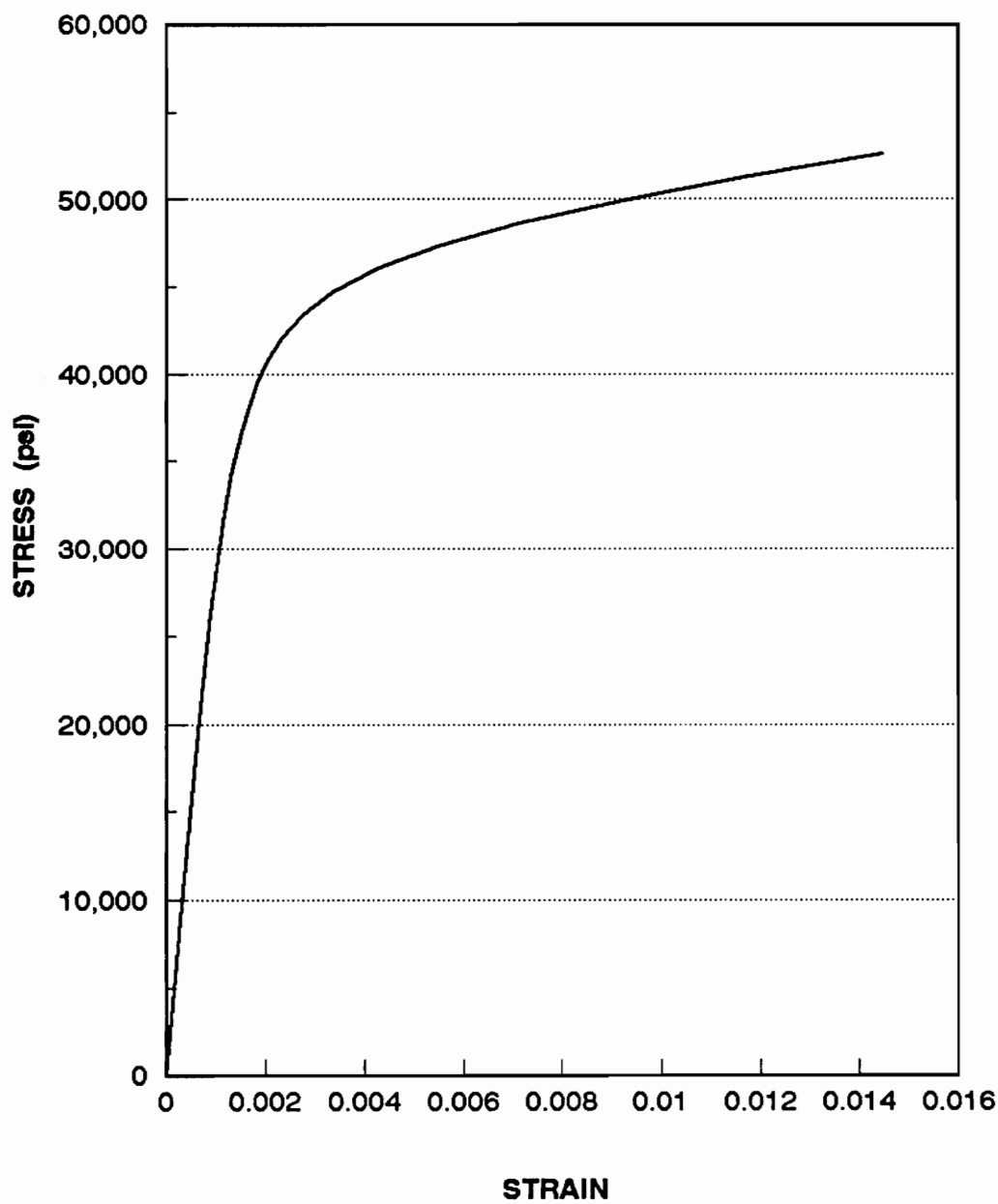


**FIG.3.9 STRESS-STRAIN GRAPH FOR THE COLUMN**

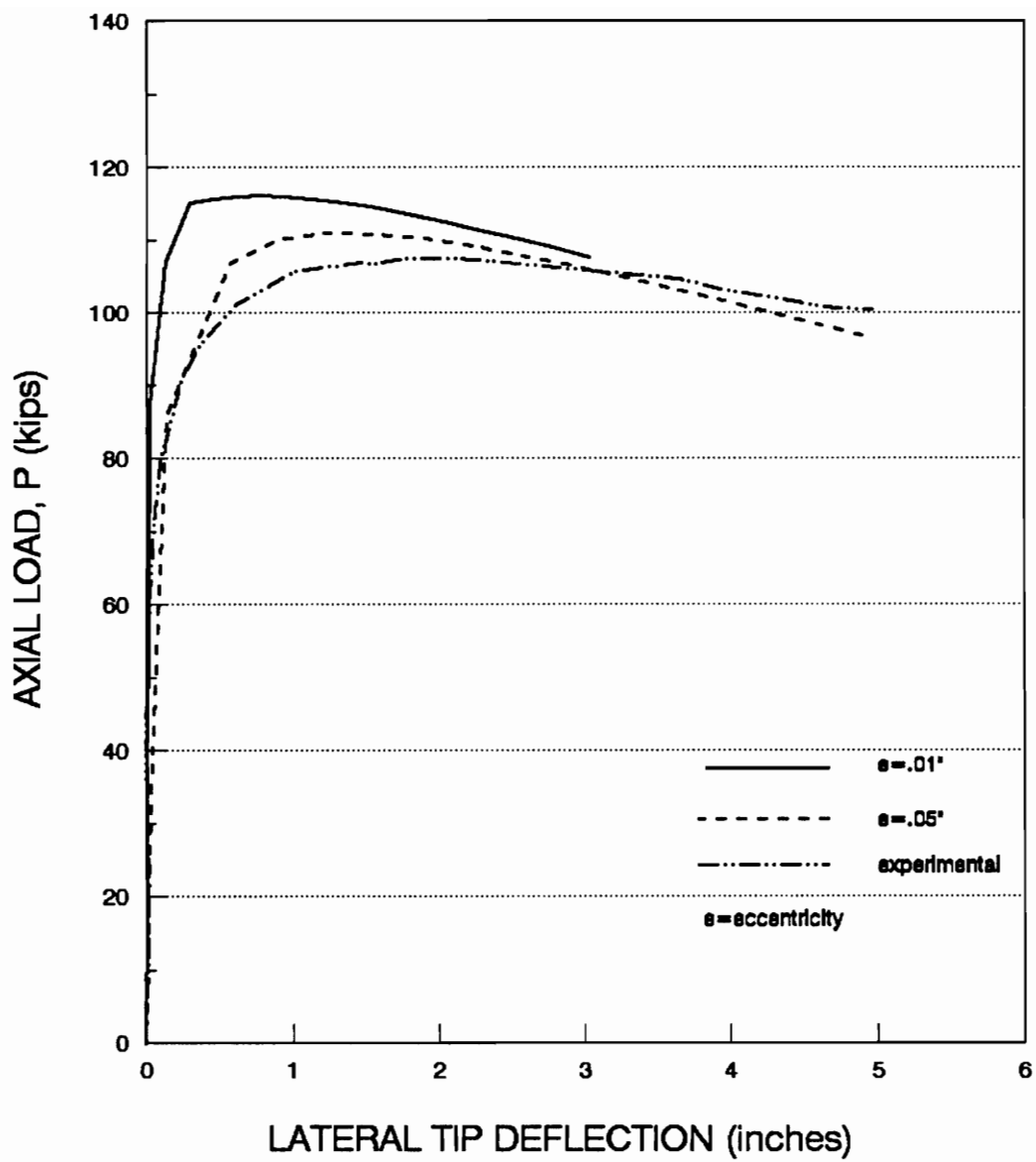


**Fig.3.10 LOAD DEFLECTION CURVE FOR THE COLUMN**

inches or the effect of a coarser mesh. The percentage difference in the limit loads for the experimental case and the analytical case with eccentricity of .05 inches is 5%

The test on the column thus indicates that the ABAQUS analyses results are consistent with the results in the experimental tests. This fact allows one to proceed with the materially nonlinear analysis of complex structures which consist of members which are subjected to combined bending and axial forces.

### **3.5 Torsion Tests on Cantilever Beam**

Two torsion tests are conducted on the cantilever beam elements. One of the tests is to verify that the torsional behavior modelled by the user subroutine is the same as modelled by the elastic or the plastic options from the library of material models available in ABAQUS. This is accomplished by analyzing a beam curved in plan, which is under combined bending and torsion.

The other test is to determine the value of the shear modulus used in the analyses by Wu (1991), Holzer, Wu, and Tissaoui (1991), and by Tissaoui (1991). To specify the shear modulus while using the elastic or plastic options, a value for

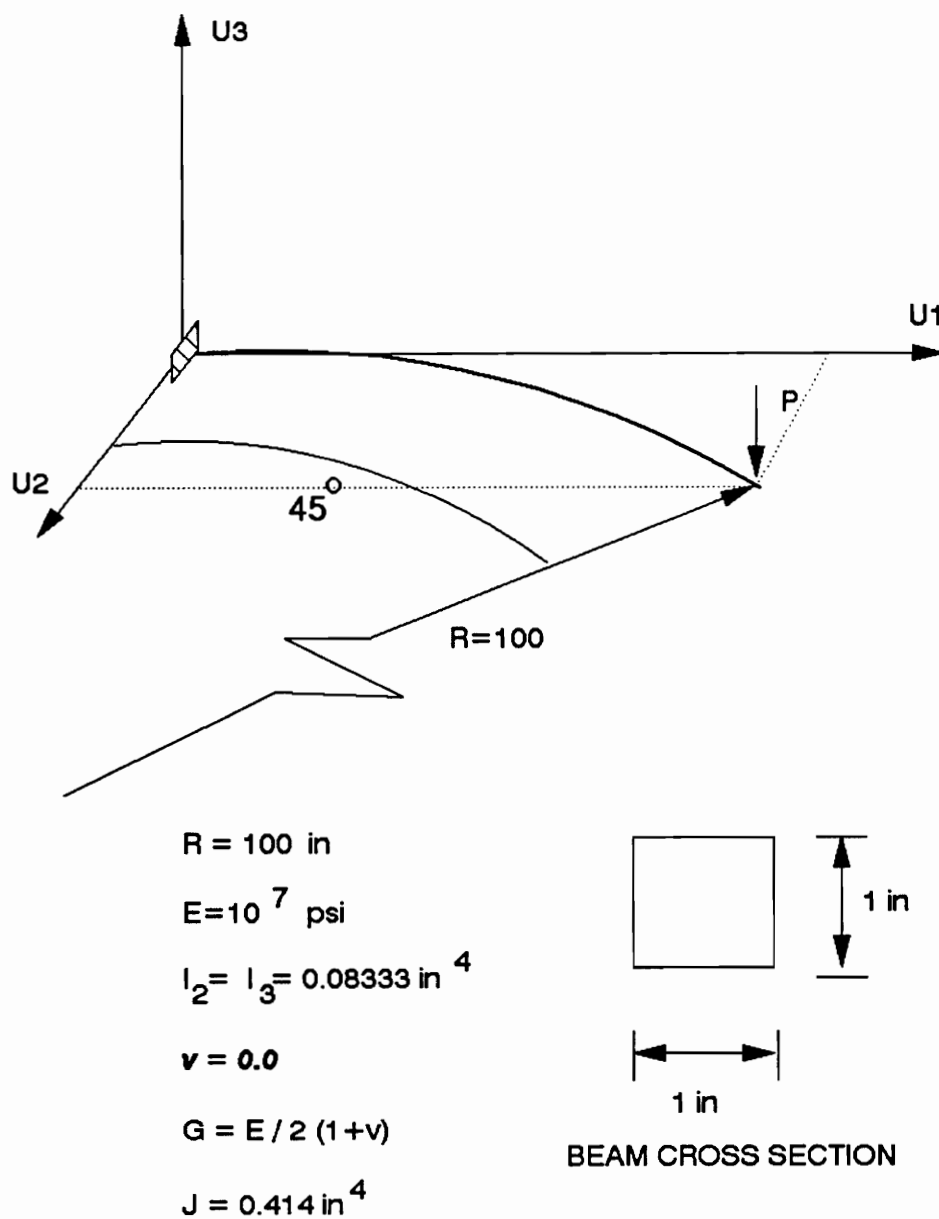


FIG.3.11 CURVED BEAM

Poisson's ratio is entered in the input file. ABAQUS then computes the shear modulus, Eq.(2.21), from the values of the Young's modulus and the Poisson's ratio. A straight cantilever beam under pure torsion is thus analysed to verify if ABAQUS computes the correct shear modulus for any value of Poisson's ratio.

It should be noted that even though the nonlinear material law is used for wooden beams, their torsional behavior is still modelled as linearly elastic. This has already been stated in Chapter 2, and in the following analyses, only linear elastic torsional behavior is verified.

### 3.5.1 Tests on Curved Cantilever Beam

The model used is a tip loaded cantilever beam of 45° bend. This model has been analysed by Bathe and Bolourchi (1979) and by Jau (1985). The beam is modelled in the present studies by eight B33 two noded beam elements. The material law is modelled by first using the user material option and then by using the elastic option. Fig.3.11 shows the cantilever beam along with the values of the various parameters. The results of the analyses using the two material modelling options are compared. Also, values obtained from the load deflection graph in the dissertation by Jau (1985) are checked against the present analyses results.

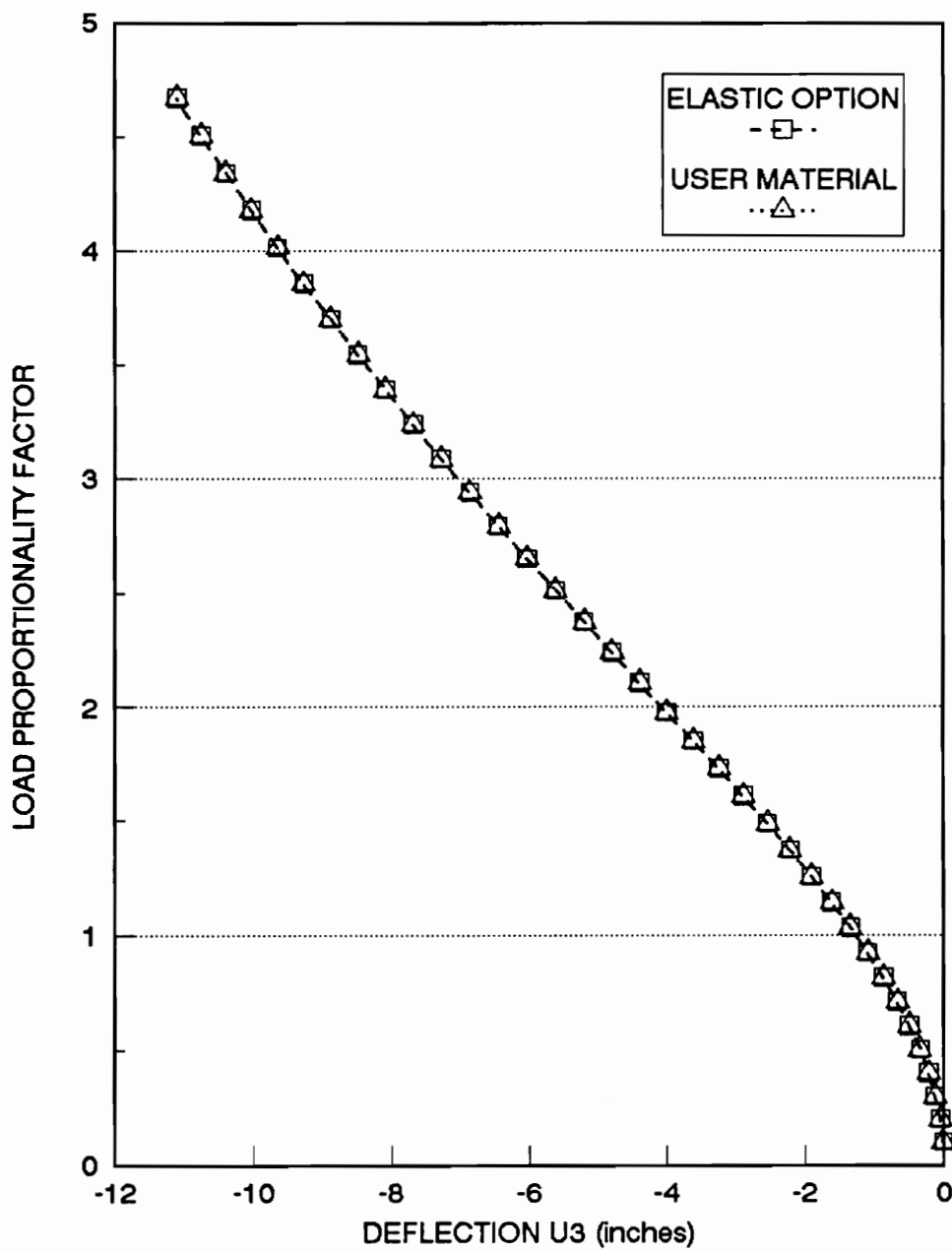


**FIG.3.12 LOAD DEFLECTION CURVE FOR THE CURVED BEAM**

The analysis results are shown in Fig.3.12. It is observed that the response obtained for the curved beam using the two material modelling options is exactly the same. The values obtained from the dissertation by Jau (1985) also agree with the present results. Therefore, the modelling of the torsional behavior as in the elastic or plastic option can be simulated correctly in the user subroutine.

### 3.5.2 Tests on Cantilever Beam

The objective of these tests is to determine if ABAQUS correctly computes the shear modulus from the values of Poisson's ratio and the Young's modulus (Eq. (2.21)).

A straight cantilever beam made up of five B33 two node beam elements is subjected to pure torsion. The length of the beam is 50 inches. Three models having different cross sections are tested. A torque of 100 pound-inch is applied at the free end. The beams are considered to be made of wood, and are assigned the linear elastic material law using the elastic option in ABAQUS.

The first model has a circular cross section of 1 in<sup>2</sup>. The shear stress obtained is 509.3 psi, while the shear strain is  $8.49 \times 10^{-4}$  psi. The shear modulus used by

ABAQUS in these computations is obtained by dividing the shear stress by the shear strain. Thus, the shear modulus used is  $6.00 \times 10^5$  psi. However, the value of shear modulus specified by Davalos (1989), Wu (1991), and Tissaoui (1991) is  $1.6 \times 10^5$  psi.

The second model has a unit square cross section. The shear stress obtained from the analysis for this model is 424.3 psi and the corresponding shear strain is  $7.07 \times 10^{-4}$ . Shear modulus of  $6.00 \times 10^5$  psi is computed from these values.

The third model has a rectangular cross section, 1 inch wide and 2 inches deep. The shear stress obtained from the analysis for this model is 134.2 psi and the shear strain is  $2.24 \times 10^{-4}$ . The shear modulus in this case too is  $6.00 \times 10^5$  psi.

From these tests, it is observed that the correct shear modulus for wood is not used by ABAQUS. The Poisson's ratio corresponding to a shear modulus of  $6.0 \times 10^5$  psi is 0.5. It is thus seen that ABAQUS limits the value of the Poisson's ratio to 0.5. Even though ABAQUS disregards the Poisson's ratio of 4.625 given in the input file and takes a default value of 0.5, it does not issue a warning or error message in the analyses results. Hence, in all the previous research conducted on elastic buckling behavior of domes by Wu (1991), by Tissaoui (1991), by Holzer, Wu, and Tissaoui (1991), and by Davalos (1989), the value of shear modulus used by ABAQUS is  $6.0 \times 10^5$  psi, instead of the expected value of  $1.6 \times 10^5$  psi.

Based on the textbook by Bodig (1975), the range of shear moduli for wood with

Young's modulus of  $1.8 \times 10^6$  psi is between  $1.14 \times 10^4$  psi and  $1.36 \times 10^5$  psi. If the Young's modulus is increased to  $2.1 \times 10^6$  psi, the shear moduli range is between  $1.25 \times 10^4$  psi and  $1.59 \times 10^5$  psi. Hence the shear modulus value used in the earlier studies of elastic buckling behavior of domes seems to be quite large. It may however be possible that certain species of wood might have higher shear modulus.

The only way of specifying the shear modulus of  $1.6 \times 10^5$  psi along with a Young's modulus of  $1.8 \times 10^6$  psi or  $2.1 \times 10^6$  psi, is by using the user subroutine option. Hence for all the further studies, the material law for even the elastic material behavior will be specified by using the user subroutine option.

Although there is a large difference between the possible range of shear moduli and the shear modulus used in the previous studies, the effect of this on the dome behavior is expected to be minimal because the previous studies by Wu (1991) and by Tissaoui (1991) show that the torsional stresses at failure are quite small.

## CHAPTER 4

# MODELLING THE DOME

In this chapter, the steps involved in creating the dome model and the subsequent writing of the ABAQUS input file is explained. In the first section, the geometry of the dome is defined. The model is created based on this geometry, and the steps involved in its creation are as follows:

- Defining the mesh sizes, the member dimensions, and the finite elements used
- Defining the boundary conditions used in the model
- Defining the material laws used for the elements
- Specifying the loading on the dome
- Creating the model graphically in I-DEAS.
- Writing an ABAQUS input file from the graphical model
- Modifying this input file to include the required boundary constraints, loading, the beam orientations, and the material laws.

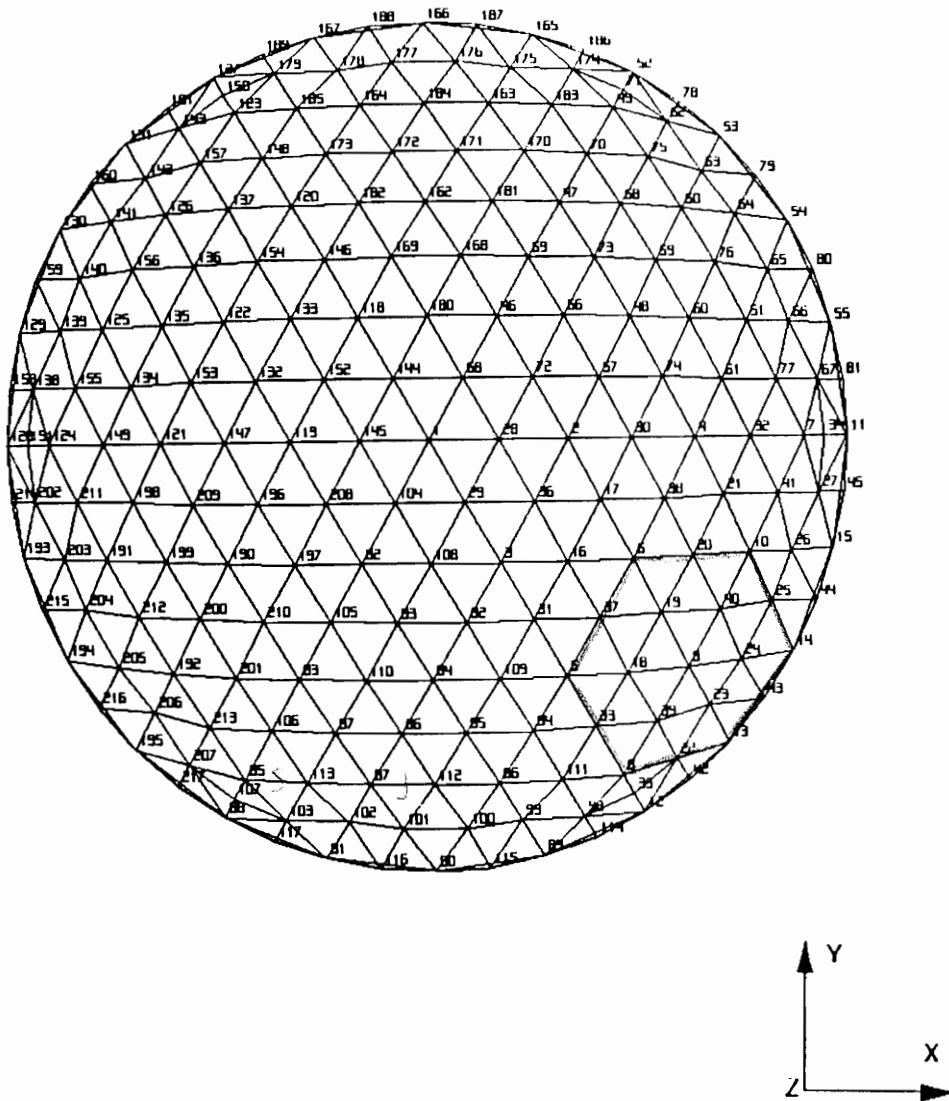


FIG.4.1 PLAN OF THE TRIAX DOME

#### **4.1. The Geometric Model**

The Crafts Pavilion Triax dome in Raleigh, North Carolina is modelled in the ongoing study. The members of the dome lie on the surface of a sphere with a radius of 1600 inches (133.33 feet). The dome has a span of 1595 inches (132.92 feet) and a height of 212.35 inches (17.70 feet). The plan of the dome is shown in Fig.4.1.

The finite element model of the dome is created by first defining its geometry on a horizontal plane which is 1387.66 inches (115.64 feet) above the center of the sphere. The geometry of the dome is a grid of equilateral triangles on this horizontal plane. The configuration of the dome is then obtained by projecting this triangular grid onto the surface of the sphere by rays originating from the sphere center.

#### **4.2 The Finite Element Model**

The finite element model of the dome is similar to that modelled by Wu (1991).

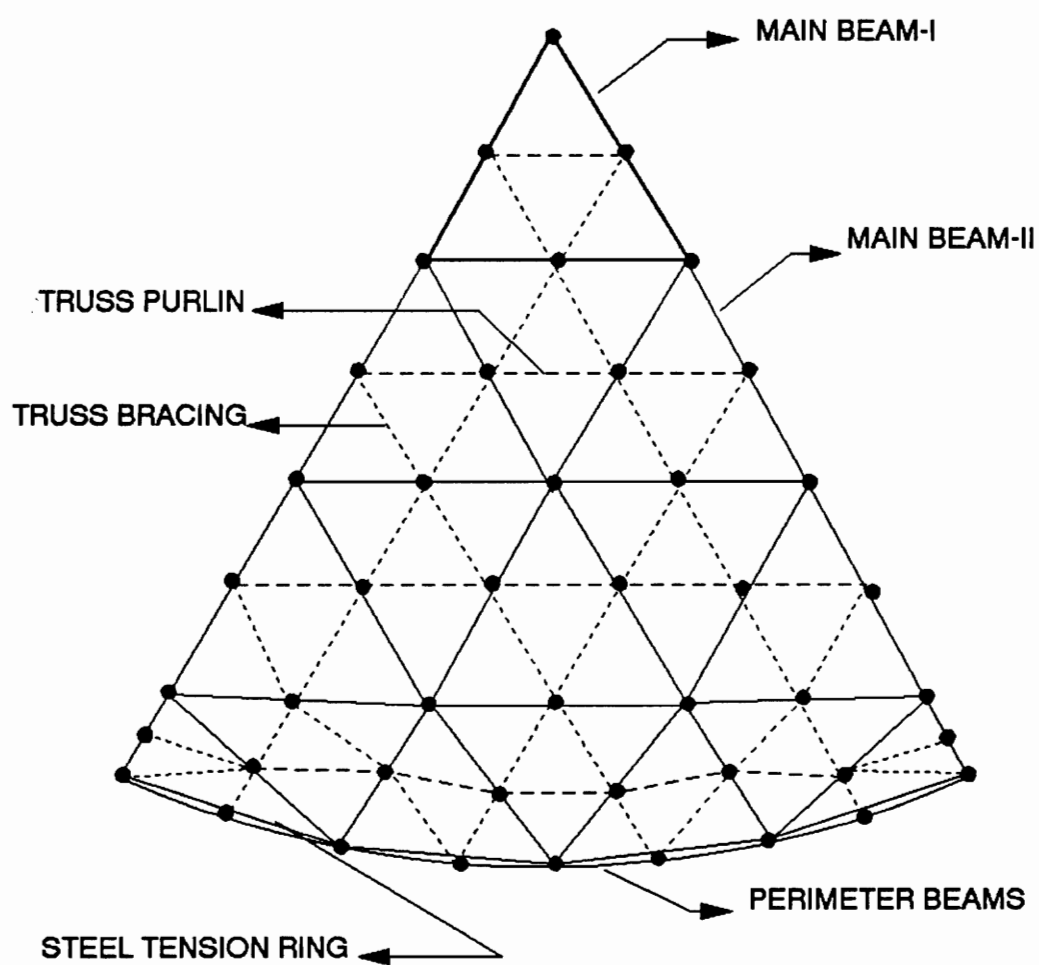


**FIG.4.2 ONE SECTOR OF THE DOME**

In the finite element model, each physical beam has been divided into two beam elements. The purlins are modelled as truss elements and the lateral bracing effect of the decking is modelled by using truss elements. The tension ring is also modelled as being made up of truss elements.

The beams are divided into three categories based on their dimensions. The set of beams forming the first ring around the apex of the dome are denoted as Main Beam-I. The beams at the base or perimeter of the dome are denoted as the Edge Beams, and the remaining beams are labelled as Main Beam-II. All the different members are shown in Fig4.2 and their dimensions are given below (Holzer, Wu, and Tissaoui, 1991) :

1. Main Beam-I : 6.75 inches  $\times$  12.0 inches
2. Main Beam-II : 5.0 inches  $\times$  11.0 inches
3. Edge Beam : 3.0 inches  $\times$  12.25 inches
4. Purlins : 3.0 inches  $\times$  8.25 inches
5. Steel Tension Ring : 1.0 inch  $\times$  12.0 inches
6. Bracing : 0.3 inch<sup>2</sup>

All the beams are modelled by B33 two noded Bernoulli-Euler elements, and the rest of the members are modelled with C1D2 two-node isoparametric truss elements (ABAQUS 4.6 User's Manual, 1991). The choice of the elements is based on the studies conducted on various dome models by Wu (1991).

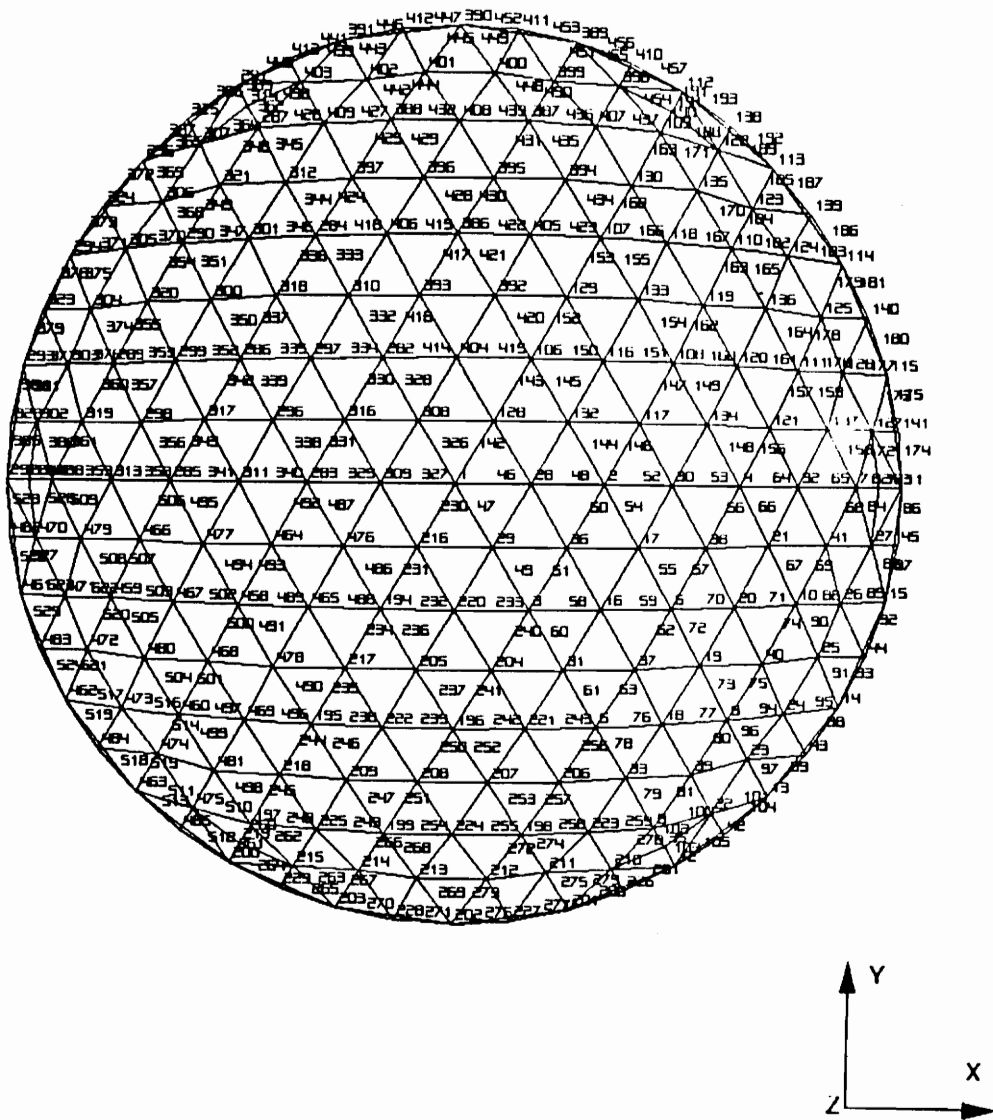


**FIG.4.3 DOME MODEL WITH REFINED MESH**

To study the effect of mesh refinement on the behavior of the dome, the above mentioned model is modified to obtain a refined mesh. In this model, each physical beam is modelled with four beam elements instead of two elements. The dome model so created is shown in Fig.4.3.

Apart from the above mentioned dome model, several models consisting of only the top ring of the dome are analysed. These models consist of only the Main Beam-I and the corresponding truss elements, and are referred to as the Dome Cap model. The mesh refinement studies are conducted by modelling each beam by four elements or by providing connector elements to the beam elements in the original dome cap model.

The connector elements are B33 beam elements with 6 inch length provided at each end of the beam element. As discussed in Chapter 3, the study on the nonlinear cantilever beam indicated that the selective refinement of the mesh gave a better response than a uniform refinement with the same number of elements. This idea is thus extended to the analyses of the Dome Cap.

The Dome Cap model and the one with the refined mesh are shown in Fig.4.4 and Fig.4.5 respectively.

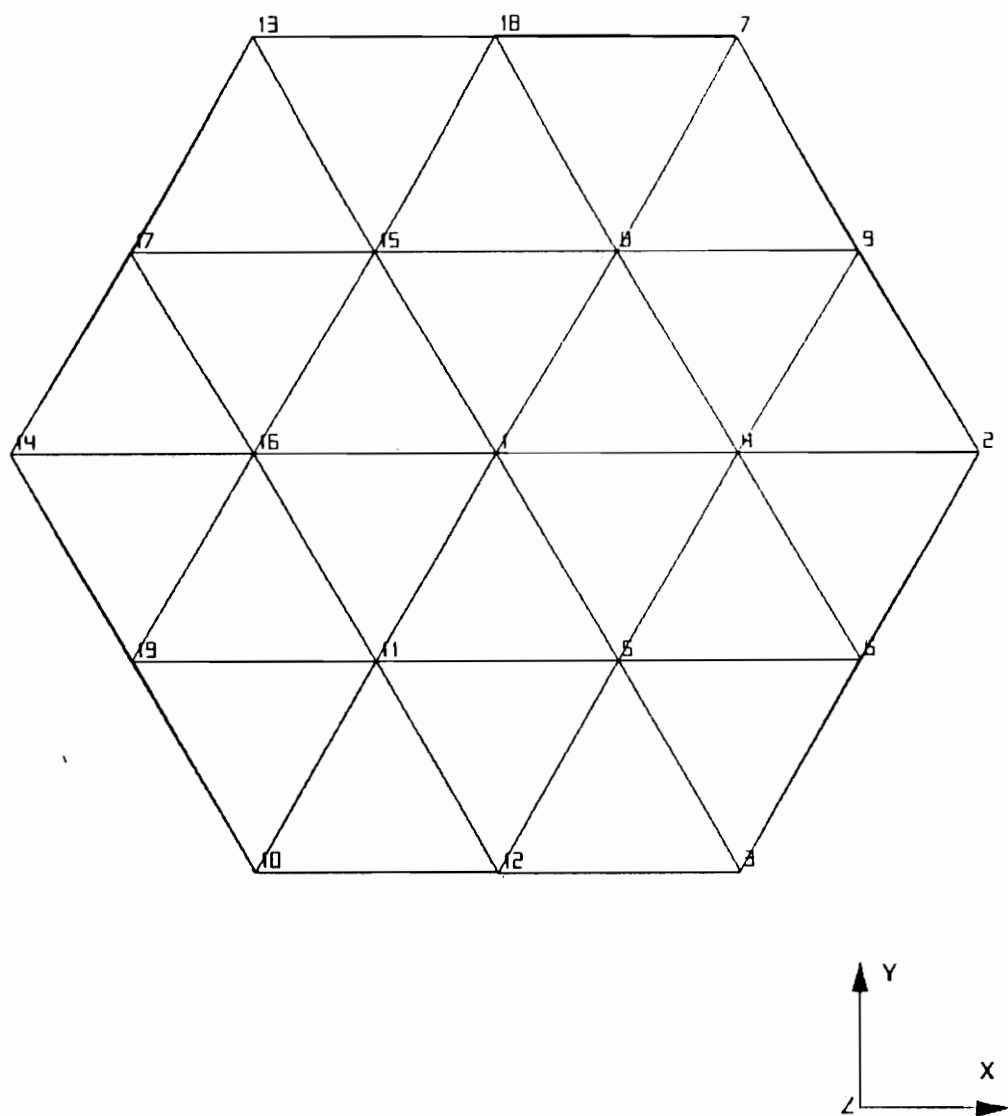


**FIG.4.4 DOME CAP MODEL**

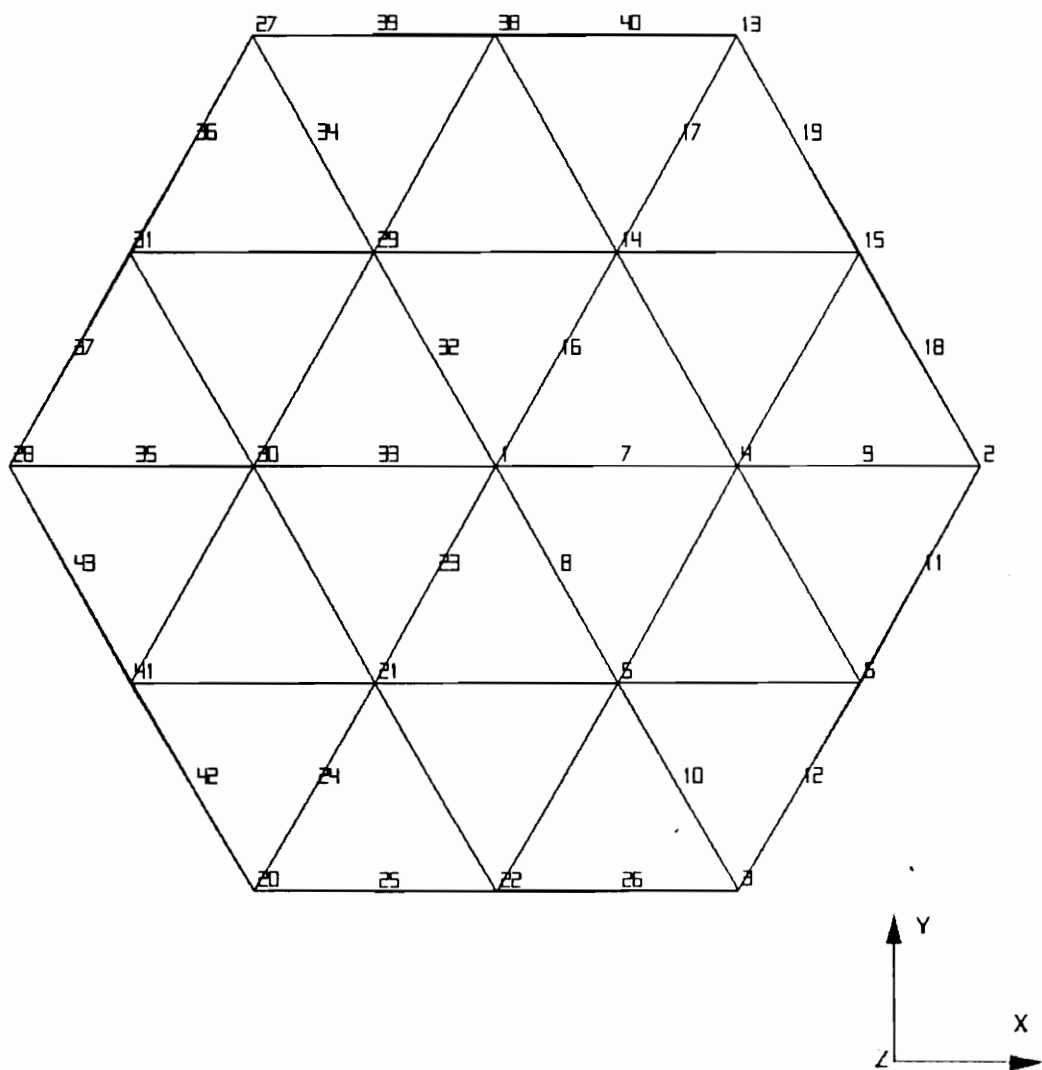


**FIG.4.5 DOME CAP MODEL WITH REFINED MESH**

### 4.3 Boundary Conditions

The boundary constraints used in the model are similar those used by Wu (1991) and Huang(1989). The selected constraints must eliminate the rigid body motion of the dome but at the same time must allow for the tension ring to move freely in the radial direction (Davalos, 1989).

The boundary constraints are applied to the perimeter nodes. All the perimeter nodes are constrained in the Z-direction to eliminate the vertical rigid body motion. To remove the rigid body rotation of the dome about the Z-axis and the rigid body translation in X and Y-directions, constraints in the X-direction are applied to base nodes on the Y-axis (nodes 90 and 166 in the dome model without mesh refinement), and constraints in the Y-direction are applied to the base nodes on the X-axis (nodes 11 and 128). The boundary constraints are shown in Fig.4.6.

For the dome models or dome cap models with refined meshes or with connector elements, extra nodes are created at the perimeter due the the mesh refinement. It is important to note that the boundary constraints in these models must be applied to the original nodes only. This is because the constraining of the extra nodes changes the boundary condition of the dome, and the model is then no longer similar to the one without the refined mesh.

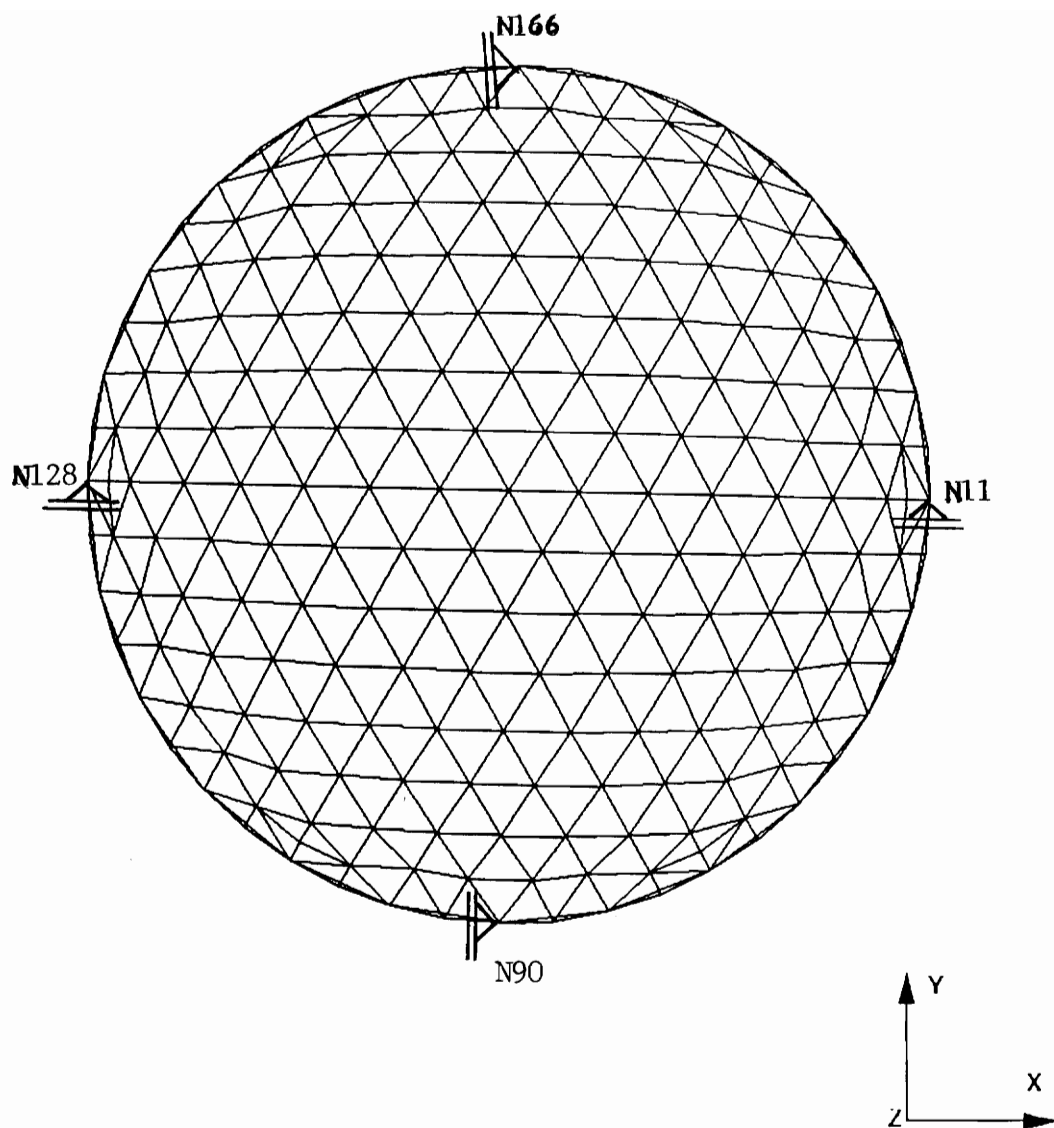
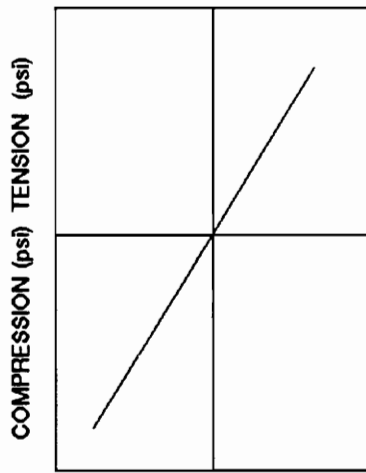


**FIG.4.6 DOME MODEL SHOWN WITH CONSTRAINTS**

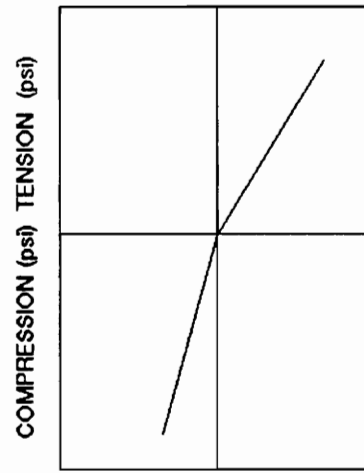
#### 4.4 Material Properties

For studying the effect of variations of the material law on the dome behavior, three linear models and one nonlinear model are defined for wood. In all the dome models, the bracing, the purlins, and the steel tension ring are assigned a linear material law. Specifically, the bracings and the purlins have a Young's modulus of  $1.8 \times 10^6$  psi and the tension ring has a Young's modulus of  $2.9 \times 10^7$  psi. The four dome models, based on the type of material law assigned to the beam elements, are given below while the shape of these stress strain curves are shown in Fig.4.7.

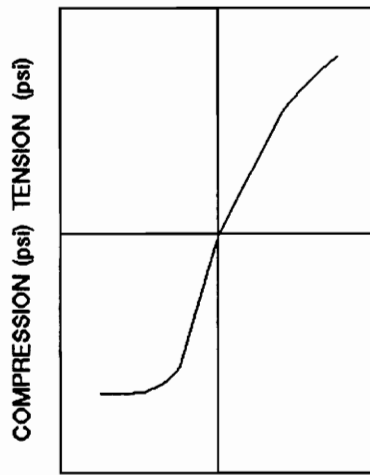
1. The first linear model is the same as that used by Wu (1991). In this model the glulam beams have the following material properties: Young's modulus  $E = 1.8 \times 10^6$  psi and the shear modulus  $G = 6.0 \times 10^5$  psi.
2. The second linear model is created to determine the effect of changes in the shear modulus on the behavior of the dome. In this model the glulam beams have a Young's modulus  $E = 1.8 \times 10^6$  psi and a shear modulus  $G = 1.6 \times 10^5$  psi.
3. The modelling of the nonlinear material law has been described in detail in Chapter 2. The mechanical property of wood in this nonlinear material law is based on the percentage moisture content and the specific gravity of the wood. In the ongoing study, the wood is considered to have a moisture content of 12% and



(a) Linear



(b) Bilinear



(c) Nonlinear

**FIG.4.7 THE TYPES OF STRESS-STRAIN CURVES  
USED IN THE DOME MODELS**

a specific gravity of 0.52 based on the oven-dry weight and green volume. Based on these values, the initial longitudinal modulus of wood in tension  $E_{(tension)}=1.81 \times 10^6$  psi and in compression  $E_{(compression)}=2.19 \times 10^6$  psi. The shear modulus is taken as  $G=1.6 \times 10^5$  psi. All the beams in the dome are modelled with this nonlinear material law.

4. To get a reasonably good assessment of the effect of the nonlinear material model on the behavior of the dome, a bilinear elastic material law is developed. In this model, the longitudinal modulus of wood in tension is  $E_{(tension)}=1.81 \times 10^6$  psi, and the longitudinal modulus in compression is  $E_{(compression)}=2.19 \times 10^6$  psi. The shear modulus is again taken as  $G=1.6 \times 10^5$  psi. In this dome model, all the beams are assigned this bilinear elastic material law.

#### 4.5 Dome Loading

The loading on the dome is divided into live loads and dead loads. The design dead load is 16 psf and the design live load is 20 psf. The dead load is due to the following self-weight of the structure.

The design dead load is obtained as follows (Wu, 1991; Davalos, 1989) :

1. beams and purlins:	2.0 psf
2. tongue and groove Decking:	5.0 psf
3. connectors, roofing and insulation:	9.0 psf
total dead load:	<hr/> 16.0 psf

The design live load is considered to be due to the snow over the dome. The value for the snow load is the same as that used by Wu (1991). It should be noted that the snow load is considered to be distributed not on the surface area, but on the plan area of the dome.

Two load cases are considered in the analyses of the dome. The first load case is the combined loading of dead load and uniform snow load over the complete dome. The second load case considered is the combined loading of dead load and uniform snow load over half of the dome. With these two load cases, the behavior of the dome under cyclically symmetrical and cyclically unsymmetrical loading can be studied.

In the earlier studies by Wu (1991) and by Holzer, Wu, and Tissaoui (1991), it was found that the load case of dead load and uniform snow load over half the dome induced the maximum stresses in the dome members at failure. This is another reason for selecting the second load case as it will allow us to study the behavior of the dome when the stresses in its members are beyond the

proportional limit.

## **4.6 Creation of the ABAQUS Input File**

The input file of the dome is created in three steps. In the first step, the dome model is generated graphically with I-DEAS (Integrated Design and Engineering Analyses Software), from which an initial ABAQUS input file is obtained. In the second step, nodal loads and beam orientations are computed and written to a file in the required ABAQUS input format. In the third step, the initial input file is modified by adding the boundary constraints, the beam orientations, the material model definition, the step definition, the nodal loadings, and the output request cards. The use of I-DEAS and the modifications of the input file is explained in the following sections.

### **4.6.1. Pre-Processing Using I-DEAS**

The dome graphics is generated in the **model preparation task** of I-DEAS. This task lies in the **pre/post processing module** which in turn lies in the **engineering**

**analyses family** in I-DEAS. The **task**, **module**, and **family** represent a hierarchy of program regions where various pre/post processing operations can be conducted.

In the model preparation task menu, the creation of the dome model requires three steps. These steps are described below:

1. First, the nodes for one sector are defined. This can be done either by reading the nodes from an existing I-DEAS file, as was done in the present analyses, or they can be defined individually by entering the node numbers and their coordinates.

The existing I-DEAS node file, as used by Wu (1991), was stored in a **Universal** file format. To read this, the **Universal** and **Read** options are picked. When prompted for the name of the file, the file name without the extension is entered. After the file is read, **Auto Scale (AU)** and **Draw (DR)** commands are issued to display the nodes on the screen.

If the nodes are to be defined directly by entering them, then the **Node** , **Create**, and **Single** options have to be entered in the mentioned order. After this, the node number and its three coordinates have to be given. After defining all the nodes, the **auto scale** and **draw** commands have to be issued to view the drawing.

2. After defining the nodes, the elements are generated. This is done by selecting the **Element** option from the menu. The **Default** option is then selected, and the

element type, and color is defined. Returning back to the **Element** menu, **Create** and **Single** options are selected. The elements are then generated by clicking on the nodes which define the element. In this way, all the elements for one sector are defined.

3. In this step, the complete dome model is created by reflecting the first sector about the sector lines. This is achieved by selecting the **Create** and **Reflect** options from the **Element** menu. The **Three Point Method** is then selected and three points forming the reflecting plane are then entered. The sector is thus reflected about this plane to form another sector with all the elements and nodes. In this fashion, all the sectors of the dome are created. The dome is saved in the **Universal** file format by selecting **Universal** and **Write** from the menu. The file name is then provided, and the dome graphics and all the related data is saved in this file.

After creating the complete dome model, the ABAQUS file is written. The writing of the ABAQUS input file is a two step process. In the first step, the node and element data is transferred into a database. I-DEAS then creates the ABAQUS input file by reading this database.

The database is created by first selecting **Pearl Data Transfer** from the menu. The **Create** option is then selected and, when prompted, the name of the database is given. Then the **Load** and **Model** options are selected. After the model is successfully loaded, the database is closed and saved by selecting the **Close** option.

Once the database is created, the **Manage Files (Man)**, **Write**, and **ABAQUS (AB)** options are selected. The program prompts for the name of the database and the ABAQUS input filename. After providing all the information, the ABAQUS input file is written, and a message as to its successful completion is provided at the end.

#### **4.6.2. Nodal Loads**

Shell elements are created in I-DEAS to discretize the uniformly distributed loads to the nodes. Three and four node thin shell elements are used for this purpose. The mesh is formed such that the shell elements form a symmetric pattern in each sector.

For the dome models with and without the connector elements, only triangular shell elements are used. By using the triangular elements, the loads are discretised only to the original nodes of the model; i.e, no loads are assigned to the extra nodes generated for the connector elements. For the models with a refined mesh, the triangular as well as the quadrilateral elements are used. By using both of these elements, the loads are discretised to the original nodes as well as to the extra nodes created due to the mesh refinement.

A linear analyses is conducted on ABAQUS to obtain the nodal loads. For this purpose all the nodes of the dome are fixed, and distributed load due to the dead weight or snow load is applied in the positive Z-direction (vertical).

Output requests are made for reaction forces at all the nodes. The reaction forces are the nodal loads on the dome. The nodal loads in the X and Y directions are relatively small as compared to those in the Z direction, and hence only the nodal loads in the Z direction are used for the loading on the dome.

#### **4.6.3. Beam Orientations and File Modifications**

The beams in the dome are oriented such that each beam lies in a plane passing through the center of the sphere (Fig.4.8). Only the edge beams are oriented differently, and are vertical. A FORTRAN program (Appendix A) is written to compute the beam orientations. This program writes the beam element definition cards, the beam cross section dimensions, and the beam orientations in the required format for the input file.

After obtaining the beam orientations, the input file as obtained from I-DEAS is

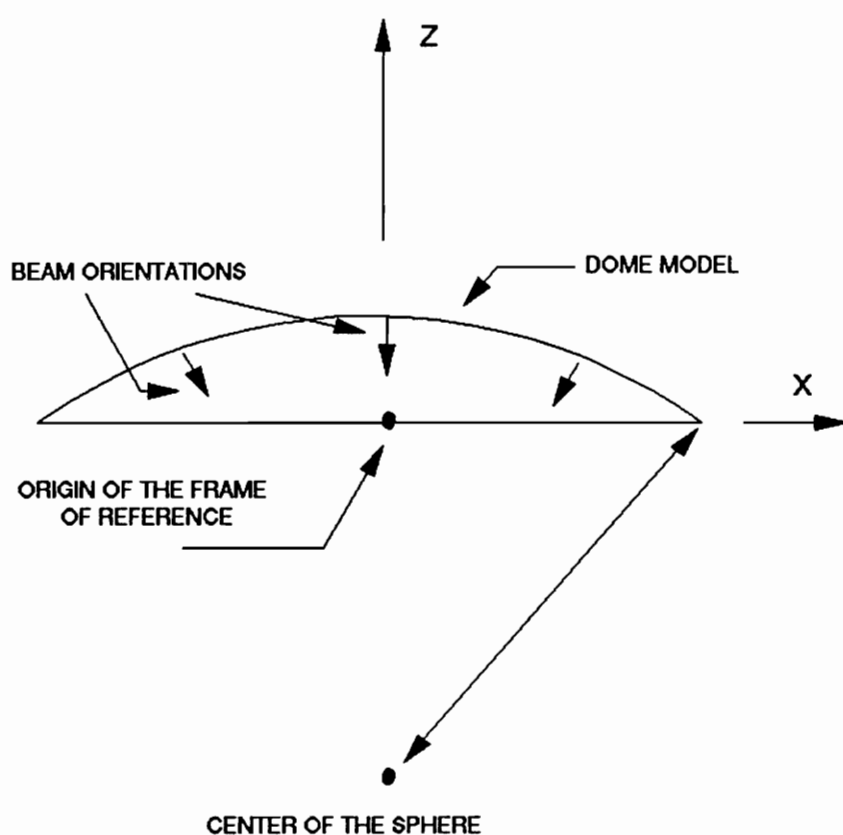


**FIG.4.8 BEAM ORIENTATIONS WITH RESPECT TO  
THE SPHERICAL CENTER**

modified. The various modifications carried out manually, in the order in which they are carried out, are listed below:

1. Boundary nodes are grouped into a node set
2. Set names are assigned to the various dome members
3. Cards for the cross sectional areas for the truss elements are added
4. The output from the beam orientation program is inserted in the input file
5. A card for the boundary condition is added
6. Material definition cards are added
7. Step definition cards and the nodal loads are inserted in the input file
8. Node and element sets for the output are defined
9. Cards for the output requests are added
10. The subroutine to define user material is added at the end of the input file

After going through this procedure, an ABAQUS input file for the nonlinear analysis is obtained. A sample of this input file is provided in the Appendix B, and the analyses results are discussed in the next chapter.

## CHAPTER 5

# DOME ANALYSES

Nonlinear analysis of various dome and the dome cap models is conducted to study the effect of the change in material properties on the stability behavior of the domes. Both, material as well as geometric nonlinearities are considered in these analyses. Critical snow loads for the dome models are determined and the load deflection curves are presented. The maximum stresses in the beams at the critical load are compared with the ultimate stresses.

### 5.1 Nonlinear Analysis Procedure

The nonlinear analysis is conducted with ABAQUS using the Riks option (ABAQUS 4.6 User's Manual, 1990). This option traces the equilibrium path

beyond the limit point. As this procedure uses automatic incrementation of the load, exact value of the limit load may not be obtained because the increment may jump over the limit load. In the following discussion, the limit point is assumed to be the highest point on the load deflection curve.

The loading on the dome is applied incrementally in two steps, which are given below:

1. The Newton-Raphson method is used in the first step to incrementally load the dome upto its full dead load (16 psf).
2. The Riks method is used in the second step to apply incrementally the snow load (20 psf) upto and beyond the limit load.

The total load at any instant is thus given by

$$P = P_D + \lambda P_L \quad (5.1)$$

where

$\lambda$  = the load proportionality factor

$P_D$  = the dead load (16 psf)

$P_L$  = the live load or snow load (20 psf)

In the following discussion, the critical load factor is the load proportionality factor at the limit point. The load deflection curves for the dome models are

obtained by plotting the load proportionality factor versus the corresponding deflection at a given node. In the nonlinear analysis of all the dome and dome cap models, the critical load is at the limit point.

Before embarking on the nonlinear analysis, linear analyses of the dome models are carried out to ascertain that there are no major defects or imperfections in the finite element models. In the linear analysis, the dome models are subjected to cyclically symmetric loads, and the reactions at all the supports, and the displacements at symmetrically placed nodes are monitored. The results of the linear analysis for all the dome models with uniformly applied dead load are found to be satisfactory.

## 5.2 Proportional Limits and the Ultimate Stresses

*revised ed. -> wood Eng handbook, 1990*

The proportional limit and the ultimate stresses are different for the linear and the nonlinear material laws. For the linear material law, these values are given in Table 5.1 (Wood Handbook (1974), Holzer, Wu, and Tissaoui (1991)). The values of proportional limit and the ultimate stresses for the bilinear stress strain law are assumed to be the same as those for the linear laws. In Table 5.1, the ultimate compressive stress represents the maximum crushing stress, while the ultimate

tensile stress is the modulus of rupture from static bending tests.

**TABLE 5.1 Proportional Limit and Ultimate stresses for linear material law**

PROPORTIONAL LIMIT	ULTIMATE COMPRESSIVE STRESS	ULTIMATE TENSILE STRESS
5900 psi	8500 PSI	14500

For the nonlinear material law, the proportional limits and the ultimate stresses are computed by using Eqs. (2.1) through Eqs. (2.17). The equations have parameters which depend on the values of the specific gravity and the moisture content of wood. For southen pine, the average values for the specific gravity is given as 0.52 and the moisture content is given as 12% (Timber Construction Manual (1985)). The values for proportional limit and ultimate stresses for the nonlinear material law are computed from Eqs. (2.1) through Eqn. (2.17) for these values of specific gravity and moisture content, and are presented in table 5.2.

TABLE 5.2 Proportional Limit and Ultimate Stresses for nonlinear material law

PROPORTIONAL LIMIT IN COMPRESSION	PROPORTIONAL LIMIT IN TENSION	ULTIMATE COMPRESSIVE STRESS	ULTIMATE TENSILE STRESS
4873 psi	2578 psi	10496 psi	14500 psi

5092

2586

OK

2

0

6882.71

5.3 Dome Cap Analysis

$$\alpha_2 = \sqrt{\frac{K_1^2 - K_2^2}{K_1^2}}$$

The dome cap models are created because they are much smaller than the complete dome models, and are cheaper to analyze in terms of computer cost and time. As the dome cap models are derived from the complete dome models, their behavior would be similar to the corresponding complete dome models from which they are derived. Thus, after analysing the dome cap models, potential modelling and analysis problems for the complete dome models can be identified.

The dome cap models are analyzed for two different loading conditions. For the loading condition of dead load and snow over the complete dome (Full Snow load condition), four different models of the dome cap are considered. These models are obtained by varying the material law for the beam elements, as described in Section 4.4. For the load case of dead load and snow load over only half of the

dome (Half Snow load condition), four models of the dome cap are considered. These are again obtained by varying the material law for the beam elements, as described in Chapter 4.

The mesh refinement studies are conducted on the dome cap for the case of half snow load only. Six different models of the dome cap are considered by varying the material laws and by refining the mesh.

#### 5.4 Effect of Shear Modulus on Dome Cap Behavior

ABAQUS computes the shear modulus from the values of Young's modulus and Poisson's ratio by using Eq. 2.21. In the domes modelled by Wu (1991), Holzer, Wu, and Tissaoui (1991), and by Tissaoui (1991), the shear modulus to be specified was  $1.6 \times 10^5$  psi and the Young's modulus was  $1.8 \times 10^6$  psi. However, as stated in Chapter 3, ABAQUS used a value of  $6.0 \times 10^5$  psi instead of  $1.6 \times 10^5$  psi for the shear modulus. It is thus important to determine the effect of this on the dome behavior, and to verify if the results from the previous research are within close proximity of those which are obtained when using the correct shear modulus.

Since wood is produced under uncontrolled natural environmental conditions, it

has variable physical properties. It is thus essential to determine if the value of  $6.0 \times 10^6$  psi is a reasonable estimate of the shear modulus. An article by Bodig (1975), gives a method to compute the shear modulus of woods from the longitudinal modulus. In the nonlinear material model, the initial longitudinal modulus in tension  $E_{(tension)} = 1.8 \times 10^6$  psi and the initial longitudinal modulus in compression  $E_{(compression)} = 2.1 \times 10^6$  psi. From the Wood Handbook (1974), it is observed that the maximum value of Young's modulus for any wood is  $2.05 \times 10^6$  psi. Hence, shear moduli computed from the elasticity moduli  $E_{(tension)}$  and  $E_{(compression)}$  respectively, will give a good estimate of the range of shear modulus for wood. The values of shear moduli computed from these longitudinal moduli values are given in Table 5.3. It is thus observed that the shear modulus value of  $6.0 \times 10^5$  psi is nearly four times larger than the largest shear modulus value in Table 5.3. Hence, it is essential to study the effect the reduction in the shear modulus will have on the stability behavior of the dome.

**TABLE 5.3 Range of Values for the Shear Modulus**

LONGITUDINAL MODULUS	TYPE OF WOOD	MAXIMUM VALUE OF SHEAR MODULUS	MINIMUM VALUE OF SHEAR MODULUS
$1.8 \times 10^6$ psi	SOFTWOOD	$1.1 \times 10^5$ psi	$1.2 \times 10^4$ psi
	HARDWOOD	$1.4 \times 10^5$ psi	$3.2 \times 10^4$ psi
$2.1 \times 10^6$ psi	SOFTWOOD	$1.2 \times 10^5$ psi	$1.3 \times 10^4$ psi
	HARDWOOD	$1.6 \times 10^5$ psi	$3.8 \times 10^4$ psi

Two dome cap models, one with shear modulus  $G=6.0 \times 10^5$  psi, and the other with a shear modulus  $G=1.6 \times 10^5$  psi are analysed. These models have the original mesh configuration, as given in Fig.4.4 and described in Section 4.2. To find the loading case under which the dome cap behavior will be more sensitive to the change in shear modulus, the full snow load and half snow load cases are considered. The nomenclature used for the dome models, and the analysis results are presented below.

For the case of snow over the complete dome (full snow load case), the following models are analysed:

1. Linear-1F with  $E=1.8 \times 10^6$  psi and  $G=6.0 \times 10^5$  psi.
2. Linear-2F with  $E=1.8 \times 10^6$  psi and  $G=1.6 \times 10^5$  psi.

And, for the case of snow over half the dome (half snow load case), the following models are analysed:

1. Linear-1H with  $E=1.8 \times 10^6$  psi and  $G=6.0 \times 10^5$  psi.
2. Linear-2H with  $E=1.8 \times 10^6$  psi and  $G=1.6 \times 10^5$  psi.

The 'F' at the end of each model name indicates the full snow load condition and the 'H' indicates the half snow load condition. As stated earlier, the critical load factors for all the dome cap models are found to be the limit loads.

For the dome cap model Linear-1F, the critical snow load factor is 12.37. The load deflection path for the node 1 in the vertical direction is shown in Fig.5.1. The stress outputs are in the form of combined axial and bending stresses. It is observed that the maximum stresses at the critical load are between the proportional limit and the ultimate stress (Table 5.1). The maximum stresses at the limit point are as follows:

Maximum tensile stress : 5665 psi, in element 5 at node 2

Maximum compressive stress : 7001 psi, in element 2 at node 2

For the dome cap model Linear-2F, the critical load factor is again 12.37. From Fig.5.1, it is seen that load deflection paths for Linear-1F and Linear-2F models coincide. This indicates that the shear modulus  $G$  is not an important parameter affecting the behavior of the dome under cyclically symmetric loading. The maximum stresses at the limit point reinforce the fact that the shear modulus does not affect at all the behavior of these two domes. The stresses obtained are:

Maximum tensile stress : 5662 psi, in element 5 at node 2

Maximum compressive stress : 6999 psi, in element 2 at node 2

The critical load factor for the dome cap model Linear-1H is 11.60. The load deflection path for node 4 in the vertical direction is shown in Fig.5.2. The maximum stresses at the limit point for this case are over 50% larger than the corresponding full snow load case. The maximum stress in tension is below the ultimate (Table 5.1) and the maximum stress in compression is beyond the ultimate stress. The values for the maximum stresses are:

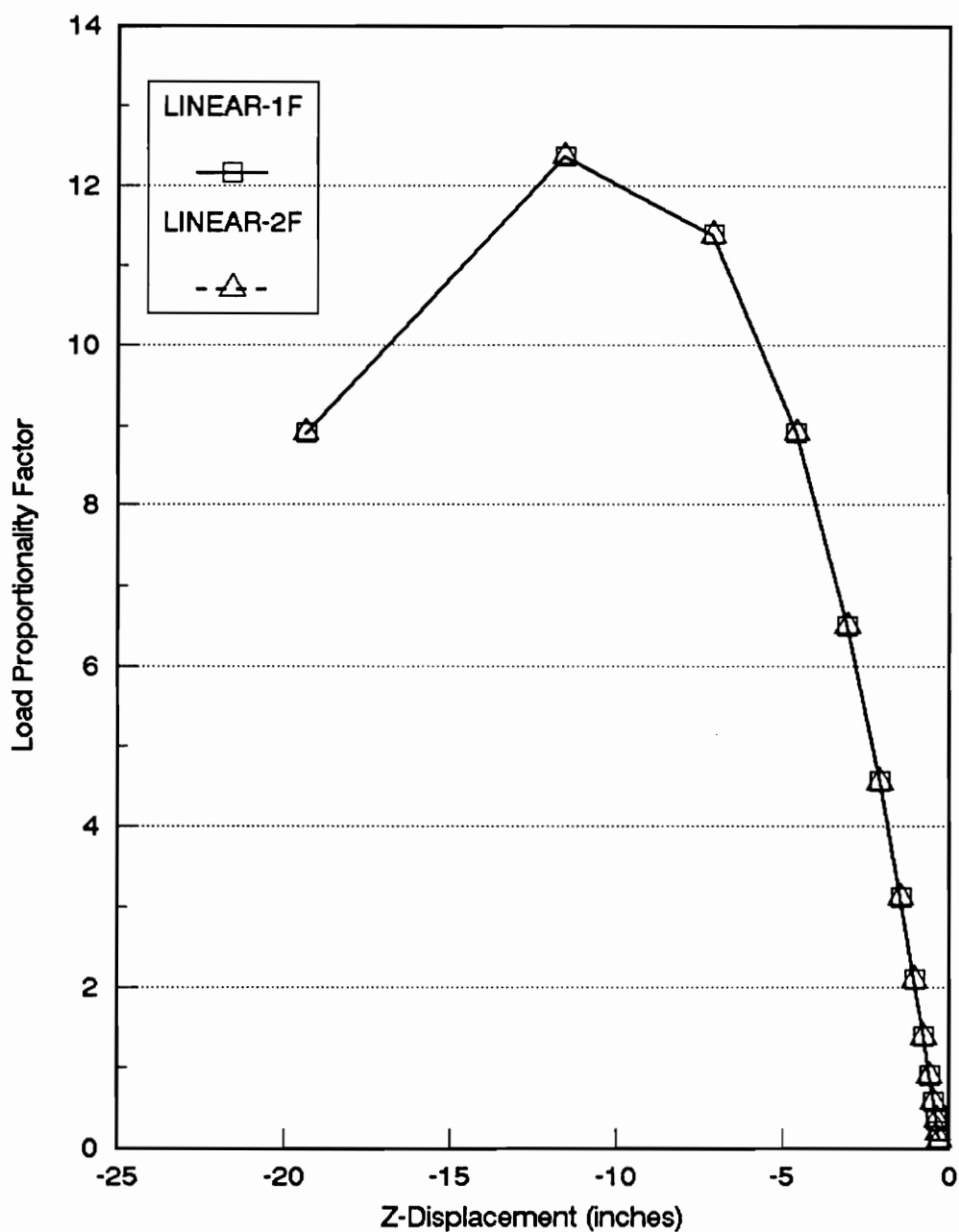


**FIG.5.1 DOME CAP WITH FULL SNOW LOAD  
RESPONSE FOR DIFFERENT VALUES OF SHEAR MODULI  
Load Proportionality Factor vs. Z-Displacement**

Maximum tensile Stress : 13588 psi, in element 5 at node 2

Maximum compressive Stress : 16571 psi, in element 1 at node 4

The critical load factor for dome cap model Linear-2H is 11.14. The load deflection path in Fig.5.2 indicates that the change in the shear modulus affects the critical load factor as well as the nature of the load deflection path. The decrease in the shear modulus makes the response of this model softer as compared to dome cap model Linear-1H. Hence, in the case of cyclically unsymmetric loading, the shear modulus does affect the response of the dome cap. In the dome with half snow load, the beams undergo torsion and hence the shear modulus causes change in their response as the shear modulus affects the torsional stiffness of the beams. There is negligible torsion in the beams for the full snow load case, hence there is no effect of the change in the shear modulus on the dome response.

The maximum stresses at limit point for the dome cap model Linear-2H are given below. It is again seen that the stresses are very large, but the tensile stress is below the ultimate where as the compressive stress is beyond the ultimate stress value (Table 5.1). The stresses in this case are higher than those in the previous case. The maximum stresses are:

Maximum tensile stress : 14099 psi, in element 5 at node 2

Maximum compressive stress : 17032 psi, in element 1 at node 4

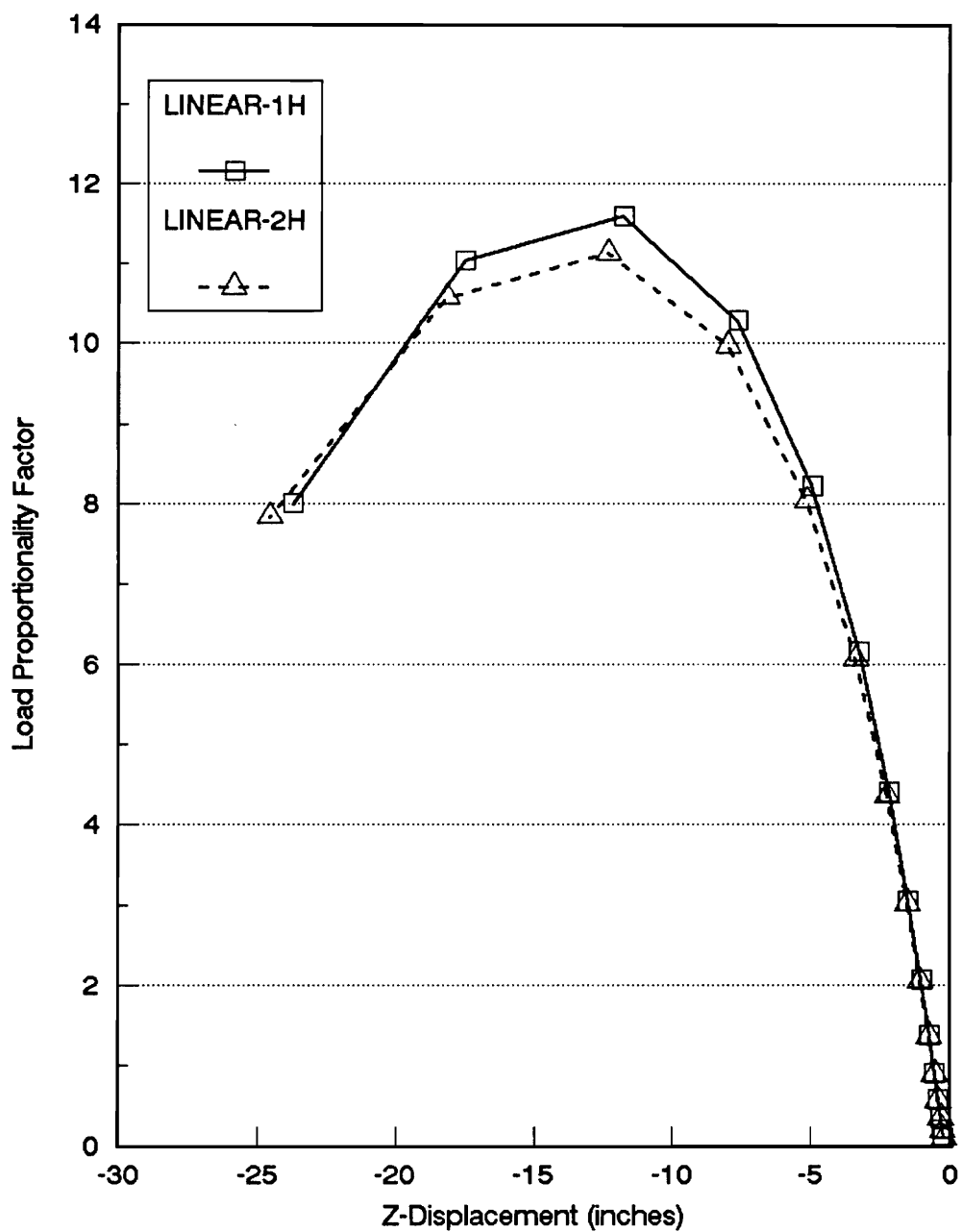


**FIG.5.2 DOME CAP WITH HALF SNOW LOAD  
RESPONSE FOR DIFFERENT VALUES OF SHEAR MODULI  
Load Proportionality Factor vs. Z-Displacement**

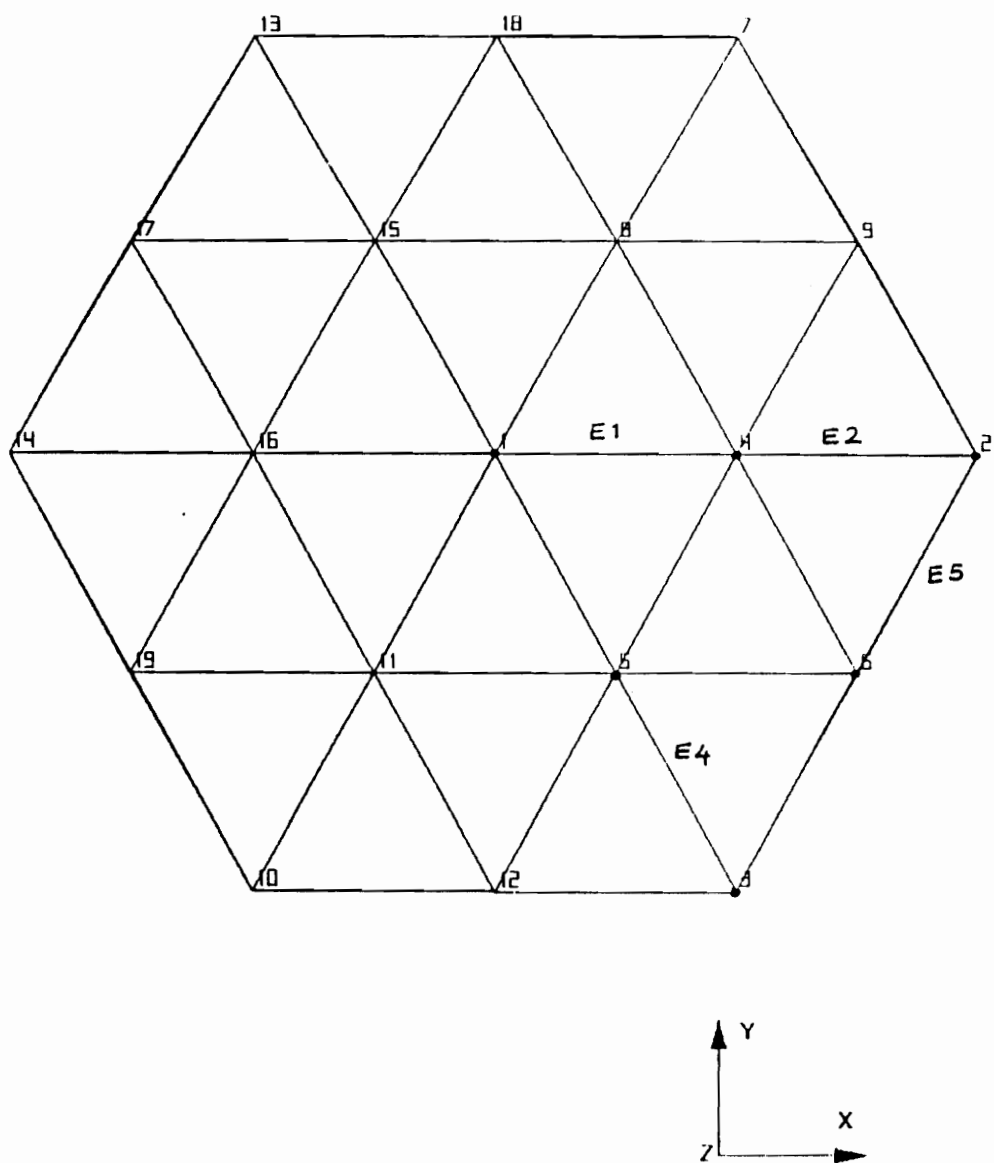


**FIG.5.3 DOME CAP NODES, ORIGINAL MESH**

The location of the nodes at which the maximum stresses occur are shown in Fig.5.3.

## **5.5 Effect of Material Nonlinearity on the Dome Cap Behavior**

The effect of nonlinearity of the material law on the stability behavior is studied by analysing several models of the dome cap under the half snow and full snow loading. The dome cap models analysed here have the original mesh configuration, where each beam is modelled by two elements. The configuration of the model is shown in Fig.4.4, and described in Section 4.2.

The nonlinearity of the stress strain law is expected to reduce the critical load for the dome cap models. It is also estimated that the dome cap models which have higher stresses at the critical load will be more influenced by the nonlinearity of the stress strain law. The justification of using the bilinear stress strain law is also verified in the following analyses.

For the case of full snow load, three different models of the dome cap are analyzed. These models are based on the material law used for the beam elements, and are labelled as followed:

1. Linear-2F with  $E=1.8 \times 10^6$  psi and  $G=1.6 \times 10^5$  psi.
2. Linear-3F with  $E=2.1 \times 10^6$  psi and  $G=1.6 \times 10^5$  psi.
3. Nonlinear-F

The results for the Linear-2F model are already presented in Section 5.4. The load deflection path for this model is again presented in Fig.5.4 to compare it with those for the other two models.

The critical load factor for dome cap model Linear-3F is 14.73 and shows a much stiffer response than that of Linear-2F. Even though there is about 19% difference in the critical load factor between this and the Linear-2F, the effect on the stresses is negligible. The deflections seem to be more sensitive to the change in modulus of elasticity than the critical load factor. The vertical deflection at the limit point at the apex for the dome cap model Linear-2F is 12.5 inches, whereas that for dome cap model Linear-3F is just about 6 inches, a difference of about 50%. The maximum stresses at the limit point in dome cap model Linear-3F are:

Maximum tensile stress : 6108 psi, in element 5 at node 2

Maximum compressive stress : 7088 psi, in element 2 at node 2

The load deflection curve for the dome cap model Nonlinear-F, in Fig.5.4, lies between those for Linear-1F and Linear-3F. It will thus be more appropriate to compare the response of the dome with nonlinear material law with a dome having a linear material law similar to the linear portion of the nonlinear material law. To check this fact, another model of the dome is created with bilinear

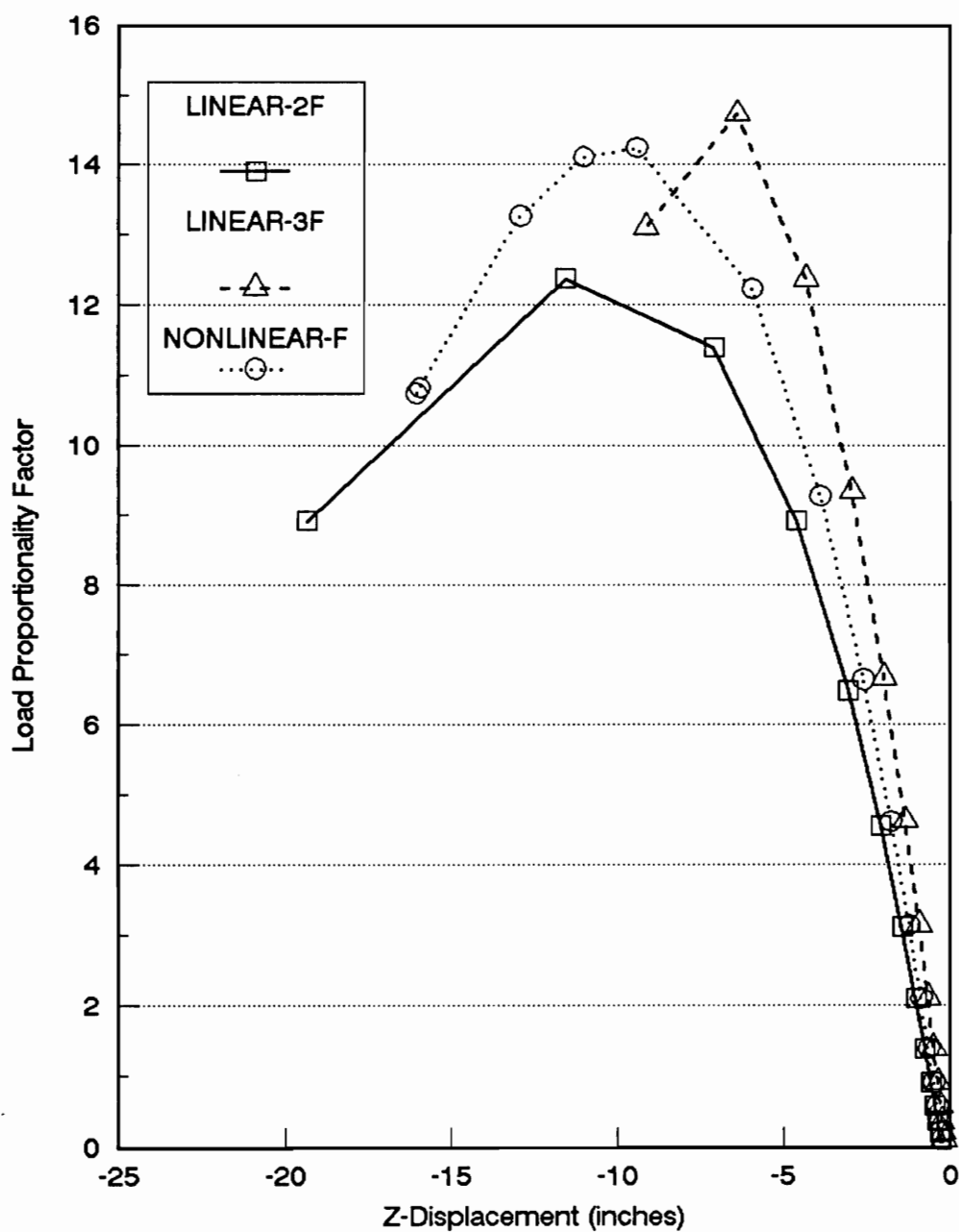


**FIG.5.4 DOME CAP WITH FULL SNOW LOAD  
RESPONSE FOR DIFFERENT MATERIAL LAWS  
Load Proportionality Factor vs. Z-Displacement**

material law for the beam elements. This model is tested for the case of half snow load to check if it is a better model for comparing the response of the dome cap with material nonlinearity.

The critical load factor for the dome cap model Nonlinear-F is 14.25. The maximum stresses at failure are found to be lower than those with linear material law. The reason for the lower stresses in the inelastic domes despite the higher critical load factors is described in detail in section 5.7. The maximum stresses at the limit point for the dome cap model Nonlinear-F are,

Maximum tensile stress : 5359 psi, in element 5 at node 2

Maximum Compressive Stress : 6919 psi, in element 2 at node 2

For the case of half snow load, two different models of the dome cap are analysed. These models are based on the material law used for the beam elements, and are labelled as :

1. Bilinear-H, with  $E_{(tension)}=1.8 \times 10^6$  psi,  $E_{(compression)}=2.1 \times 10^6$  psi and  $G=1.6 \times 10^5$  psi.
2. Nonlinear-H

The critical load factor for the dome cap model Bilinear-H is 12.68. The load deflection path is shown in Fig.5.5, and the maximum stresses at the limit point are presented below. It is seen that the tensile stress is lower than that for dome cap model Linear-2H (Section 5.4), whereas the compressive stress is higher than

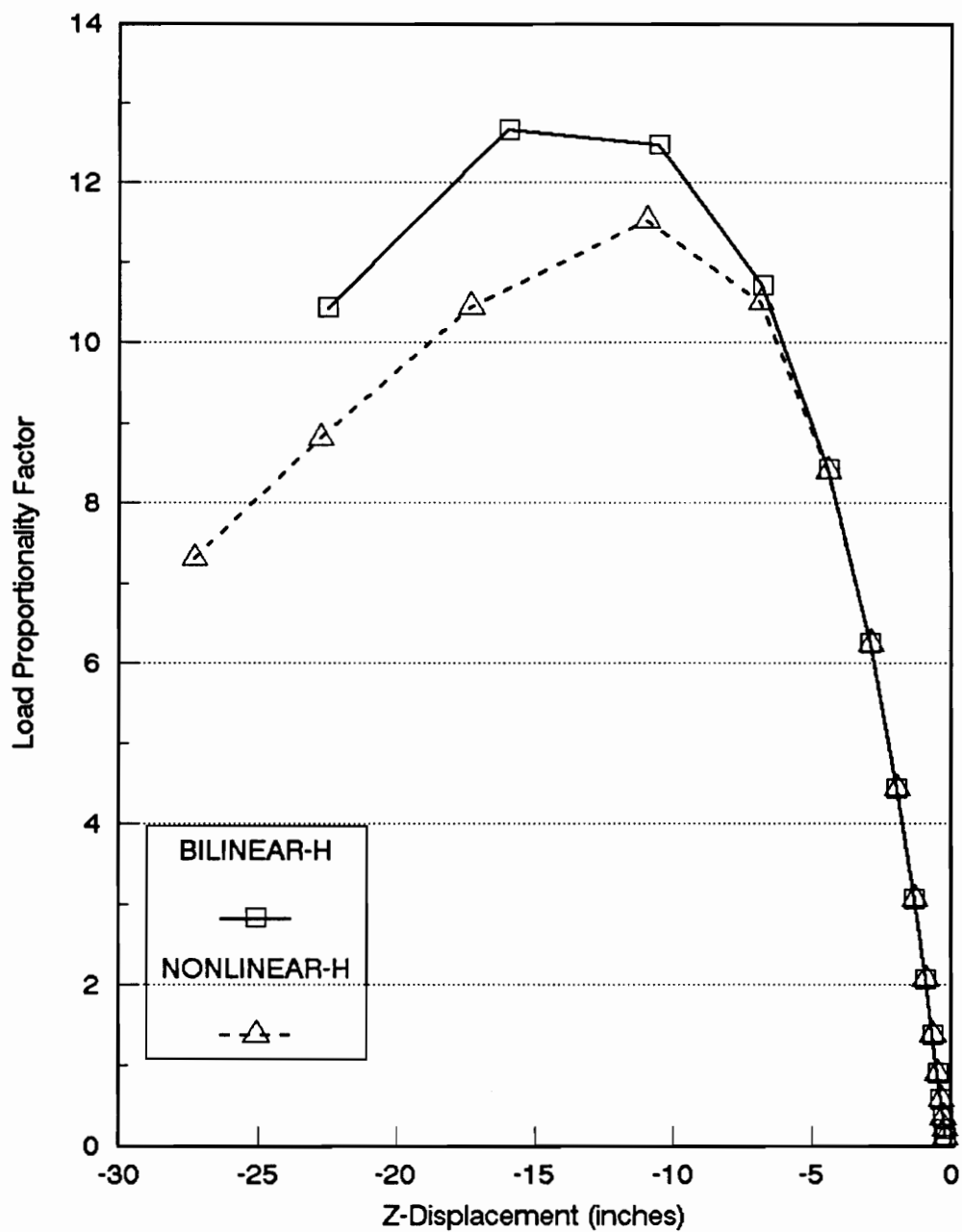


**FIG.5.5 DOME CAP WITH HALF SNOW LOAD  
RESPONSE FOR DIFFERENT MATERIAL LAWS  
Load Proportionality Factor vs. Z-Displacement**

before. Again, the tensile stress is below the ultimate while the compressive stress is above the ultimate stress value (Table 5.1).

Maximum tensile stress : 12673 psi, in element 5 at node 2

Maximum Compressive Stress : 17923 psi, in element 1 at node 4

The bilinearity of the stress strain law seems to force the beams to undergo larger compressive stresses and smaller tensile stresses as compared to the model with linear material law.

The critical load factor for the dome cap model Nonlinear-H is 11.53. The load deflection path in Fig.5.5 coincides for the initial linear range with that for the dome cap model Bilinear-H. After a certain load though, the load deflection path for the Nonlinear-H case shows a softer response, indicating the gradual yielding of the material. The maximum stresses at failure for the Nonlinear-H model are given below.

Maximum tensile stress : 11457 psi, in element 5 at node 2

Maximum Compressive Stress : 10496 psi, in element 4 at node 5

The location of nodes where maximum stresses occur are shown in Fig.5.3.

## 5.6 Mesh Refinement Studies on the Dome Cap

For the mesh refinement studies, only the half snow load condition is considered. Six dome cap models are analysed. Out of these, three models have nonlinear material law for the beams while the other three have the bilinear law. Three different mesh configurations make up the three models under each material law. The mesh configurations are discussed in Section 4.2 and the original mesh and the refined mesh configurations are shown in Fig.4.4 and Fig.4.5 respectively. The models with bilinear material law are labelled as follows:

1. Bilinear-H, the model with the original mesh.
2. Bilinear-HR, where the 'R' stands for the refined mesh.
3. Bilinear-HC, where the 'C' stands for the connector elements.

Similarly, the inelastic models are labelled as:

1. Nonlinear-H, the model with the original mesh.
2. Nonlinear-HR, where the 'R' stands for the refined mesh.

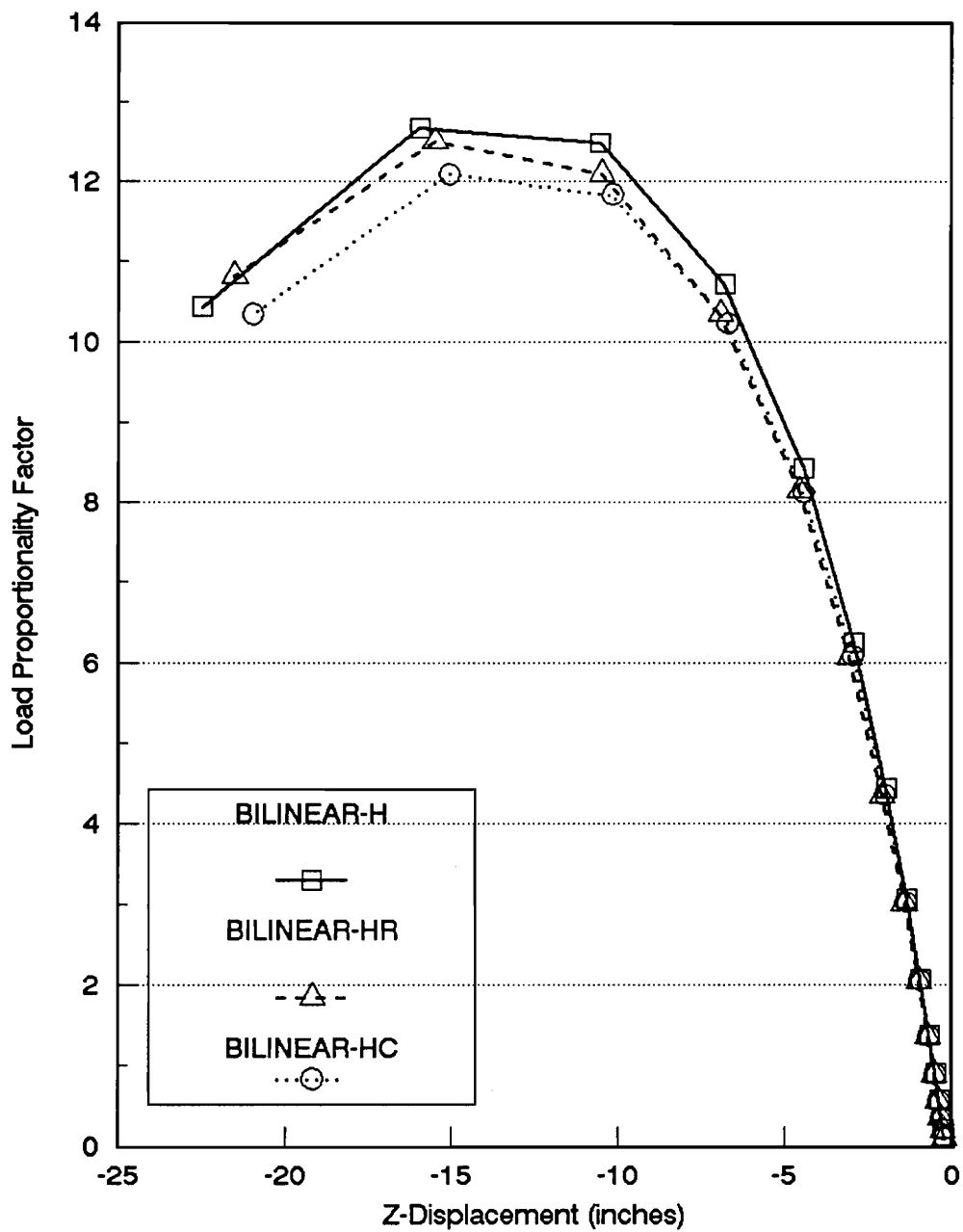


**FIG.5.6 DOME CAP MESH REFINEMENT STUDIES  
BILINEAR MATERIAL LAW AND HALF SNOW LOAD  
Load Proportionality Factor vs. Z-Displacement**

### 3. Nonlinear-HC, where the 'C' stands for the connector (or hinge) elements.

The critical load factor for the dome cap model Bilinear-HR is 12.51 while that for the Bilinear-HC is 12.09. The load deflection curves for the dome cap with bilinear elastic material law are given in Fig.5.6. It can be seen that the mesh refinement

softens the response of the dome. The model with connector elements show the softest response, followed by the model with refined mesh and then the original model. It is thus observed that sufficient refinement of the mesh would give results closest to the response of an ideal dome. It is also observed that the selective refinement of the mesh, i.e. inserting connector or hinge elements, gives a better response for the dome cap because the finite element solution converges to the continuum solution when the mesh is refined.

The critical load factors for the dome cap model Nonlinear-HR is 11.29 and that for Nonlinear-HC is 11.07. The nature of the load deflection paths for the inelastic dome caps are similar to those for the bilinear dome caps. These are given in Fig.5.7.

As the mesh is refined, the lengths of successive load increments past the limit point start decreasing. This indicates the increasing effort required to get a convergent solution. For the dome cap model Nonlinear-HC, the final few points are nearly coincident, indicating the beginning of convergence problems.

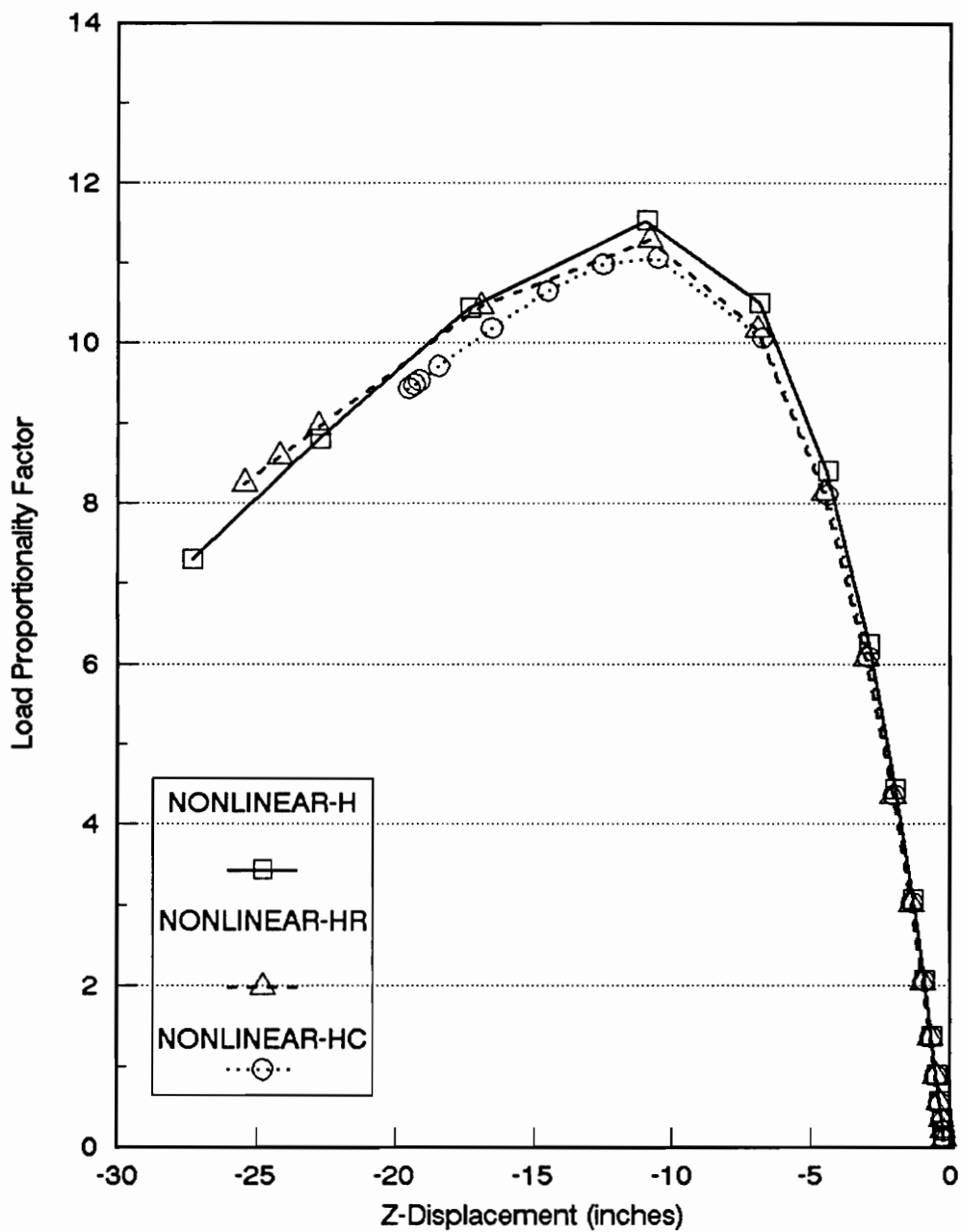


**FIG.5.7 DOME CAP MESH REFINEMENT STUDIES  
NONLINEAR MATERIAL LAW AND HALF SNOW LOAD  
Load Proportionality Factor vs. Z-Displacement**

Of the six models analysed, the convergence problems occur only in the Nonlinear-HC model. Several analysis runs of the Nonlinear-HC models were attempted by relaxing the convergence tolerances for loads and moments. The load tolerances were gradually relaxed from 1% to 20% of the nodal load at the apex. The relaxing of the tolerances did not help in alleviating the convergence problems. Further relaxation of tolerances would be futile, as it would keep reducing the accuracy of the solution with no guarantee of solving the convergence problems. It can be inferred from the program runs that the convergence problems are not due to a very tight tolerance value. The cause for the convergence problems could be due to the combined effect of the inelastic material law and the size of the connector elements, effectively causing very stiff elements next to very soft ones.

## **5.7 Analyses of the Dome**

A limited number of cases are analysed for the complete dome model. The comparative study of the dome is divided into three classes. In each of these classes the effect of only a specific group of properties on the dome behavior is studied.

In two of the three groups, only one load condition of half snow load is considered.

In the remaining group, the dome models are analysed for both half and full snow load conditions. The different models in each group are obtained by varying the material law for the beam elements.

Except in the case of mesh refinement studies, the dome models have the original configuration where each physical beam is modelled with two elements. The dome model is discussed in Section 4.2, and is illustrated in Fig.4.1.

In the analysis of the complete dome models it is observed that the critical loads for the dome models correspond to the limit points, thus are also the limit loads.

## **5.8 Effect of Shear Modulus on the Dome Behavior**

Tests are conducted on two dome models. The first model is similar to the model used by Wu (1991). It has elastic material law and has the shear modulus same as used by Wu (1991). The only difference is that Wu (1991) has used connector elements with variable stiffness to model the triax joints. The case with 100% joint stiffness would be the same as the model being analysed here. The second model is same as the first model except the shear modulus is reduced. The nomenclature used for the models, and the values for the moduli are given below:

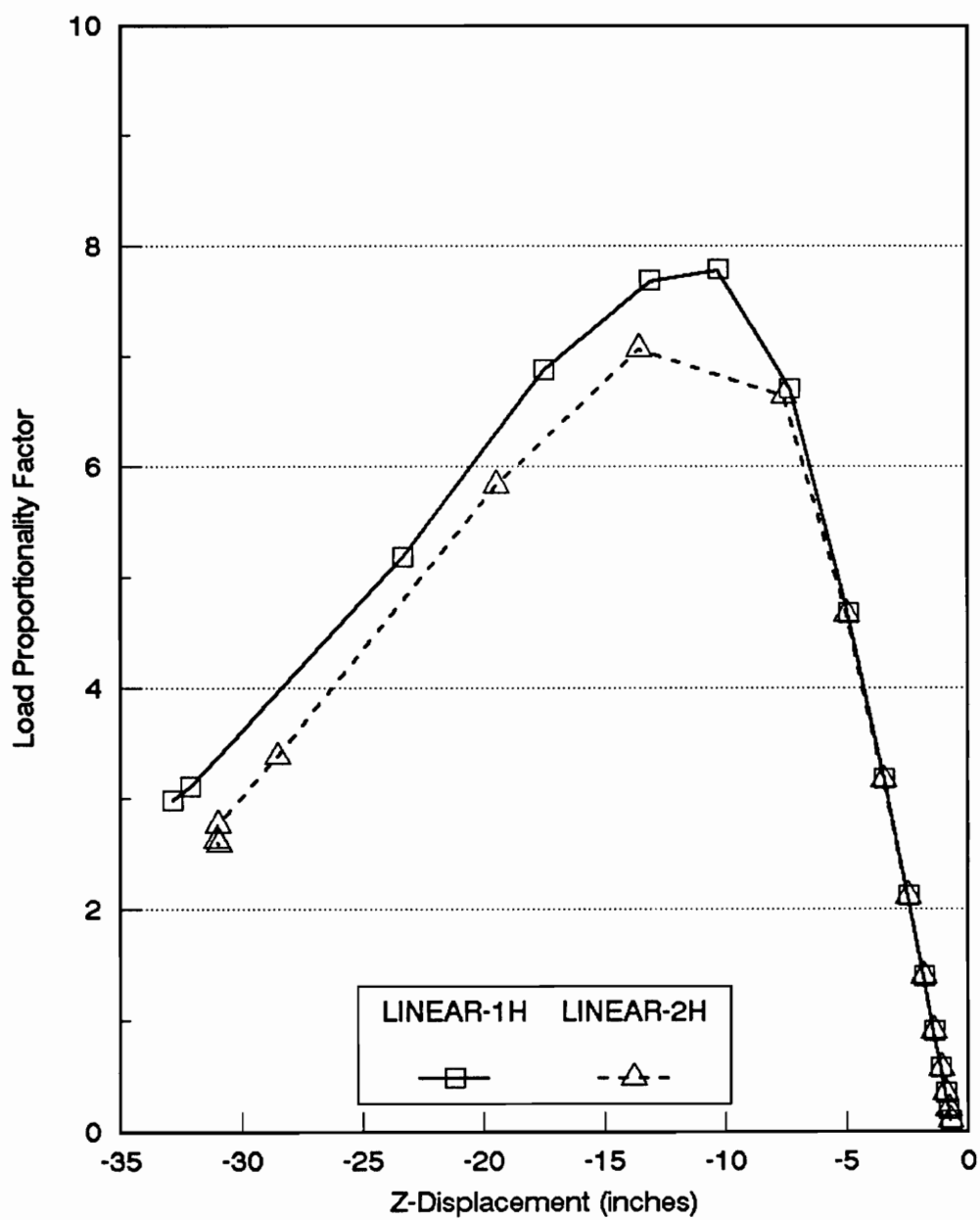


**FIG.5.8 DOME WITH HALF SNOW LOAD  
EFFECT OF CHANGE IN SHEAR MODULUS  
Load Proportionality Factor vs. Z-Displacement**

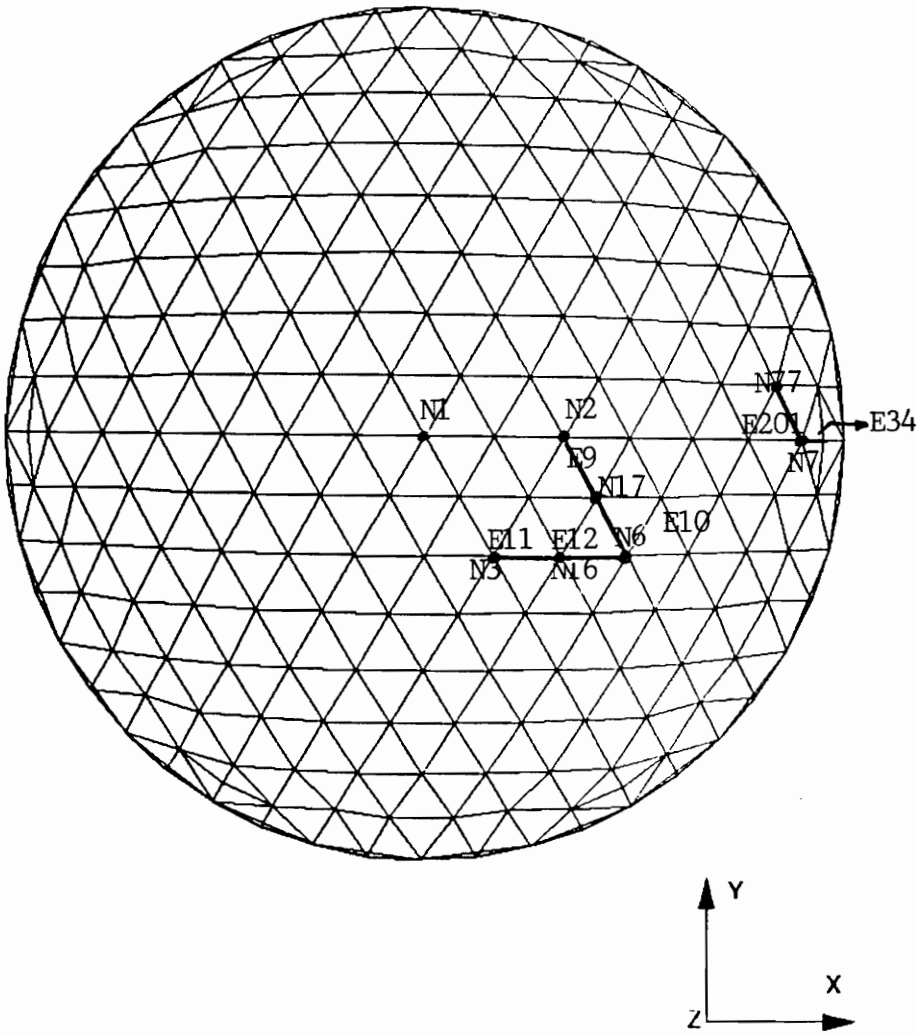


**FIG.5.9 DOME NODES, ORIGINAL MESH**

1. Linear-1H with  $E=1.8 \times 10^6$  psi and  $G=6.0 \times 10^5$  psi. (Wu's (1991) model )
2. Linear-2H with  $E=1.8 \times 10^6$  psi and  $G=1.6 \times 10^5$  psi.

The 'H' stands for half snow load.

The critical load factor for the dome model Linear-1H is 7.72, which is the same as that obtained by Wu (1991). The load deflection path is shown in Fig.5.8. The maximum stresses at failure in the dome model Linear-1H are:

Maximum tensile stress : 8099 psi, in element 11 at node 16

Maximum compressive Stress : 17363 psi, in element 11 at node 16

The critical load factor for the dome model Linear-2H is 7.08. It is observed that the change in the shear modulus has a considerable effect on the load deflection path and the critical load, Fig.5.8. The lowering of the shear modulus causes the dome response to be softer. The maximum stresses at failure for this dome model are much lower than those for the dome model Linear-1H. It is observed that the reduction in the shear modulus tends to reduce the critical load factor, and the maximum stresses at failure. The maximum stresses at failure are below the ultimate stress values (Table 5.1).

Maximum tensile stress : 4971 psi, in element 10 at node 17

Maximum Compressive Stress : 8811 psi, in element 11 at node 16

The nodes where the maximum stresses occur are shown in Fig.5.9.

The buckling modes for both the models are similar. They show local buckling in the form of small dimples on the side of the applied snow load.

## 5.9 Effect of Material Nonlinearity on the Behavior of the Dome Models

Four models are tested to study the behavior of the complete dome with nonlinear material law. A model with bilinear material law and one with nonlinear material law are analysed for full snow and half snow load conditions. The nomenclature used for the dome models is given below. For the full snow load condition, the models are:

1. Bilinear-F, with  $E_{(tension)}=1.8 \times 10^6$  psi,  $E_{(compression)}=2.1 \times 10^6$  psi and  $G=1.6 \times 10^5$  psi.
2. Nonlinear-F

The 'F' stands for the full snow load condition. For half snow load condition the extension 'H' is used. The models with half snow load condition are:

1. Bilinear-H, with  $E_{(tension)}=1.8 \times 10^6$  psi,  $E_{(compression)}=2.1 \times 10^6$  psi and  $G=1.6 \times 10^5$  psi.

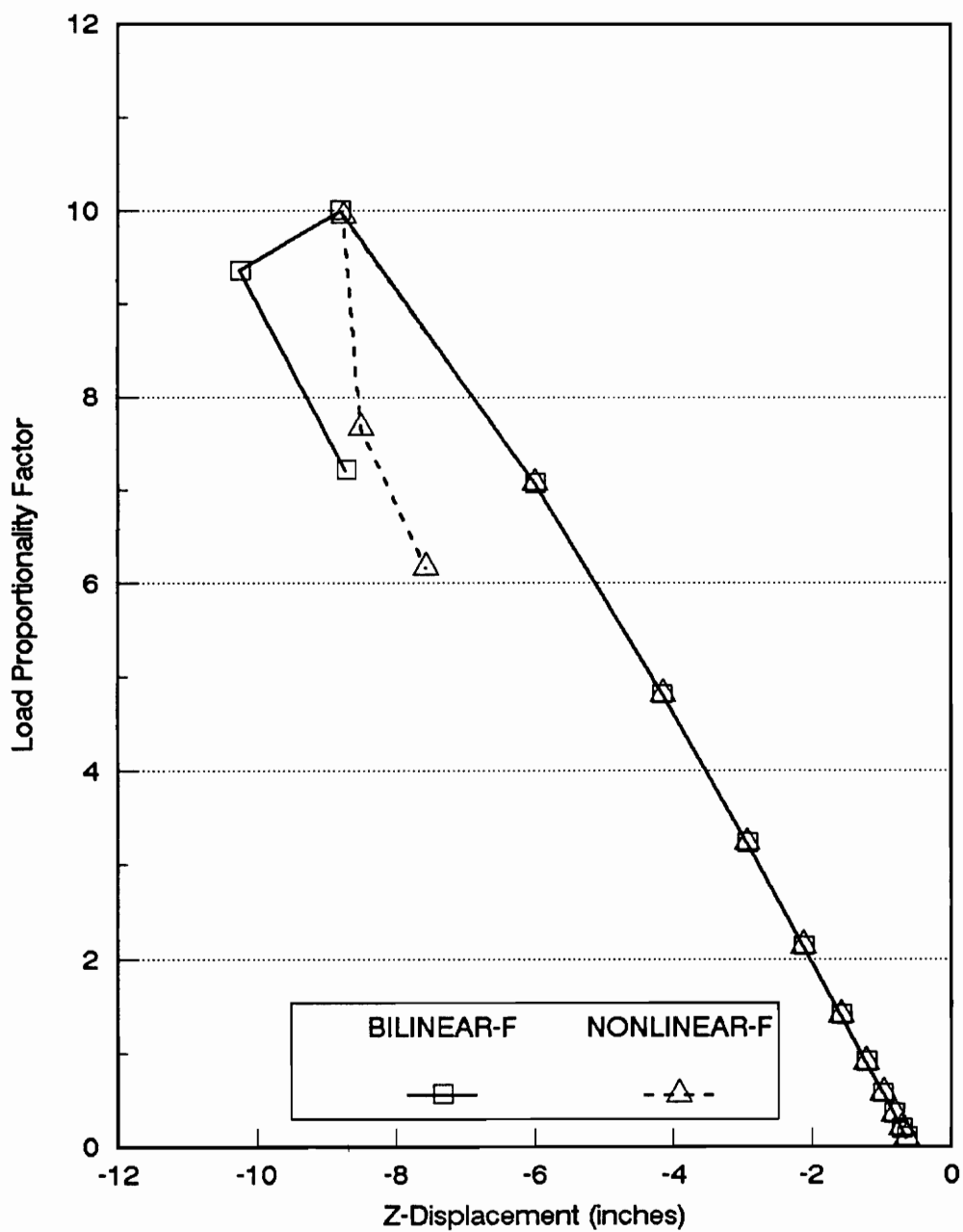


**FIG.5.10 DOME WITH FULL SNOW LOAD  
DOME BEHAVIOR FOR BILINEAR AND NONLINEAR MATERIAL  
Load Proportionality Factor vs. Z-Displacement**

## 2. Nonlinear-H

The critical load factor for the dome model Bilinear-F is 9.99. The load deflection path is shown in Fig.5.10. The maximum stresses at the limit point are given below. The maximum compressive stress is beyond the proportional limit whereas the Maximum tensile stress is below the proportional limit (Table 5.1).

Maximum tensile stress : 3747 psi, in element 201 at node 77

Maximum compressive Stress : 11535 psi, in element 37 at node 7

The critical load factor for the dome model Nonlinear-F is 9.94. From the load deflection path in Fig.5.10, it can be seen that for full snow load case, the inelastic behavior is not much different from the elastic behavior. The maximum compressive stress and the maximum tensile stress at the limit point are between the proportional limit and the ultimate stress (Table 5.2). The maximum stresses are:

Maximum tensile stress : 3740 psi, in element 201 at node 77

Maximum compressive Stress : 9985 psi, in element 37 at node 7

The nodes at which the maximum stresses occur are shown in Fig.5.9.

The buckling load is at the limit point, and the buckling mode is in the form of cyclically symmetric failure around the base of the dome with the formation of dimples at the location of failure. The failure modes for both the models are identical.

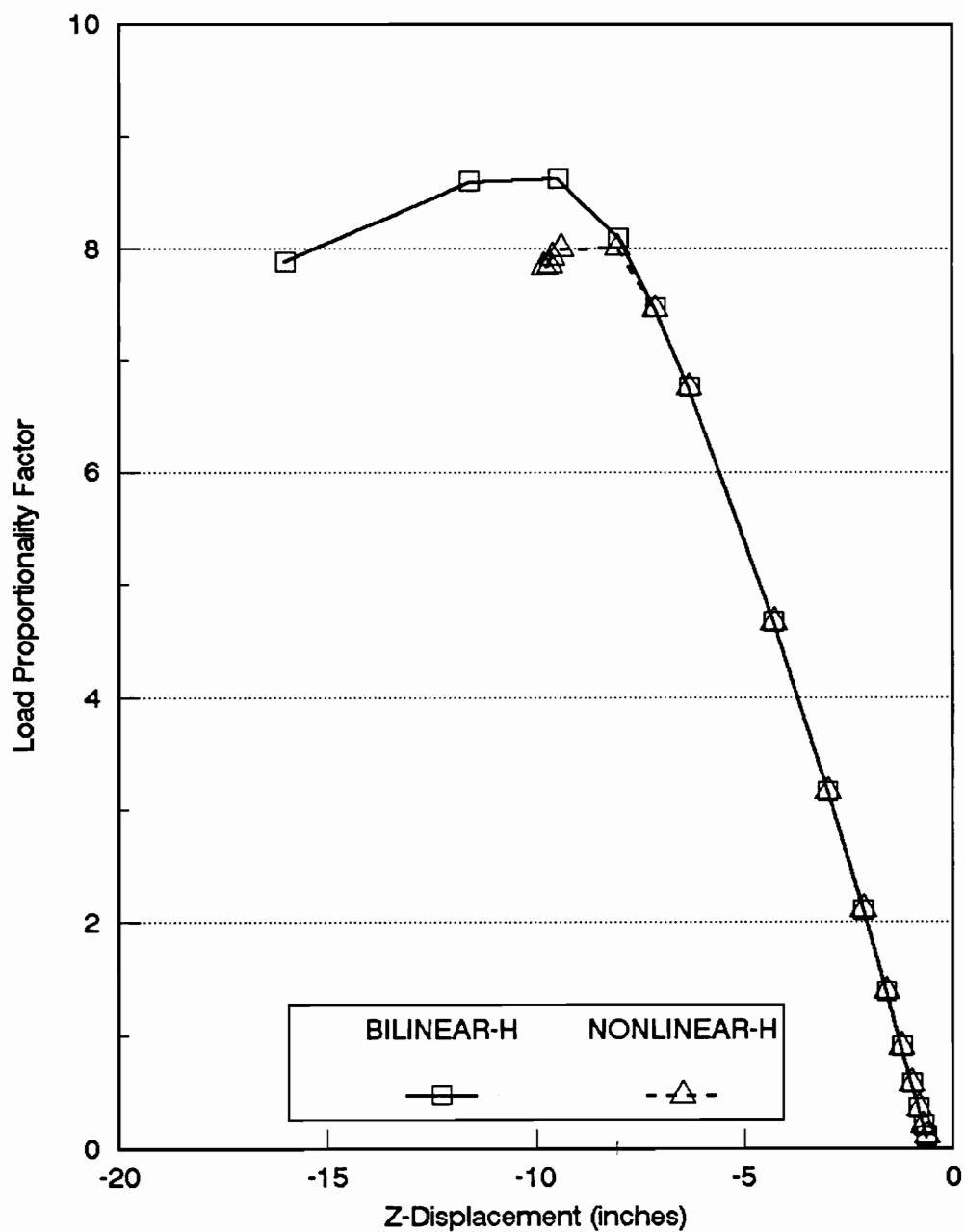


**FIG.5.11 DOME WITH HALF SNOW LOAD  
DOME BEHAVIOR FOR BILINEAR AND NONLINEAR MATERIAL  
Load Proportionality Factor vs. Z-Displacement**

The analysis results for dome models with half snow load and nonlinear material law are given below.

The critical load factor for the dome model Bilinear-H is 8.63. The load deflection path for this model is shown in Fig.5.11. The maximum stresses at critical load, which is also the limit load, are given below. The maximum compressive stress is beyond the ultimate stress while the maximum tensile stress is between the proportional limit and the ultimate stress (Table 5.1).

Maximum tensile stress : 5862 psi, in element 9 at node 17

Maximum Compressive Stress : 16546 psi, in element 11 at node 16

For the dome model Nonlinear-H, the critical load factor is 8.01. From the load deflection path shown in Fig.5.11, it can be observed that the materially nonlinear behavior of the dome with half snow load is thus softer than the elastic behavior. The stresses at failure are given below. The maximum compressive stress is at the plastic stress level. The maximum tensile stress lies between the proportional limit and the ultimate stress (Table 5.2).

Maximum tensile stress : 7467 psi, in element 11 at node 16

Maximum Compressive Stress : 10496 psi, in element 12 at node 6

The nodes at which the maximum stresses occur are shown in Fig.5.9.

The buckling mode for the dome models with half snow loads shows localised dimples on the side of the applied snow load, indicating local failure at the

location of these dimples. The buckling modes are the same for the dome models with linear and nonlinear material laws for the load case of half snow load.

#### **5.10 Mesh Refinement Studies of the Dome Model**

For the mesh refinement studies, only the half snow load condition is considered. Four models are analysed. Of these four, two have bilinear material laws, whereas the other two have nonlinear material laws. Two different mesh configurations make up the two models under each material law. The descriptions of the meshes are given in Section 4.1 and illustrated in Fig.4.1 and Fig.4.3. In the original mesh, each physical beam is modelled by two elements while in the refined mesh, four elements are used to model each physical beam. Hence the mesh in the refined mesh model is twice as fine as the dome model with the original mesh. The models with linear material law are labeled as:

1. Bilinear-H, the model with the original mesh.
2. Bilinear-HR, where the 'R' stands for the refined mesh.

Similarly, the inelastic models are labeled as:

1. Nonlinear-H, the model with the original mesh.

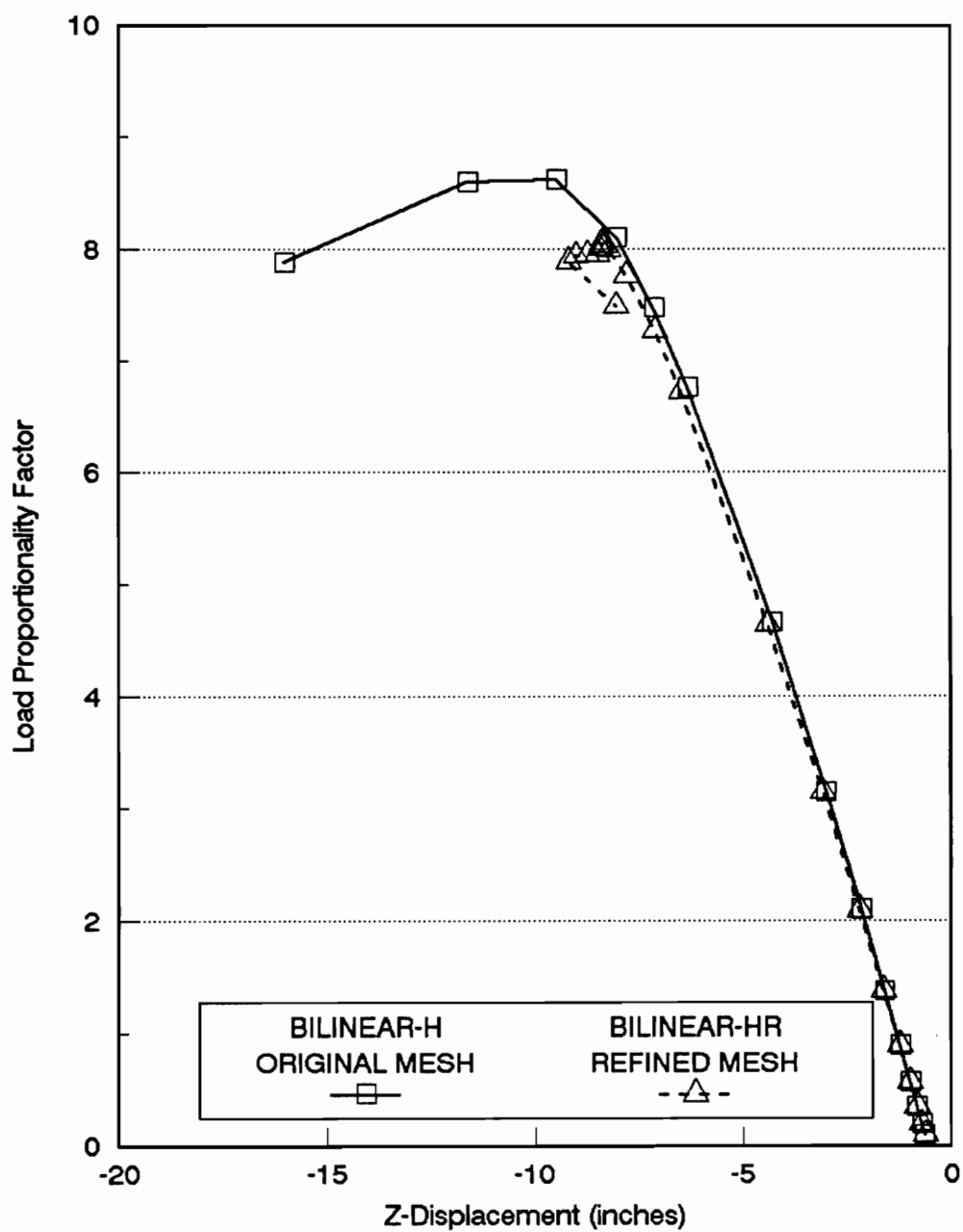


**FIG.5.12 DOME WITH HALF SNOW LOAD  
MESH REFINEMENT STUDIES, BILINEAR RESPONSE  
Load Proportionality Factor vs. Z-Displacement**

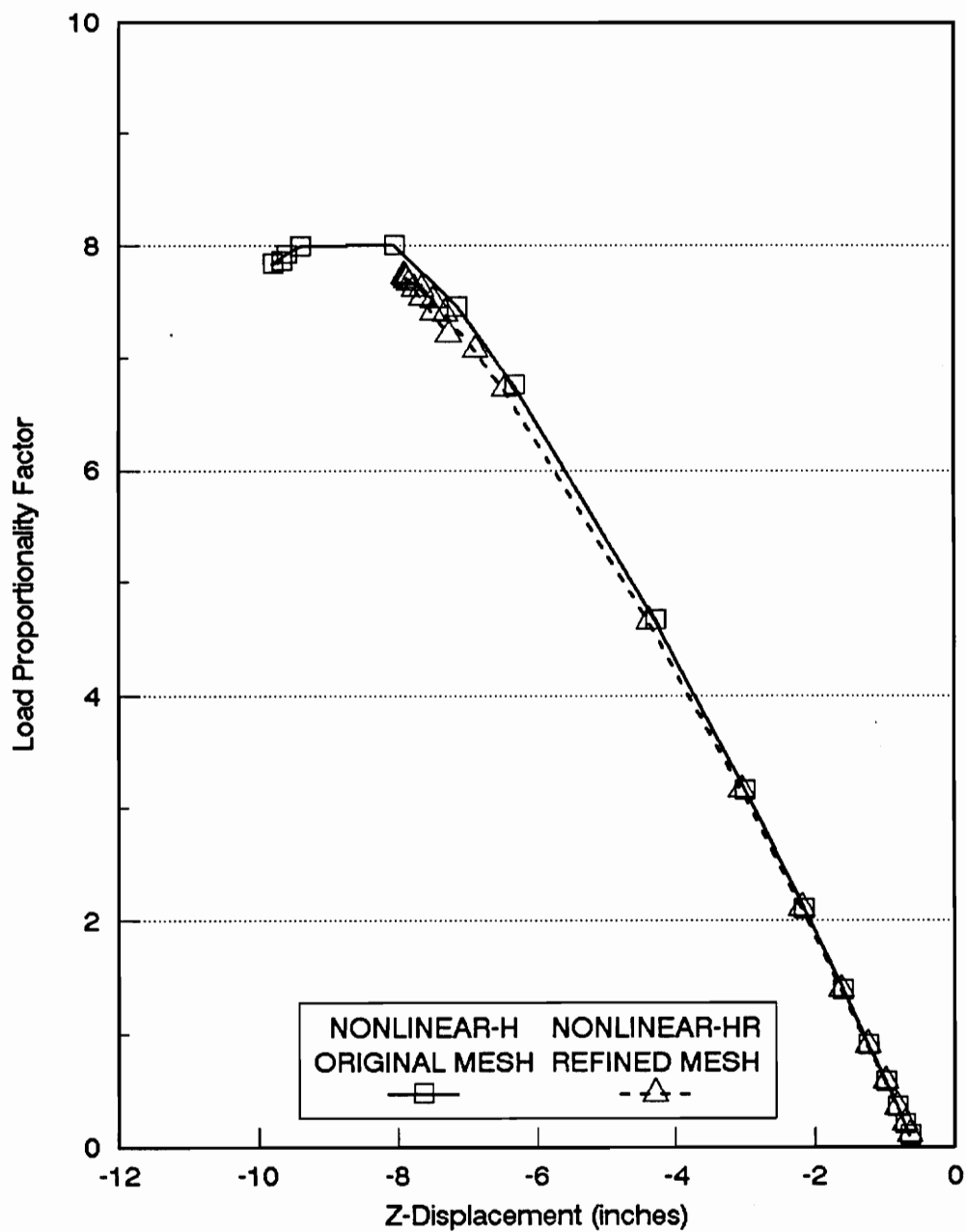


**FIG.5.13 DOME WITH HALF SNOW LOAD  
MESH REFINEMENT STUDIES, NONLINEAR RESPONSE  
Load Proportionality Factor vs. Z-Displacement**

2. Nonlinear-HR, where the 'R' stands for the refined mesh.

The use of connector (hinge) elements in the dome models did not give good results, and are not presented here. The analysis of the dome model with connector elements and inelastic material law gave convergence problems. These convergence problems are attributed to the combined effect of the size of the connector elements and the inelastic material law. Further studies need to be done by using different sizes of connector elements and different element types.

The critical load factor for the dome model Bilinear-H is 8.63 while that for the Bilinear-HR is 8.06. The load deflection curves for the dome with bilinear elastic material law are given in Fig.5.12. It can be seen that the mesh refinement softens the response of the dome. Although the difference in the critical loads for the two models is not very large, sufficient refinement of the mesh would give results closest to the response of an ideal dome.

The critical load factors for the dome model Nonlinear-H is 8.01 and that for Nonlinear-HR is 7.74. The nature of the load deflection paths for the inelastic dome caps are similar to those for the bilinear dome caps. These are given in Fig.5.13.

The buckling modes for the dome models with original and refined mesh configurations are very similar. The failure is in the form of local buckling of members on the side of the applied snow load. The failure is indicated by the

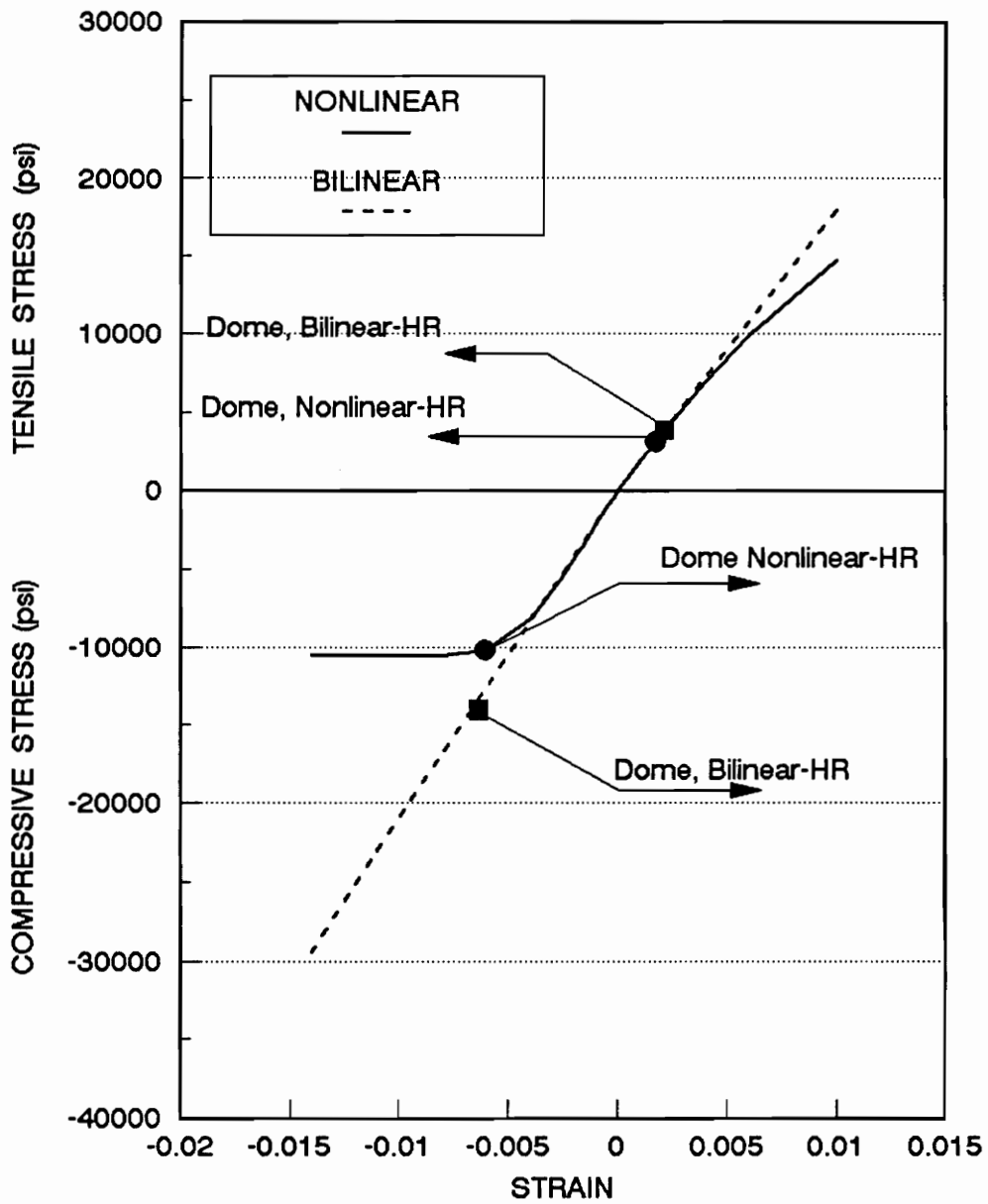


**FIG.5.14 STRESS AND STRAINS AT LIMIT POINT FOR THE DOME WITH REFINED MESH**

presence of dimples at the location of localised buckling.

The stress and the corresponding strain at the limit point for the dome models with refined meshes and half snow load are plotted in Fig.5.14. These stresses and strains are superimposed on the plot of the bilinear and the nonlinear stress-strain curves for wood. From the figure it can be seen that the compressive strains at the limit point for both the models are nearly the same, while the stresses are markedly different. This difference arises due to the curvature of the nonlinear stress-strain law. Since the nonlinear stress-strain law curves and becomes horizontal, for the same strain, a smaller stress reading is obtained as compared to that for the linear stress strain law.

The compressive strain at failure for the dome model Inelastic-HR is  $6.07 \times 10^{-3}$  and the corresponding stress is 10188 psi. Considering linear behavior, the stress for this strain value would be 12747 psi. As the inelastic stress strain curve levels off, the difference in the stresses at the same strain values for the inelastic and the elastic material laws would become greater. It is also seen that the strain value at failure for the dome model Bilinear Elastic-HR is  $6.38 \times 10^{-3}$ . This value is very close to that for the inelastic case, but the corresponding stress at failure, 14011 psi, is much higher. This explains the rather large difference between the stresses at failure for the elastic and the inelastic dome models.

## CHAPTER 6

# CONCLUSIONS AND RECOMMENDATIONS

### 6.1 Conclusions

From the studies conducted in this research, it is found that:

1. The nonlinear material law of wood can be successfully modelled and incorporated in the finite element program ABAQUS.
2. The selective refinement of the mesh in inelastic analysis gives a softer response as compared to complete mesh refinement, although it gives convergence problems and does not work for the complete dome.
3. Torsion studies on cantilever beams show that the shear modulus value used

by ABAQUS in the computations is different from those specified by Wu (1991), Tissaoui (1991), and by Davalos (1989) because ABAQUS defaults at Poisson's ratio of 0.5, thus computing the corresponding shear modulus as  $6.0 \times 10^5$  psi instead of as  $1.6 \times 10^5$  psi.

4. For full snow load cases (cyclically symmetric loading) the effect of variation in the shear modulus on the dome behavior is negligible, whereas considerable effect is seen for the half snow load cases (cyclically unsymmetric loading).

5. The materially nonlinear response of the dome is softer than the materially linear response.

6. The mesh refinement causes a softer response, and lowers the critical load as compared to that for the dome model with a coarser mesh.

8. The selective refinement of the mesh gave better results than the uniform mesh refinement in the dome cap models. But for the dome model, the selective mesh refinement, i.e., providing connector (hinge) elements caused convergence problems.

9. The buckling modes for all the dome models with linear and nonlinear material law were the same, and the critical loads were at the limit points.

10. For the elastic dome analyses, the compressive stresses at the limit load were

beyond the ultimate, while the tensile stresses were between the proportional limit and the ultimate stress.

11. For the dome with nonlinear material law, the compressive stresses at the limit load were in the plastic region of the stress strain curve (plateau region) while the tensile stresses were between the proportional limits and the ultimate stress.

## **6.2 Recommendations**

1. The nonlinear response of the cantilever beam must be compared with experimental results
2. The material law modelled in this research is for small clear timber. Experimental tests must be conducted on glulam beams to find the differences, if any, in their nonlinear behavior. These differences must then be incorporated in the material model.
- 3 The results of finite element analyses of the dome models should be verified by experimental tests of the dome models.

4. Dome models with different geometry and rise to span ratios should be analysed. Inelastic analyses of domes with different geometry would give a more clearer understanding of the behavior of domes with nonlinear stress-strain laws, and of the effect of the rise to span ratios on this behavior.
5. Further studies should be conducted by modelling the connector (hinge) elements with B32 beam elements to determine the cause of the convergence problems in the complete dome model.
6. Various other loading conditions should be used to study their effect on the nonlinear behavior of the domes.
7. A more realistic model of decking should be used to study its effect on the dome behavior.
8. The maximum stresses at failure occur at the beam joints. Hence, it is important to determine if the connectors would fail before the members. The connectors should thus be modelled and monitored in the future studies.
10. The method of combined linear and nonlinear buckling prediction method (Wu, 1991; Tissaoui, 1991; Holzer, Wu, and Tissaoui, 1991) should be used to study its applicability and usefulness in the buckling analyses of domes with nonlinear material laws.

## REFERENCES

1. ABAQUS, General-Purpose Finite Element System, Hibbit, Karlsson and Sorensen, Inc., 100 Medway Street, Providence, RI 02906, U.S.A.
2. American Institute of Timber Construction, Timber Construction Mannul, 3<sup>rd</sup> edition, John Wiley and Sons, Inc, New York, 1985.
3. Bathe, K. J., Finite Element Procedures in Engineering Analyses, Prentice-Hall, Englewood Cliffs, NJ, 1982.
4. Bathe, K. J., and Bolourchi, S., "Large Displacement Analysis of Three-Dimensional Beam Structures", International Journal for Numerical Methods in Engineering, vol. 14, 1979, pp. 961-986.
5. Bodig, J., Wood Structures, American Society of Civil Engineers, Structures

Division, 1975.

6. Broyles, L. D., Triax Dome Modelling with I-DEAS 4.1, M. S. Thesis, Virginia Polytechnic Institute and State University, January 1990.
7. Conners, T. E., "Segmented Models for Stress-Strain Diagrams", Wood Science and Technology, vol. 23, 1989, pp. 65-73.
8. Cook, R. D., Malkus, D. S., and Plesha, M. E., Concepts and Applications of Finite Element Analysis, 3<sup>rd</sup> edition, John Wiley and Sons, 1989.
9. Davalos, J. F., Geometrically Nonlinear Finite Element Analysis of a Glulam Timber Dome, Ph.D. Dissertation, Virginia Polytechnic Institute and State University, July 1989.
10. Holzer, S. M., and Loferski, J. R., "Background for Research on Glulam Lattice Domes", Proceedings of the Sixth Annual Structures Congress, ASCE Structures Division, Orlando, Fl, August 1987, pp. 305-308.
11. Holzer, S. M., Wu, C. H., and Tissaoui, J., "Finite Element Stability Analysis of a Glulam Dome", International Journal of Space Structures, to appear.
12. Huang, C. Y., Geometrically Nonlinear Finite Element Analysis of a Lattice Dome, M. S. Thesis, Virginia Polytechnic Institute and State University, November 1989.

13. I-DEAS, Engineering Analysis, Model Solution, and Optimization, Macneal-Schwendler, Structural Dynamics Research Corporation, 2000 Eastman Drive, Milford, Ohio, U.S.A.
14. Jau, J. J., Geometrically Nonlinear Finite Element Analysis of Space Frames, Ph.D. Dissertation, Virginia Polytechnic Institute and State University, February 1985.
15. Kaliszky, S., Plasticity : Theory and Engineering Applications, Elsevier, New York, 1989.
16. McGowan, D., Ultimate Capacity of Offshore Platform Conductor Strings, M. S. Thesis, Virginia Polytechnic Institute and State University, January 1991.
17. Smith, J. O., and Sidebottom, O. M., Inelastic Behavior of Load-Carrying Members, John Wiley and Sons, 1965.
18. Tissaoui, J., Stability Analysis of the Church of the Nazarene Varax Dome, M. S. Thesis, Virginia Polytechnic Institute and State University, February 1991.
19. United States Department of Agriculture, Wood Handbook, U.S Forest Products Laboratory, 1974.

- ✓  
20. Wu, C. H., Modelling and Stability Investigation of a Glulam Dome, M. S. Thesis, Virginia Polytechnic Institute and State University, March 1991.

## APPENDIX A

```

C      =====C
C  PROGRAM TO COMPUTE THE DIRECTION COSINES OF THE BEAM ELEMENTS C
C  AND TO WRITE THE SECTION PROPERTIES AND ELEMENT SETS          C
C                                                                C
C  USER: NIKET M. TELANG.....951 3071.                        C
C  PROGRAM WRITTEN SEPT 1991                                     C
C                                                                C
C  THE PROGRAM READS THE DATA FILES NAMED IN THE COMMENT      C
C  STATEMENTS                                                    C
C                                                                C
C  VARIABLES:                                                    C
C  N:                    NODE NUMBERS                            C
C  X, Y, Z:              ELEMENT NUMBER                          C
C  R:                    RADIUS OF THE DOME                      C
C  XCOS, YCOS, ZCOS:     ARRAY FOR THE NODES                    C
C  XNORM:                MAGNITUDE OF THE 1 AXIS VECTOR         C
C  XCC, YCC, ZCC:        DIRECTION COSINES FOR THE BEAMS        C
C  =====C
C
C  DECLARE THE VARIABLES
C
C  REAL X, Y, Z
C  REAL XCOS(800), YCOS(800), ZCOS(800)
C  REAL XC(800), YC(800), ZC(800)
C  REAL XCC(800), YCC(800), ZCC(800)
C  REAL R
C  R=1387.6
C
C  OPEN NODE COORDINATES AND BEAM CONNECTIVITY DATA FILES
C
C  OPEN(UNIT=55,STATUS='OLD')

```

```

OPEN(UNIT=60,STATUS='OLD')
OPEN(UNIT=65,STATUS='OLD')
OPEN(UNIT=70,STATUS='OLD')
C
C   OPEN OUTPUT DATA FILES
C
OPEN(UNIT=88,STATUS='UNKNOWN')
OPEN(UNIT=98,STATUS='UNKNOWN')
C
C   READ NODES FROM NODES.DAT
C
DO 10 I=1,217
  READ (55,*) N, X, Y, Z
  XCOS(I) = X
  YCOS(I) = Y
  ZCOS(I) = Z + 1387.66
  ZCOS1(I) = Z+1387.66
10 CONTINUE
C
C   READ CONNECTIVITY FOR MAIN BEAMS-I FROM MBEAM1.DAT
C
WRITE(88,350)
WRITE(98,350)
DO 20 J=1,24
  READ (60,*) NE, N1, N2
  XC(NE) = YCOS(N1) * ZCOS(N2) - ZCOS(N1) * YCOS(N2)
  YC(NE) = -(XCOS(N1) * ZCOS(N2) - ZCOS(N1) * XCOS(N2))
  ZC(NE) = XCOS(N1) * YCOS(N2) - YCOS(N1) * XCOS(N2)
  XNORM = (XC(NE)**2+YC(NE)**2+ZC(NE)**2) ** 0.5
  XCC(NE) = XC(NE) / XNORM
  YCC(NE) = YC(NE) / XNORM
  ZCC(NE) = ZC(NE) / XNORM
  WRITE (88,200) NE
  WRITE (88,220) NE, N1, N2
  WRITE (98,230) NE
  WRITE (98,240)
  WRITE (98,300) XCC(NE),YCC(NE),ZCC(NE)
  WRITE (98,310)
  WRITE (98,320)
20 CONTINUE
C
C   READ CONNECTIVITY FOR MAIN BEAM-II FROM MBEAM2.DAT
C
WRITE(88,360)
WRITE(98,360)
DO 30 II=1,240
  READ (65,*) NE, N1, N2
  XC(NE) = YCOS(N1) * ZCOS(N2) - ZCOS(N1) * YCOS(N2)
  YC(NE) = -(XCOS(N1) * ZCOS(N2) - ZCOS(N1) * XCOS(N2))

```

```

      ZC(NE) = XCOS(N1) * YCOS(N2) - YCOS(N1) * XCOS(N2)
      XNORM = (XC(NE)**2+YC(NE)**2+ZC(NE)**2) ** 0.5
      XCC(NE) = XC(NE) / XNORM
      YCC(NE) = YC(NE) / XNORM
      ZCC(NE) = ZC(NE) / XNORM
      WRITE (88,200) NE
      WRITE (88,220) NE, N1, N2
      WRITE (98,230) NE
      WRITE (98,245)
      WRITE (98,300) XCC(NE),YCC(NE),ZCC(NE)
      WRITE (98,310)
      WRITE (98,320)
30  CONTINUE
C
C  READ CONNECTIVITY FOR EDGE (PERIMETER) BEAMS FROM EDBEAM.DAT
C
      WRITE(88,370)
      WRITE(98,370)
      DO 40 II=1,48
        READ (70,*) NE, N1, N2
        XC(NE) = YCOS(N1) * ZCOS(N2) - ZCOS(N1) * YCOS(N2)
        YC(NE) = -(XCOS(N1) * ZCOS(N2) - ZCOS(N1) * XCOS(N2))
        ZC(NE) = XCOS(N1) * YCOS(N2) - YCOS(N1) * XCOS(N2)
        XNORM = (XC(NE)**2+YC(NE)**2+ZC(NE)**2) ** 0.5
        XCC(NE) = XC(NE) / XNORM
        YCC(NE) = YC(NE) / XNORM
        ZCC(NE) = ZC(NE) / XNORM
        WRITE (88,200) NE
        WRITE (88,220) NE, N1, N2
        WRITE (98,230) NE
        WRITE (98,250)
        WRITE (98,300) XCC(NE),YCC(NE),ZCC(NE)
        WRITE (98,310)
        WRITE (98,320)
40  CONTINUE
C
C  FORMAT STATEMENTS FOR WRITING THE OUTPUTS
C
200  FORMAT (T1,'*ELEMENT,TYPE=B33,ELSET=E',T26,I4)
220  FORMAT (1X,I4,',',I4,',',I4)
230  FORMAT (T1,'*BEAM SECTION,SECTION=RECT,MATERIAL=UWOOD,ELSET=E'
      $      ,T50,I4)
240  FORMAT (2X,'6.75, 11.0')
245  FORMAT (2X,'5.0, 11.0')
250  FORMAT (2X,'12.25, 3.0')
300  FORMAT (1X,F8.4,',',F8.4,',',F8.4)
310  FORMAT ('*TRANSVERSE SHEAR STIFFNESS')
320  FORMAT (2X,'9972128.26, 9972128.26')
350  FORMAT ('**-----MAIN BEAMS 1')

```

```
360  FORMAT ('**-----MAIN BEAMS 2')
370  FORMAT ('**-----EDGE BEAMS')
      END
```

## APPENDIX B

```
*HEADING, CORE=15000000
SDRC I-DEAS ABAQUS FILE TRANSLATOR 10-OCT-91 22:26:18
** NIKET M. TELANG 9513071 INPUTFILE FOR DOME
** NONLINEAR RIKS ANALYSES/ HALF SNOW LOAD/ USER MATERIAL ALL BEAMS
** NONLINEAR MATERIAL LAW
**----- NODES
*NODE, SYSTEM=R, NSET=ALL
  1, 0.0000E+00, 0.0000E+00, 2.1234E+02
  2, 2.6374E+02, 0.0000E+00, 1.9046E+02
  3, 1.3187E+02,-2.2840E+02, 1.9046E+02
  4, 5.0721E+02, 0.0000E+00, 1.2982E+02
  5, 2.5361E+02,-4.3926E+02, 1.2982E+02
  6, 3.8528E+02,-2.2244E+02, 1.4925E+02
  7, 7.1710E+02, 0.0000E+00, 4.2643E+01
  8, 3.5855E+02,-6.2103E+02, 4.2644E+01
  9, 4.8911E+02,-4.2359E+02, 7.5678E+01
 10, 6.1139E+02,-2.1179E+02, 7.5677E+01
 11, 7.9650E+02, 0.0000E+00, 4.8828E-04
 12, 3.9825E+02,-6.8978E+02, 4.8828E-04
 13, 5.6321E+02,-5.6321E+02, 4.8828E-04
 14, 6.8978E+02,-3.9825E+02, 4.8828E-04
 15, 7.6936E+02,-2.0615E+02, 4.8828E-04
 16, 2.5941E+02,-2.2615E+02, 1.7490E+02
 17, 3.2556E+02,-1.1158E+02, 1.7489E+02
 18, 3.7243E+02,-4.3266E+02, 1.0704E+02
 19, 4.3841E+02,-3.2391E+02, 1.1663E+02
 20, 4.9972E+02,-2.1772E+02, 1.1663E+02
  .
  .
  .
  .
```

```

.
.
.
.
.
.

200,-4.3841E+02,-3.2391E+02, 1.1663E+02
201,-3.7243E+02,-4.3266E+02, 1.0704E+02
202,-7.4494E+02,-1.0331E+02, 2.4569E+01
203,-6.9140E+02,-2.0928E+02, 3.9982E+01
204,-6.5207E+02,-3.0572E+02, 4.1096E+01
205,-5.9079E+02,-4.1185E+02, 4.1096E+01
206,-5.2695E+02,-4.9413E+02, 3.9982E+01
207,-4.6194E+02,-5.9348E+02, 2.4569E+01
208,-1.9848E+02,-1.1459E+02, 1.9584E+02
209,-4.4766E+02,-1.1157E+02, 1.4439E+02
210,-3.2045E+02,-3.3190E+02, 1.4438E+02
211,-6.6610E+02,-1.0619E+02, 6.3212E+01
212,-5.5186E+02,-3.1862E+02, 7.9969E+01
213,-4.2502E+02,-5.2377E+02, 6.3212E+01
214,-7.8968E+02,-1.0396E+02, 0.0000E+00
215,-7.3587E+02,-3.0480E+02, 0.0000E+00
216,-6.3190E+02,-4.8487E+02, 0.0000E+00
217,-4.8488E+02,-6.3190E+02, 0.0000E+00

*-----BOUNDARY NODES
*NSET,NSET=SUPPORT
    12,    195,    15,    88,    89,    90
    91,    52,    53,    11,    127,    128
    129,    130,    165,    166,    167,    131
    13,    54,    55,    14,    193,    194
    78,    79,    80,    81,    186,    187
    188,    189,    158,    159,    160,    161
    214,    215,    216,    217,    114,    115
    116,    117,    42,    43,    44,    45

**-----ELEMENT INCIDENTS
**-----TRUSS ELEMENTS
**-----TENSION RING
*ELEMENT,TYPE=C1D2,ELSET=RING
232 53 52
231 54 53
230 55 54
229 11 55
893 88 195
894 195 194
895 194 193
896 193 128
61 11 15
733 127 167

```

```

62 15 14
576 129 128
575 130 129
574 131 130
573 127 131
734 167 166
735 166 165
736 165 52
400 89 12
399 90 89
398 91 90
397 88 91
63 14 13
64 13 12

```

```

**-----PURLINS

```

```

*ELEMENT,TYPE=C1D2 ,ELSET=PURLIN

```

```

242 67 66
235 57 56
234 30 57
240 59 58
75 26 25
76 25 24
739 169 168
589 140 139
588 141 140
587 142 141
72 19 18
586 143 142
738 146 169
585 134 149
584 135 134
583 136 135
582 137 136
65 28 29
66 30 17

```

```

.
.
.
.
.
.

```

```

748 177 176
401 104 29
402 105 93
403 93 92
404 92 31
405 106 97
406 97 96
407 96 95

```

```

408 95 94
409 94 33
410 103 102
411 102 101
412 101 100
413 100 99
414 99 98
749 176 175
750 175 174
909 204 203
741 148 173
590 139 138
236 56 69

```

```

**-----TRUSS BRACING

```

```

*ELEMENT,TYPE=C1D2 ,ELSET=BRACE

```

```

417 108 93
418 108 92
419 105 110
420 93 110
421 92 109
422 31 109
423 110 97
424 110 96
765 172 184
415 104 108

```

```

.
.
.
.
.

```

```

610 157 142
760 182 172
612 156 140
613 155 139
614 155 138
615 143 150
616 143 127
617 143 161
618 142 160
619 141 160
620 140 159
624 138 151
622 138 158
623 138 128
776 179 127

```

```

**-----BEAM ELEMENTS

```

```

**-----MAIN BEAMS 1

```

```

*ELEMENT,TYPE=B33,ELSET=E 1

```

```

1, 1, 28

```

```

*ELEMENT,TYPE=B33,ELSET=E 2
  2, 28, 2
*ELEMENT,TYPE=B33,ELSET=E 3
  3, 1, 29
*ELEMENT,TYPE=B33,ELSET=E 4
  4, 29, 3
*ELEMENT,TYPE=B33,ELSET=E 5
  5, 2, 36
*ELEMENT,TYPE=B33,ELSET=E 6
  6, 36, 3
*ELEMENT,TYPE=B33,ELSET=E 178
  178, 68, 46
*ELEMENT,TYPE=B33,ELSET=E 180
  180, 72, 46
*ELEMENT,TYPE=B33,ELSET=E 850
  850, 208, 119
*ELEMENT,TYPE=B33,ELSET=E 849
  849, 82, 208
*ELEMENT,TYPE=B33,ELSET=E 345
  345, 1, 104
*ELEMENT,TYPE=B33,ELSET=E 346
  346, 104, 82
*ELEMENT,TYPE=B33,ELSET=E 347
  347, 82, 108
*ELEMENT,TYPE=B33,ELSET=E 348
  348, 108, 3
*ELEMENT,TYPE=B33,ELSET=E 513
  513, 1, 144
*ELEMENT,TYPE=B33,ELSET=E 514
  514, 144, 118
*ELEMENT,TYPE=B33,ELSET=E 515
  515, 1, 145
*ELEMENT,TYPE=B33,ELSET=E 516
  516, 145, 119
*ELEMENT,TYPE=B33,ELSET=E 517
  517, 118, 152
*ELEMENT,TYPE=B33,ELSET=E 518
  518, 152, 119
*ELEMENT,TYPE=B33,ELSET=E 690
  690, 180, 46
*ELEMENT,TYPE=B33,ELSET=E 689
  689, 118, 180
*ELEMENT,TYPE=B33,ELSET=E 177
  177, 1, 68
*ELEMENT,TYPE=B33,ELSET=E 179
  179, 2, 72
**-----MAIN BEAMS 2
*ELEMENT,TYPE=B33,ELSET=E 23
  23, 6, 20

```

```

*ELEMENT,TYPE=B33,ELSET=E 24
  24, 20, 10
*ELEMENT,TYPE=B33,ELSET=E 25
  25, 6, 19
*ELEMENT,TYPE=B33,ELSET=E 26
  26, 19, 9
*ELEMENT,TYPE=B33,ELSET=E 27
  27, 5, 18
*ELEMENT,TYPE=B33,ELSET=E 28
  28, 18, 9
*ELEMENT,TYPE=B33,ELSET=E 29
  29, 5, 33
*ELEMENT,TYPE=B33,ELSET=E 30
  30, 33, 8
*ELEMENT,TYPE=B33,ELSET=E 31
  31, 7, 41
*ELEMENT,TYPE=B33,ELSET=E 32
  32, 41, 10
*ELEMENT,TYPE=B33,ELSET=E 33
  33, 10, 40
*ELEMENT,TYPE=B33,ELSET=E 34
  34, 40, 9
.
.
.
.
.
.
.
*ELEMENT,TYPE=B33,ELSET=E 363
  363, 84, 96
*ELEMENT,TYPE=B33,ELSET=E 364
  364, 96, 87
*ELEMENT,TYPE=B33,ELSET=E 365
  365, 84, 95
*ELEMENT,TYPE=B33,ELSET=E 366
  366, 95, 86
*ELEMENT,TYPE=B33,ELSET=E 367
  367, 5, 94
*ELEMENT,TYPE=B33,ELSET=E 368
  368, 94, 86
*ELEMENT,TYPE=B33,ELSET=E 369
  369, 85, 113
*ELEMENT,TYPE=B33,ELSET=E 370
  370, 113, 87
*ELEMENT,TYPE=B33,ELSET=E 388
  388, 98, 89
*ELEMENT,TYPE=B33,ELSET=E 387
  387, 8, 98

```

\*ELEMENT,TYPE=B33,ELSET=E 386  
 386, 99, 89  
 \*ELEMENT,TYPE=B33,ELSET=E 385  
 385, 86, 99  
 \*ELEMENT,TYPE=B33,ELSET=E 371  
 371, 87, 112  
 \*ELEMENT,TYPE=B33,ELSET=E 382  
 382, 101, 90  
 \*ELEMENT,TYPE=B33,ELSET=E 379  
 379, 87, 102  
 \*ELEMENT,TYPE=B33,ELSET=E 378  
 378, 103, 91  
 \*ELEMENT,TYPE=B33,ELSET=E 377  
 377, 85, 103  
 \*ELEMENT,TYPE=B33,ELSET=E 376  
 376, 107, 88  
 \*ELEMENT,TYPE=B33,ELSET=E 375  
 375, 85, 107  
 \*ELEMENT,TYPE=B33,ELSET=E 374  
 374, 111, 8  
 \*ELEMENT,TYPE=B33,ELSET=E 373  
 373, 86, 111  
 \*ELEMENT,TYPE=B33,ELSET=E 372  
 372, 112, 86

\*\*-----EDGE BEAMS

\*ELEMENT,TYPE=B33,ELSET=E 891  
 891, 193, 214  
 \*ELEMENT,TYPE=B33,ELSET=E 572  
 572, 158, 128  
 \*ELEMENT,TYPE=B33,ELSET=E 221  
 221, 11, 81  
 \*ELEMENT,TYPE=B33,ELSET=E 389  
 389, 88, 117  
 \*ELEMENT,TYPE=B33,ELSET=E 390  
 390, 117, 91  
 \*ELEMENT,TYPE=B33,ELSET=E 391  
 391, 91, 116  
 \*ELEMENT,TYPE=B33,ELSET=E 392  
 392, 116, 90  
 \*ELEMENT,TYPE=B33,ELSET=E 393  
 393, 90, 115  
 \*ELEMENT,TYPE=B33,ELSET=E 394  
 394, 115, 89  
 \*ELEMENT,TYPE=B33,ELSET=E 56  
 56, 44, 14

.  
 .  
 .  
 .

```

.
.
.
.
.
.
*ELEMENT,TYPE=B33,ELSET=E 888
888, 216, 194
*ELEMENT,TYPE=B33,ELSET=E 889
889, 194, 215
*ELEMENT,TYPE=B33,ELSET=E 890
890, 215, 193
*ELEMENT,TYPE=B33,ELSET=E 60
60, 42, 12
*ELEMENT,TYPE=B33,ELSET=E 59
59, 13, 42
*ELEMENT,TYPE=B33,ELSET=E 58
58, 43, 13
*ELEMENT,TYPE=B33,ELSET=E 57
57, 14, 43
*ELEMENT,TYPE=B33,ELSET=E 565
565, 127, 161
*ELEMENT,TYPE=B33,ELSET=E 566
566, 161, 131
*ELEMENT,TYPE=B33,ELSET=E 567
567, 131, 160
*ELEMENT,TYPE=B33,ELSET=E 568
568, 160, 130
*ELEMENT,TYPE=B33,ELSET=E 569
569, 130, 159
*ELEMENT,TYPE=B33,ELSET=E 570
570, 159, 129
*ELEMENT,TYPE=B33,ELSET=E 54
54, 45, 15
**-----SECTION PROPERTIES
**-----TRUSS ELEMENTS
*SOLID SECTION, ELSET=RING, MATERIAL=STEEL
12.
*SOLID SECTION, ELSET=PURLIN, MATERIAL=WOOD
24.75
*SOLID SECTION, ELSET=BRACE, MATERIAL=WOOD
0.3
**-----BEAM ELEMENTS
**-----MAIN BEAMS 1
*BEAM SECTION,SECTION=RECT,MATERIAL=UWOOD,ELSET=E 1
6.75, 11.0
0.0000, 1.0000, 0.0000
*TRANSVERSE SHEAR STIFFNESS
9972128.26, 9972128.26

```

```

*BEAM SECTION,SECTION=RECT,MATERIAL=UWOOD,ELSET=E 2
6.75, 11.0
0.0000, 1.0000, 0.0000
*TRANSVERSE SHEAR STIFFNESS
9972128.26, 9972128.26
*BEAM SECTION,SECTION=RECT,MATERIAL=UWOOD,ELSET=E 3
6.75, 11.0
0.8660, 0.5000, 0.0000
*TRANSVERSE SHEAR STIFFNESS
9972128.26, 9972128.26
*BEAM SECTION,SECTION=RECT,MATERIAL=UWOOD,ELSET=E 4
6.75, 11.0
0.8660, 0.5000, 0.0000
*TRANSVERSE SHEAR STIFFNESS
9972128.26, 9972128.26
*BEAM SECTION,SECTION=RECT,MATERIAL=UWOOD,ELSET=E 5
6.75, 11.0
0.8571, -0.4948, -0.1432
*TRANSVERSE SHEAR STIFFNESS
9972128.26, 9972128.26
*BEAM SECTION,SECTION=RECT,MATERIAL=UWOOD,ELSET=E 6
6.75, 11.0
0.8571, -0.4949, -0.1432
*TRANSVERSE SHEAR STIFFNESS
9972128.26, 9972128.26
*BEAM SECTION,SECTION=RECT,MATERIAL=UWOOD,ELSET=E 178
6.75, 11.0
-0.8660, 0.5000, 0.0000
*TRANSVERSE SHEAR STIFFNESS
9972128.26, 9972128.26
.
.
.
.
.
.
.
**-----MAIN BEAMS 2
*BEAM SECTION,SECTION=RECT,MATERIAL=UWOOD,ELSET=E 23
5.0, 11.0
0.0000, 0.9897, 0.1432
*TRANSVERSE SHEAR STIFFNESS
9972128.26, 9972128.26
*BEAM SECTION,SECTION=RECT,MATERIAL=UWOOD,ELSET=E 24
5.0, 11.0
0.0000, 0.9897, 0.1432
*TRANSVERSE SHEAR STIFFNESS
9972128.26, 9972128.26
*BEAM SECTION,SECTION=RECT,MATERIAL=UWOOD,ELSET=E 25
5.0, 11.0

```

0.8571, 0.4948, -0.1432  
 \*TRANSVERSE SHEAR STIFFNESS  
 9972128.26, 9972128.26  
 \*BEAM SECTION,SECTION=RECT,MATERIAL=UWOOD,ELSET=E 26  
 5.0, 11.0  
 0.8571, 0.4948, -0.1433  
 \*TRANSVERSE SHEAR STIFFNESS  
 9972128.26, 9972128.26  
 \*BEAM SECTION,SECTION=RECT,MATERIAL=UWOOD,ELSET=E 27  
 5.0, 11.0  
 0.0000, 0.9606, 0.2781  
 \*TRANSVERSE SHEAR STIFFNESS  
 9972128.26, 9972128.26  
 \*BEAM SECTION,SECTION=RECT,MATERIAL=UWOOD,ELSET=E 28  
 5.0, 11.0  
 0.0001, 0.9606, 0.2780  
 \*TRANSVERSE SHEAR STIFFNESS  
 9972128.26, 9972128.26  
 .  
 .  
 .  
 .  
 .  
 .  
 .  
 \*BEAM SECTION,SECTION=RECT,MATERIAL=UWOOD,ELSET=E 376  
 5.0, 11.0  
 0.8660, -0.5001, -0.0001  
 \*TRANSVERSE SHEAR STIFFNESS  
 9972128.26, 9972128.26  
 \*BEAM SECTION,SECTION=RECT,MATERIAL=UWOOD,ELSET=E 375  
 5.0, 11.0  
 0.8660, -0.5000, 0.0000  
 \*TRANSVERSE SHEAR STIFFNESS  
 9972128.26, 9972128.26  
 \*BEAM SECTION,SECTION=RECT,MATERIAL=UWOOD,ELSET=E 374  
 5.0, 11.0  
 0.0001, 0.9173, 0.3983  
 \*TRANSVERSE SHEAR STIFFNESS  
 9972128.26, 9972128.26  
 \*BEAM SECTION,SECTION=RECT,MATERIAL=UWOOD,ELSET=E 373  
 5.0, 11.0  
 -0.0001, 0.9173, 0.3983  
 \*TRANSVERSE SHEAR STIFFNESS  
 9972128.26, 9972128.26  
 \*BEAM SECTION,SECTION=RECT,MATERIAL=UWOOD,ELSET=E 372  
 5.0, 11.0  
 0.0000, 0.9173, 0.3983  
 \*TRANSVERSE SHEAR STIFFNESS

```

9972128.26, 9972128.26
**-----EDGE BEAMS
*BEAM SECTION,SECTION=RECT,MATERIAL=UWOOD,ELSET=E 891
12.25, 3.0
0.0000, 0.0000, -1.0000
*TRANSVERSE SHEAR STIFFNESS
9972128.26, 9972128.26
*BEAM SECTION,SECTION=RECT,MATERIAL=UWOOD,ELSET=E 572
12.25, 3.0
0.0000, 0.0000, 1.0000
*TRANSVERSE SHEAR STIFFNESS
9972128.26, 9972128.26
*BEAM SECTION,SECTION=RECT,MATERIAL=UWOOD,ELSET=E 221
12.25, 3.0
0.0000, 0.0000, 1.0000
*TRANSVERSE SHEAR STIFFNESS
9972128.26, 9972128.26
*BEAM SECTION,SECTION=RECT,MATERIAL=UWOOD,ELSET=E 228
12.25, 3.0
0.0000, 0.0000, 1.0000
*TRANSVERSE SHEAR STIFFNESS
9972128.26, 9972128.26
*BEAM SECTION,SECTION=RECT,MATERIAL=UWOOD,ELSET=E 227
12.25, 3.0
0.0000, 0.0000, 1.0000
*TRANSVERSE SHEAR STIFFNESS
9972128.26, 9972128.26
.
.
.
.
.
.
*BEAM SECTION,SECTION=RECT,MATERIAL=UWOOD,ELSET=E 569
12.25, 3.0
0.0000, 0.0000, 1.0000
*TRANSVERSE SHEAR STIFFNESS
9972128.26, 9972128.26
*BEAM SECTION,SECTION=RECT,MATERIAL=UWOOD,ELSET=E 570
12.25, 3.0
0.0000, 0.0000, 1.0000
*TRANSVERSE SHEAR STIFFNESS
9972128.26, 9972128.26
*BEAM SECTION,SECTION=RECT,MATERIAL=UWOOD,ELSET=E 54
12.25, 3.0
0.0000, 0.0000, -1.0000
*TRANSVERSE SHEAR STIFFNESS
9972128.26, 9972128.26
**-----MATERIAL PROPERTIES

```

```

*MATERIAL, NAME=WOOD
*ELASTIC
  1.8E+06, 4.625
*MATERIAL, NAME=UWOOD
*USER MATERIAL, CONSTANT=3
  12.00, 0.52, 1.6E5
*MATERIAL, NAME=STEEL
*ELASTIC
  2.9E+07, 0.3
**-----BOUNDARY CONDITIONS
*BOUNDARY
SUPPORT, 3
11, 2
128, 2
90, 1
166, 1
**-----APPLICATION OF DEAD LOAD
**-----NEWTON RAP. STEP
*STEP, NLGEOM, INC=100, CYCLE=12
*STATIC, PTOL=100.0, MTOL=1000.0
0.1, 1., 0.0, ,
*CLOAD
  1, 3, -0.1687E+04
  2, 3, -0.1622E+04
  3, 3, -0.1622E+04
  4, 3, -0.1448E+04
  5, 3, -0.1448E+04
  6, 3, -0.1502E+04
  7, 3, -0.9599E+03
  8, 3, -0.9599E+03
  9, 3, -0.1225E+04
 10, 3, -0.1225E+04
 11, 3, -0.3694E+03
 12, 3, -0.3695E+03
 13, 3, -0.4273E+03
 14, 3, -0.5313E+03
 15, 3, -0.4273E+03
 16, 3, -0.1591E+04
  .
  .
  .
  .
  .
  .
  .
100, 3, -0.1097E+04
101, 3, -0.1097E+04
102, 3, -0.9952E+03
103, 3, -0.8781E+03
104, 3, -0.1689E+04

```

105, 3, -0.1559E+04  
106, 3, -0.1344E+04  
107, 3, -0.3452E+03  
108, 3, -0.1656E+04  
109, 3, -0.1502E+04  
110, 3, -0.1502E+04  
111, 3, -0.1182E+04  
112, 3, -0.1303E+04  
113, 3, -0.1182E+04

.  
. .  
. .  
. .  
. .  
. .  
. .

190, 3, -0.1502E+04  
191, 3, -0.1225E+04  
192, 3, -0.1225E+04  
193, 3, -0.4273E+03  
194, 3, -0.5313E+03  
195, 3, -0.4273E+03  
196, 3, -0.1591E+04  
197, 3, -0.1591E+04  
198, 3, -0.1394E+04  
199, 3, -0.1419E+04  
200, 3, -0.1419E+04  
201, 3, -0.1394E+04  
202, 3, -0.8781E+03  
203, 3, -0.9952E+03  
204, 3, -0.1097E+04  
205, 3, -0.1097E+04  
206, 3, -0.9952E+03  
207, 3, -0.8781E+03  
208, 3, -0.1656E+04  
209, 3, -0.1502E+04  
210, 3, -0.1502E+04  
211, 3, -0.1182E+04  
212, 3, -0.1303E+04  
213, 3, -0.1182E+04  
214, 3, -0.1957E+03  
215, 3, -0.4934E+03  
216, 3, -0.4934E+03  
217, 3, -0.1957E+03

\*\*-----OUTPUT REQUEST

\*NSET, NSET=APEX1

1

\*ELSET, ELSET=ELE1

12

```

*PRINT, RESIDUAL=NO
*NODE PRINT, NSET=APEX1, SUMMARY=NO, FREQUENCY=5
U
*NODE PRINT, NSET=APEX1, SUMMARY=NO, FREQUENCY=5
CF
*EL PRINT, ELSET=ELE1, SUMMARY=NO, FREQUENCY=20
3, 23
S
*END STEP
**-----APPLICATION OF LIVE LOAD
**-----RIKS STEP
*STEP, NLGEOM, INC=20, CYCLE=16
*STATIC, PTOL=100., MTOL=1000., RIKS
0.1, 1., 0.0, ,20.0, 1, 3, -20.0
**-----DEAD LOAD + HALF SNOW LOAD
*CLOAD
  1, 3, -0.1687E+04
  2, 3, -0.1622E+04
  3, 3, -0.1622E+04
  4, 3, -0.1448E+04
  5, 3, -0.1448E+04
  6, 3, -0.1502E+04
  7, 3, -0.9599E+03
  8, 3, -0.9599E+03
  9, 3, -0.1225E+04
 10, 3, -0.1225E+04
 11, 3, -0.3694E+03
 12, 3, -0.3695E+03
 13, 3, -0.4273E+03
 14, 3, -0.5313E+03
 15, 3, -0.4273E+03
 16, 3, -0.1591E+04
 17, 3, -0.1591E+04
  .
  .
  .
  .
  .
  .
  .
 174, 3, -0.8781E+03
 175, 3, -0.9952E+03
 176, 3, -0.1097E+04
 177, 3, -0.1097E+04
 178, 3, -0.9952E+03
 179, 3, -0.8781E+03
 180, 3, -0.1656E+04
 181, 3, -0.1502E+04
 182, 3, -0.1502E+04

```

183, 3, -0.1182E+04  
 184, 3, -0.1303E+04  
 185, 3, -0.1182E+04  
 186, 3, -0.1957E+03  
 187, 3, -0.4934E+03  
 188, 3, -0.4935E+03  
 189, 3, -0.1957E+03  
 190, 3, -0.1502E+04  
 191, 3, -0.1225E+04  
 192, 3, -0.1225E+04  
 193, 3, -0.4273E+03  
 194, 3, -0.5313E+03  
 195, 3, -0.4273E+03  
 196, 3, -0.1591E+04  
 197, 3, -0.1591E+04  
 198, 3, -0.1394E+04  
 199, 3, -0.1419E+04  
 200, 3, -0.1419E+04  
 201, 3, -0.1394E+04  
 202, 3, -0.8781E+03  
 203, 3, -0.9952E+03  
 204, 3, -0.1097E+04  
 205, 3, -0.1097E+04  
 206, 3, -0.9952E+03  
 207, 3, -0.8781E+03  
 208, 3, -0.1656E+04  
 209, 3, -0.1502E+04  
 210, 3, -0.1502E+04  
 211, 3, -0.1182E+04  
 212, 3, -0.1303E+04  
 213, 3, -0.1182E+04  
 214, 3, -0.1957E+03  
 215, 3, -0.4934E+03  
 216, 3, -0.4934E+03  
 217, 3, -0.1957E+03  
 1, 3, -0.1053E+04  
 2, 3, -0.9986E+03  
 3, 3, -0.1997E+04  
 4, 3, -0.8582E+03  
 5, 3, -0.1716E+04  
 6, 3, -0.1803E+04  
 7, 3, -0.5402E+03  
 8, 3, -0.1080E+04  
 9, 3, -0.1404E+04  
 10, 3, -0.1404E+04  
 11, 3, -0.2020E+03  
 12, 3, -0.4040E+03  
 13, 3, -0.4691E+03  
 14, 3, -0.5844E+03

15, 3, -0.4691E+03  
 16, 3, -0.1939E+04  
 17, 3, -0.1939E+04  
 18, 3, -0.1627E+04  
 19, 3, -0.1665E+04  
 20, 3, -0.1665E+04  
 .  
 .  
 .  
 .  
 .  
 .  
 .  
 119, 3, -0.9986E+03  
 121, 3, -0.8582E+03  
 124, 3, -0.5402E+03  
 128, 3, -0.2020E+03  
 145, 3, -0.1051E+04  
 147, 3, -0.9442E+03  
 149, 3, -0.7745E+03  
 151, 3, -0.1899E+03  
 190, 3, -0.1803E+04  
 191, 3, -0.1404E+04  
 192, 3, -0.1404E+04  
 193, 3, -0.4690E+03  
 194, 3, -0.5845E+03  
 195, 3, -0.4691E+03  
 196, 3, -0.1939E+04  
 197, 3, -0.1939E+04  
 198, 3, -0.1627E+04  
 199, 3, -0.1666E+04  
 200, 3, -0.1665E+04  
 201, 3, -0.1627E+04  
 202, 3, -0.9713E+03  
 203, 3, -0.1108E+04  
 204, 3, -0.1225E+04  
 205, 3, -0.1225E+04  
 206, 3, -0.1108E+04  
 207, 3, -0.9713E+03  
 208, 3, -0.2046E+04  
 209, 3, -0.1797E+04  
 210, 3, -0.1797E+04  
 211, 3, -0.1342E+04  
 212, 3, -0.1495E+04  
 213, 3, -0.1343E+04  
 214, 3, -0.2139E+03  
 215, 3, -0.5421E+03  
 216, 3, -0.5421E+03  
 217, 3, -0.2139E+03

\*\*-----NODE, ELEMENT SETS AND OUTPUTS

\*NSET, NSET=APEX

1

\*NSET, NSET=NWATCH

1, 17, 38, 6, 16

\*ELSET, ELSET=EWATCH

37, 9, 10, 11, 12, 201

\*\*-----OUTPUT REQUESTS

\*PRINT, RESIDUAL=NO

\*EL PRINT, ELSET=EWATCH, POSITION=NODES

S

\*NODE PRINT, NSET=NWATCH

U

\*NODE PRINT, NSET=APEX

CF

\*NODE FILE, NSET=ALL

U

\*END STEP

\*USER SUBROUTINE

```
*****
*****                      SUBROUTINE TO DEFINE USER MATERIAL          *****
*****                      *****
*****      NIKET M. TELANG .....10 APRIL'91                          *****
*****
```

C

```
  SUBROUTINE UMAT(STRESS,STATEV,DDSDDE,SSE,SPD,SCD,
 1 RPL,DDSDDT,DRPLDE,DRPLDT,
 2 STRAN,DSTRAN,TIME,DTIME,TEMP,DTEMP,PRED,DPRED,CMNAME,
 3 NDI,NSHR,NTENS,NSTATV,PROPS,NPROPS,COORDS,DROT)
```

C

```
  IMPLICIT REAL*8(A-H,O-Z)
```

C

C

```
  DIMENSION STRESS(NTENS),STATEV(NSTATV),
 1 DDSDDE(NTENS,NTENS),
 2 DDSDDT(NTENS),DRPLDE(NTENS),
 3 STRAN(NTENS),DSTRAN(NTENS),PRED(1),DPRED(1),
 4 PROPS(NPROPS),COORDS(3),DROT(3,3)
```

C

C

```
  INITIALIZE DDSDDE(I,J)
```

C

```
  DO 20 I=1,NTENS
    DO 10 J=1,NTENS
```

```

        DDSDDDE(I,J)=0.0
10    CONTINUE
20    CONTINUE
C
C    *LONGITUDINAL STRESS*
C
    TS=0.0
    TS=STRAN(1) + DSTRAN(1)
C
C    *TENSION ZONE*
C
    IF(TS .GT. 0.0)THEN
C
        BETA1= 1822300. - 9.8*(PROPS(1)**3)
        BETA2= 1934700.0
        BETA3= 37045400. - 2204.*(PROPS(1)**3) - 150737800.*PROPS(2)
        AK1= (BETA1 - BETA2)/(2.*BETA3)
        ALFA1= BETA3*(AK1**2)
C
C    HAND COMPUTED VALUES FOR: SG=0.52, MC=12%
C
CC    BETA1=1805365.6
CC    BETA2=1934700.0
CC    BETA3=-45146768.0
CC    AK1=1.43237E-03
CC    ALFA1=-92.62689
C
    IF(TS .LT. AK1)THEN
        DDSDDDE(1,1)=BETA1
        STRESS(1)=BETA1*TS
    ELSEIF(TS .GE. AK1)THEN
        DDSDDDE(1,1)= BETA2 + (2.*BETA3*STRAN(1))
        STRESS(1)=ALFA1 + BETA2*TS + BETA3*(TS**2)
    ENDIF
C
C    *COMPRESSION ZONE*
C
    ELSEIF(TS .LE. 0.0)THEN
C
        BETA1= 143900. + 441996*PROPS(1) - 28997.*(PROPS(1)**2)
1      + 534.*(PROPS(1)**3)
        BETA2= 5719340. - 258850.*PROPS(1) + 4280*(PROPS(1)**2)
        BETA3= -1065588500. + 3449729*PROPS(1) +
1      1540914880.*PROPS(2)
        AK1= (BETA1 - BETA2)/(2.*BETA3)
        AK2= (-BETA2)/(2.*BETA3)
        ALFA1= BETA3*(AK1**2)
        ALFA2= BETA3*((AK1**2)-(AK2**2))
C

```

```

C      HAND COMPUTED VALUES FOR: SG=0.52, MC=12%
C
CC      BETA1=2195036.0
CC      BETA2=3229460.0
CC      BETA3=-222916014.1
CC      AK1=2.3202E-03
CC      AK2=7.24367E-03
CC      ALFA2=10496.5409
CC      ALFA1=-1200.03
C
      AK1C=-AK1
      AK2C=-AK2
      IF(TS .GE. AK1C)THEN
        DDSDE(1,1)=BETA1
        STRESS(1)=-BETA1*ABS(TS)
      ELSEIF(TS .LT. AK1C .AND. TS .GE. AK2C)THEN
        DDSDE(1,1)=BETA2 + 2.*BETA3*ABS(STRAN(1))
        STRESS(1)=- (ALFA1 + BETA2*ABS(TS) +
1          BETA3*((ABS(TS))**2))
      ELSEIF(TS .LT. AK2C)THEN
        DDSDE(1,1)=0.0
        STRESS(1)=-ALFA2
      ENDIF
    ENDIF
C
C      *TORSIONAL SHEAR STRESS*
C
      TT=0.0
      TT=STRAN(2) + DSTRAN(2)
C
      DDSDE(2,2)=PROPS(3)
      STRESS(2)=DDSDE(2,2)*TT
C
C
      RETURN
      END

```

## VITA

Niket M. Telang was born in Bombay, India in January of 1968. He graduated in First Class with Honors with the Bachelor of Engineering degree from Victoria Jubilee Technical Institute, University of Bombay. He started his studies towards the Master of Science degree in Civil Engineering in January 1990 at Virginia Polytechnic Institute and State University, which is his mother's Alma Matar. He is a member of the Honor Societies of Tau Beta Pi and Phi Kappa Phi. He is planning to work for a while as a Civil Engineer in the U.S.A. before continuing his studies towards a Ph.D. degree.

A handwritten signature in black ink, reading "Niket M. Telang". The signature is written in a cursive, flowing style with a large initial 'N' and a trailing flourish.